CLIMATIC CHANGE IN THE HISTORICAL AND THE INSTRUMENTAL PERIODS

R. Brázdil

Department of Geography, Faculty of Science, J. E. Purkyně University, Kotlářská 2, 611 37 Brno, Czechoslovakia

Received for publication: August 1989

On the occasion of the 70th anniversary of the foundation of J. E. Purkyně University in Brno (CSSR) the Department of Geography of its Faculty of Science organized an international conference entitled „Climatic Change in the Historical and the Instrumental Periods" held from 12—16 June, 1989. The beginnings of Brno climatology are closely connected with the establishment of the University Institute of Geography in 1921, when the works of *F. Koláček, F. Říkovský, B. Hrudička* and *F. Vitásek* laid the foundations of the Brno school of climatology. After the death of the first three above teachers in the fascist concentration camp Mauthausen the post-war development of Brno climatology was connected above all with the name of *Prof. M. Nosek.* Climatological research of the Department of Geography is at present oriented at local climatological research activities, the study of temporal and spatial regularities of atmospheric precipitation in the CSSR, changes and fluctuations of the climate in Europe and climatological research at Svalbard.

At the conference held under the auspices of *Prof. M. Yoshino* from Tsukuba University, Japan, chairman of the climatological commission of the International Geographical Union (IGU), 55 participants from the CSSR and 60 participants from 19 countries in Europe, Asia and North America took part, representing above all universities, research institutes of the academies of sciences, meteorological service and other institutions. After a ceremonial opening at which, besides *Prof. Yoshino,* speeches were held by the vice-rector of Brno University, *Prof. R. Rozkošný,* and the vice-chairman of the Czechoslovak Academy of Sciences, *Prof. V. Bucha,* altogether 35 papers were read in the plenary section, 42 others being presented in the form of posters. The presented papers covered a broad spectrum of global and regional climatic problems.

Several papers were devoted to the present warming of the Earth atmosphere. From the global point of view problems of climate diagnostics were discussed as a starting point of climatological modelling (*K.—H. Bernhardt, GDR*), the detection of the greenhouse effect by means of observational data (*C.—D. Schönwiese, FRG*) and the strategy of the reduction control of the effects of climatic change, above all the greenhouse effect (*W. Bach, FRG*). Further contributions concerned the effects of climatic changes, above all in economy and landscape ecology (*F. Eybergen, the Netherlands; M. Lapin, CSSR*; *M. Škoda* and *L. Špaček, CSSR*) and in the actual application to the CSR (*O. Šebek, CSSR*). A biophysical model for climatic changes and deforestation was presented (*L. C. Nkemdirim,*

Canada). With respect to the global warming of the Earth it is important to estimate the relative sensitivity and expressions of regional climate related to global changes (*J. Mika, Hungary*; *L. K. Kleshchenko* and *V. T. Radiuhin, USSR*). From the viewpoint of revealing the causes of climatic changes very important was the contribution presenting the theory of compensation of non-equilibrium states in the Earth atmosphere (*F. Pechala, CSSR*). Connections between the 80-year cycle of solar activity and climate fluctuation were mentioned (*M. Kopecký, CSSR*). The fluctuations found can be clarified by circulation changes. In this respect the presented papers concerned the relation between circulation processes and atmospheric precipitation in Europe (*V. V. Popova, USSR*), in Rumania (*A. Busuioc et al., Rumania*) and in Bohemia (*V. Brůžek, CSSR*), circulation anomalies in Europe (*D. Metaxas, Greece*), the effect of the changes of the Azores anticyclone on the circulation anomalies in Europe (*T. J. Makrogiannis et al., Greece*), the circulation anomalies of the 1980s in western Europe in comparison with the preceding decades (*A. H. Perry, UK*), the continuity of circulation anomalies with the occurrence of etesian-wind in Greece (*T. J. Makrogiannis* and *J. C. Dikaiakos, Greece*) and change of the 500 hPa level in the Atlantic-European sector (*C. Pop* and *R. Stroe, Rumania*).

Of extraordinary importance in the study of climatic changes are the applicable data sets and the methods of their study, both from the point of view of the diagnostics of the present state and with respect to possible forecasts. Besides instrumental data also historical data are important, as has been shown for central Europe (*Ch. Pfister, Switzerland; E. Młostek, Poland; J. Munzar, CSSR*; *K. Pejml* and *J. Munzar, CSSR*), the same as indirect and paleogeographical data (*G. A. Fogel* and *M. M. Chernavskaya*; *A. Tarand*; *R. K. Klige* and *O. Selivanov, USSR*), from which it is possible to evaluate climatic changes in the last millenium (*M. M. Chernavskaya*; *G. A. Fogel* and *N. N. Zolotokrylin, USSR*). Certain information can also be obtained by studying the tree-rings (*J. Kyncl et al., CSSR*). In the sphere of the methods of analysis of climatic changes attention was paid to the problems of changes in the spectral behaviour of climatic series (*M. Olberg, GDR*), to modelling the variability of time series (*C. Boroneant* and *N. Rîmbu, Rumania*), to the homogenization of climatic series on the example of Brussels-Uccle (*R. Sneyers et al., Belgium*), to the application of the method of robust regression (*J. Kalvová, CSSR*), to the statistical description of the behaviour of the extremes in meteorological series (*F.-W. Gerstengarbe* and *P. C. Werner, GDR*), to the occurrence of rare meteorological events (*C. Mareş, Rumania*), to data sources, methodology and software for the study of climate structure and variability (*R. G. Reitenbakh* and *A. M. Sterin, USSR*).

Global warming of the Earth atmosphere is also reflected by the increase in temperature of the superficial layer of the oceans, which in the tropics results in increased evaporation and the content of water vapour in the atmosphere, which can assist further intensification of the greenhouse effect (*A. Kapala, FRG*). The utilization of satellites makes it possible to apply the information obtained by them in the study of global characteristics of meteorological fields, as is the case in the snow cover, including its possible effects on other meteorological elements (*J. Bartholy, Hungary*). With respect of the necessity of solving the problem of linking up regional climatic changes with global climatic changes, valuable were the studies dealing with the fluctuation of air temperature (*G. Koppány* and *Z. Bottyán, Hungary*) and air pressure (*J. Trepińska, Poland*) in Europe, the same as

the analysis of the fluctuation of air pressure and temperature, sunshine duration, precipitation and snow patterns in central Europe (*R. Brázdil* and *T. N. Tam, CSSR* and *Vietnam*). Information about the fluctuation of temperature fields and geopotential fields in free atmosphere was presented for Europe (*J. L. Pyka, Poland*). The objective of further regional studies were dry and wet periods in the French part of the Mediterranean (*A. Douguédroit, France*), the correlation of climatic fluctuations between Cuba and Europe (*A. N. Krenke* and *M. M. Chernavskaya, USSR*), the comparison of temperature patterns in Europe and in North America (*S. Paczos, Poland*), the teleconnection of fluctuation of climatic elements in Poland and SST in north Atlantic (*M. Sadowski, Poland*), the fluctuation of precipitation in the GDR (*G. Malitz, GDR*), in Greece (*A. A. Flocas et al., Greece*), of temperature and precipitation in Bulgaria (*D. Toplijskij, Bulgaria*). Papers concerning Asia included the study of the relation of the climate and the yield of rice for the last 100 years (*M. Yoshino* and *K. Koga, Japan*) and the reconstruction of the period of precipitation of early summer in east Asia in the historical period (*M. Yoshino, Japan*). A variety of further papers dealt with the fluctuation of meteorological elements at one or several stations and/or in a certain region. Further papers discussed the effects of urbanization on the climate of Bucharest, the abnormally cold winter of 1986/87 in the European part of the USSR, the occurrence of floods in the Vltava river in relation to meteorological observations in Prague, and present-day changes of the topoclimate.

The conference was concluded by the final word of the chairman of the climatological commission of IGU, *Prof. Yoshino*, who stressed the fact that it was a useful exchange of information from the sphere of climatological changes between western and eastern countries in which a number of regionally different approaches and results were presented. He pointed out the necessity of continuing further studies oriented at the methods of analysis of climatic changes, creating corresponding data sets, the study of impacts of human activity on the climatic system, particularly in agriculture, forestry and land-use, and recommended continuing similar conferences of this type.

For the participants in the conference a one-day excursion was organized into the area of the Moravian Karst and the territory of the Battle of Austerlitz.

The seventy-two contributions have been included into the Proceedings of the Conference (Climatic Change in the Historical and the Instrumental Periods, edited by R. Brázdil, Brno, 1990). In this issue of the Journal of Scripta Fac. Sci. Nat. Univ. Purk. Brun., Vol. 20, Geographia 1—2, Brno, 1990, are further published graphical supplements to the above contributions.

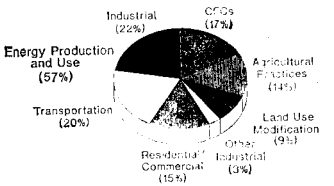

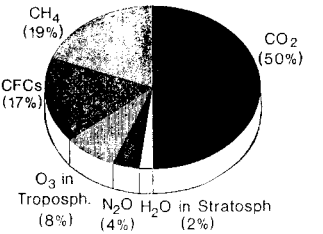

Fig. 1. Contribution of activities to global warming in the 1980's. Data Source: *Lashof* and *Tirpak* (1989)

Fig. 2. Contribution of greenhouse gases to global warming in the 1980's. Data Source: *Enquete–Kommission* (1988)

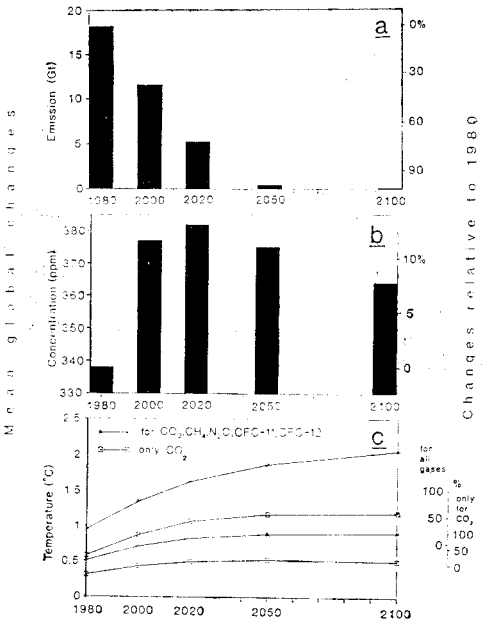

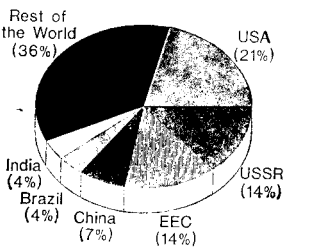

Fig. 3. Contribution of regions to global warming in the 1980's. Data Source: *Lashof* and *Tirpak* (1989)

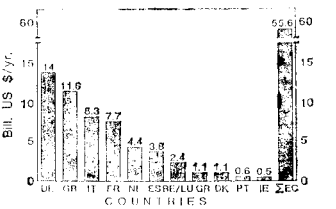

Fig. 4. Required CO_2–emission reduction to limit global mean surface warming to 1–2 °C in 2100 (a), resulting CO_2–concentration change (b), and temperature change due to CO_2 plus the other indicated trace gases (c)

Fig. 5. Share of EC–countries in CO_2-fund at c 0.5 per kWh of fossil fuel use

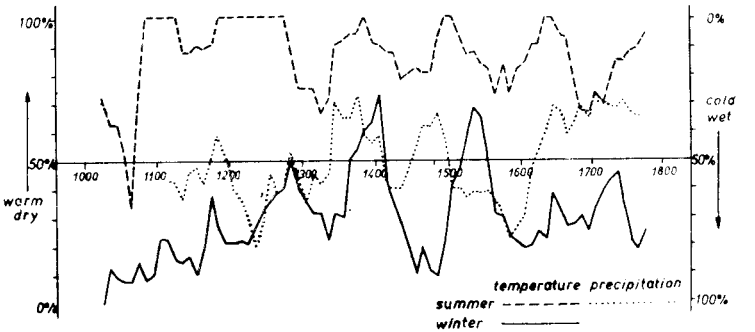

Fig. 1. Percentage of reports on warm/cool, dry/wet summer and mild/severe winter seasons in relation to the total number of significant weather event reports for the seasons under consideration. 50-year running means, calculated by *Bernhardt* and *Mäder* (1987) from the catalogue compiled by *Hennig* (1904)

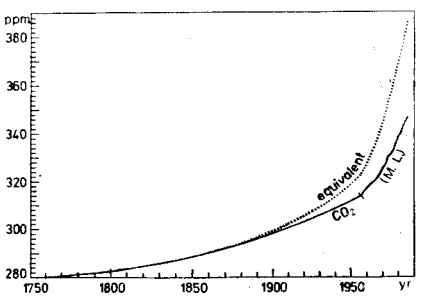

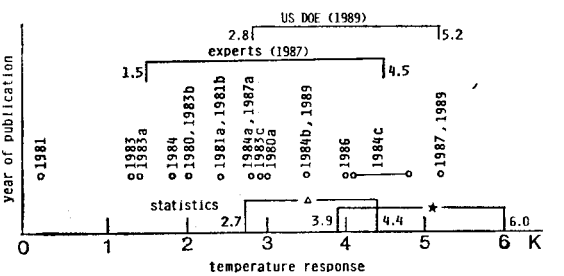

Fig. 1. Measured (Mauna Loa, Hawaii, M.L., since 1958) and reconstructed annual mean atmospheric CO_2 concentration (data from *Keeling*, 1985, 1987; *Neftel et al.*, 1985), in addition „equivalent" CO_2 increase, dotted line (data from *Tricot* and *Berger*, 1987)

Fig. 2. Annual and global mean temperature increase (near surface) in case of an atmospheric CO_2 doubling as projected by GCM experiments including a mixed layer ocean, publications (years indicated) since 1890, expert statements (WMO), outcome of a recent US DOE Workshop (*Schlesinger, ed.*, 1989) and statistical assessments (this contribution) with (*) and without (Δ) phase shift of the temperature response in relation to trace gas forcing

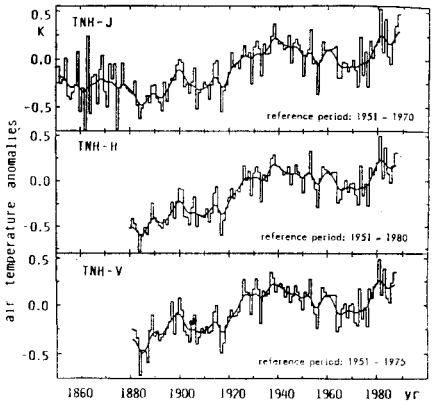

Fig. 3. Comparison of mean northern hemisphere air temperature fluctuations, annual means and 10 yr low-pass filtered 1851/1880–1987/1988, as reconstructed by *Jones et al.* (1982, 1989), *J*, *Hansen* and *Lebedeff* (1987, 1988), *H*, and *Vinnikov et al.* (1989), *V*

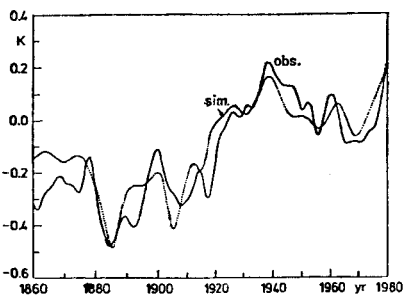

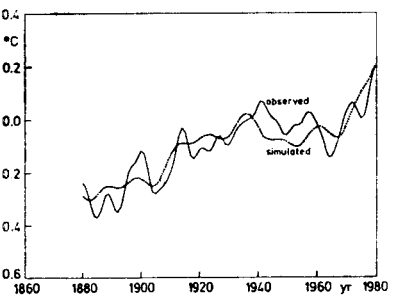

Fig. 4. Observed mean northern hemisphere air temperature fluctuations, data from *Jones et al.* (1982, 1988), 10 yr low-pass filtered, solid line, and reproduction by means of the statistical multivariate regression model described in the text, best fit (multiple correlation coefficient $r_m = 0.90$, unfiltered data implying ENSO $r_m = 0.76$) using the volcanic SVI*, the solar TSD and the „equivalent" trace gas (CO_2E) forcing, phase shift 20 yr

Fig. 5. Similar to ***Fig. 4.***, but southern hemisphere data from ***Hansen*** and ***Lebedeff*** (1987), solid line, best fit without phase shift ($r_m = 0.90$, unfiltered data implying ENSO $r_m = 0.68$)

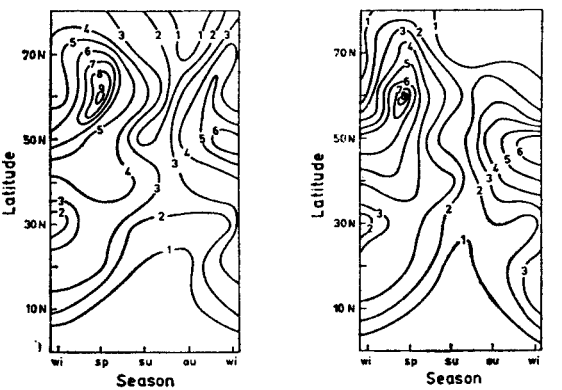

Fig. 6. Contour lines of temperature increase (K) in case of a CO_2 doubling, zonal mean seasonal statistical assessments, average of all combinations, left side without and right side including ENSO forcing, data base *Jones et al.* (*US CDIAC*, 1988)

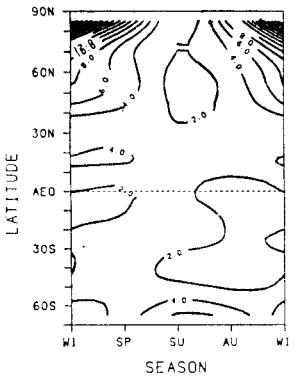

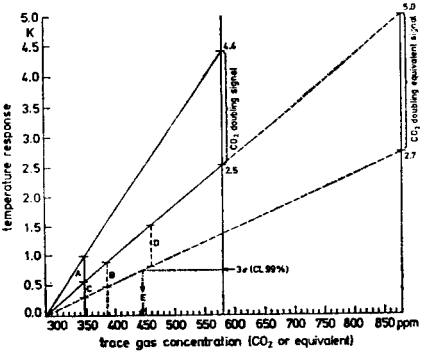

Fig. 7. Similar to *Fig. 6*, but global and data base *Hansen* and *Lebedeff* (1988)

Fig. 8. Global and annual mean temperature response in case of a CO_2 doubling, assessments TGL–J from *Table 1*, where A = ,,industrial" CO_2 signal, C = similar but reduced, B = ,,equivalent industrial" signal (all equilibrium assessments), and D = ,,equivalent industrial" signal implying a phase shift of 20 yr. The three times standard deviation of the observational data may be exceeded, using the lower ,,equivalent" assessment, if the ,,equivalent" concentration exceeds approximately 445 ppm (E). According to *Tricot* and *Berger* (1987) this may occur sometime between the years 2000 and 2005 (from *Schönwiese*, 1989)

ARSKY, A., MOKHOV, I., PETUKHOV, V. K.: STUDY OF VARIABILITY CHARACTERISTICS EVOLUTION OF THE EARTH'S CLIMATE SYSTEM IN THE ENERGY-BALANCE MODEL

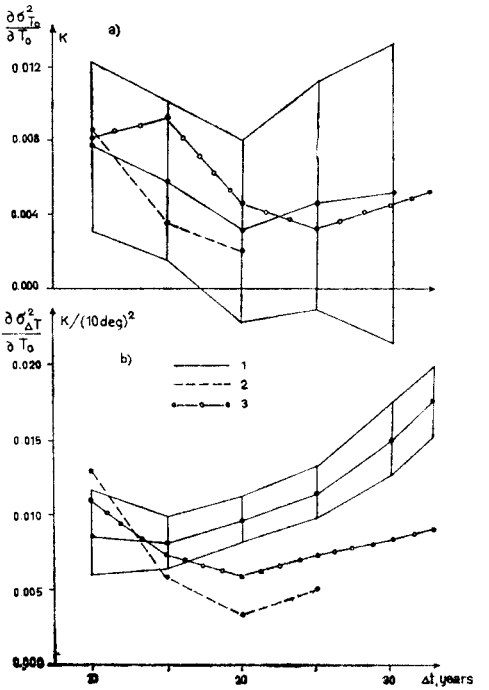

Fig. 1. The regression coefficients $\frac{\delta\sigma T_0}{\delta T_0}$ (a) and $\frac{\delta\sigma_{\Delta T}}{\delta T_0}$ (b) as functions of time moving average Δt: 1 – initial data set (vertical bars – root-mean square deviations), 2 – initial data set but with omitted moving averages, 3 – initial data set but with omitted linear trends at the intervals Δt

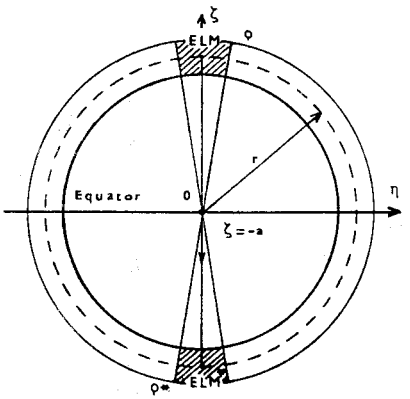

Fig. 1. Auxiliary picture to the gravitational principle of compensation of non-equilibrium states (NES)

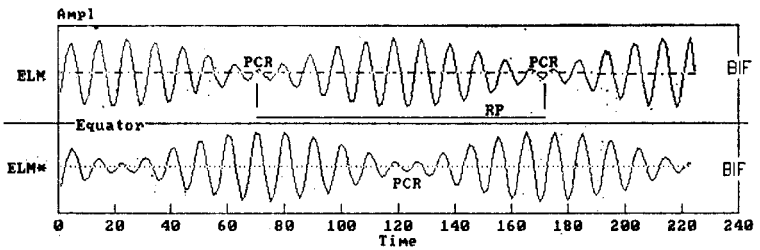

Fig. 2. Graphic representation of the solution of Eq. (12). The elementary compensation process with frequencies w and w^* (PCR – point of circulation reverse, RP – repete period)

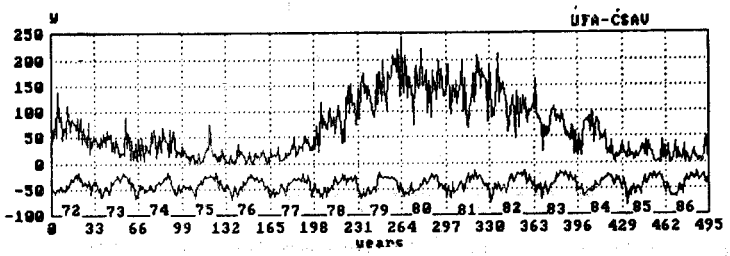

Fig. 3. Solar and circulation activity in the time interval 1/1 1972 – 31/12 1986 (eleven-year average of Wolf's numbers and AT 500 hPa – 600 hPa)

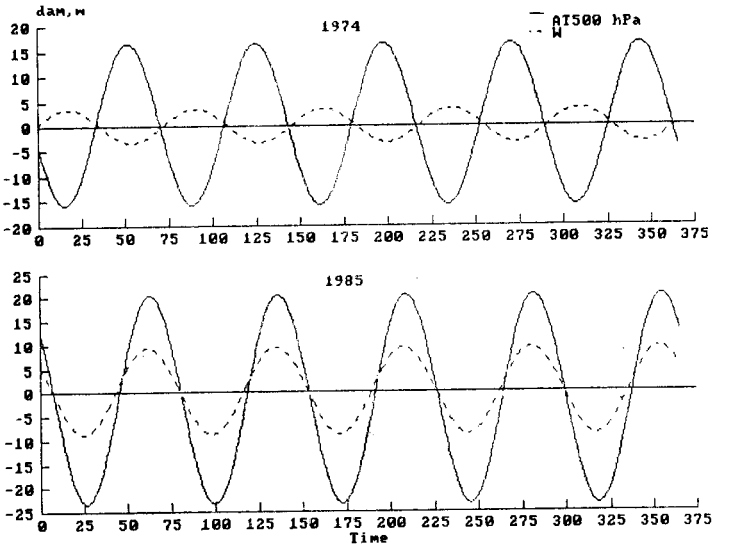

Fig. 4. Circulation and solar activity for $T = 72.989$ days in the years 1974 and 1985 for Prague

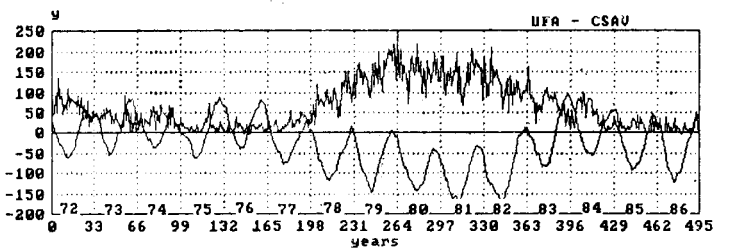

Fig. 5. March of solar activity and global residual non−equilibrium states (GRNES) for the time interval 1/1 1972 − 31/12 1986 (eleven-day averages)

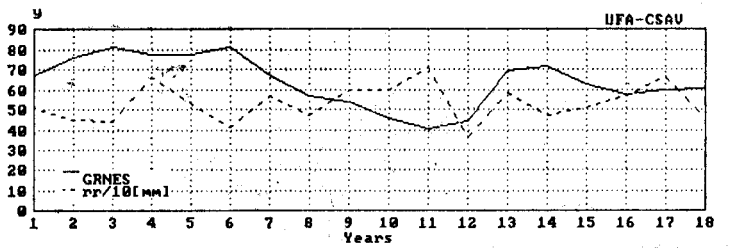

Fig. 6. Marches of annual GRNES and of precipitation for the time interval 1971−1988

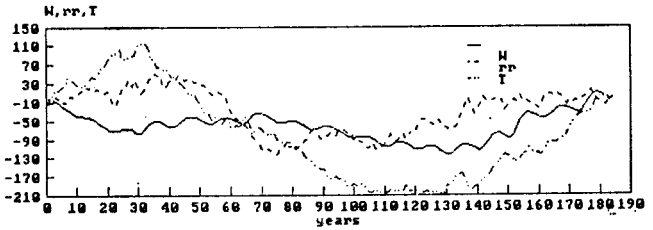

Fig. 7. Integral curve of solar activity (*W*), precipitation (*rr*) and temperature (*T*) for Prague in 1805–1989

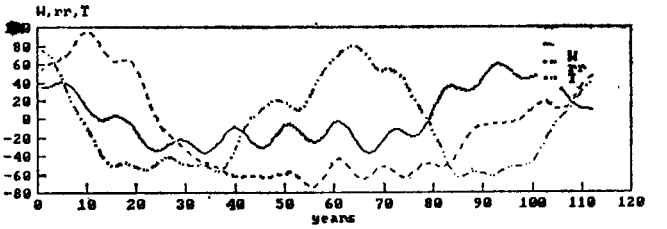

Fig. 8. Forecasts of integral curves of solar activity (*W*), precipitation (*rr*) and temperature (*T*) for Prague. Time interval 1990–2100

NKEMDIRIM, L. C.: MODELING THE POTENTIAL HYDROCLIMATIC CONSEQUENCE OF LARGE SCALE REMOVAL OF THE BOREAL FOREST: A PRELIMINARY REPORT

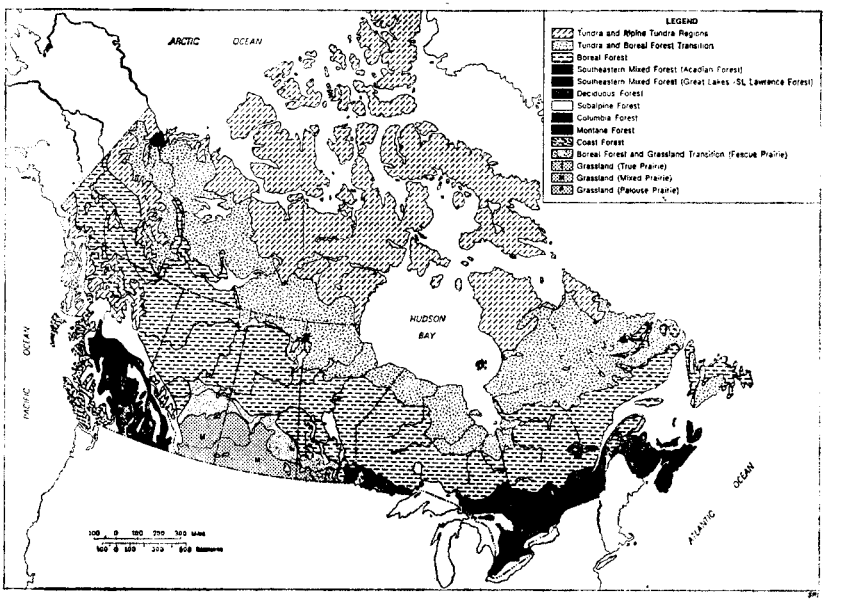

Fig. 1. The Boreal forest in Canada

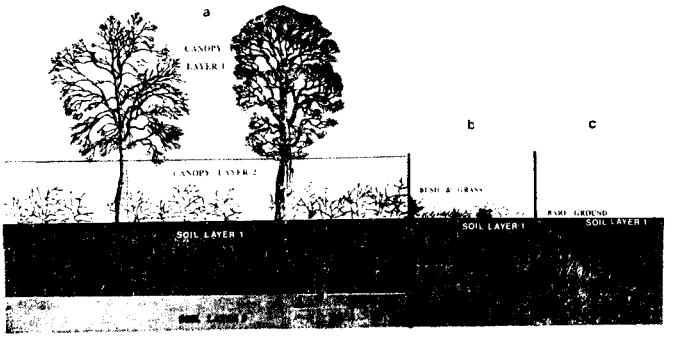

Fig. 2. Schematic representation of domains within which energy and moisture are exchanged in (a) forest stand, (b) bush-grass complex, (c) bare ground. Note the reduction in the size of the soil moisture reservoir from (a) to (c). Erosion and leaching are the major factors behind the change

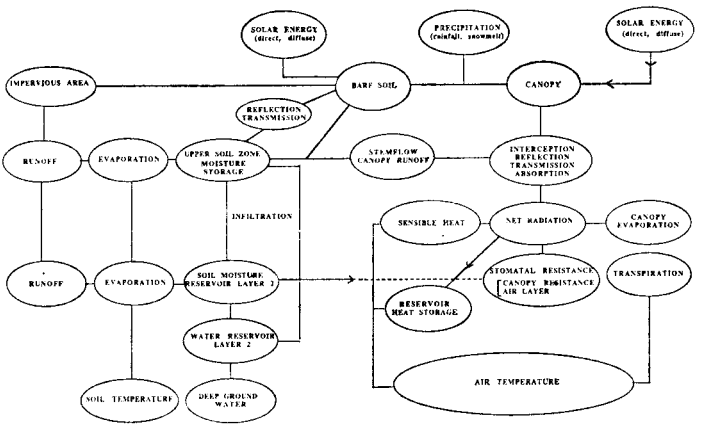

Fig. 3. Schematic representation of the path followed by moisture and energy. Equations specifying connectivity are given in *Sellers et al.* (1986), *Hansen et al.* (1983) and the HEC model (*US Corps of Eng.*, 1973)

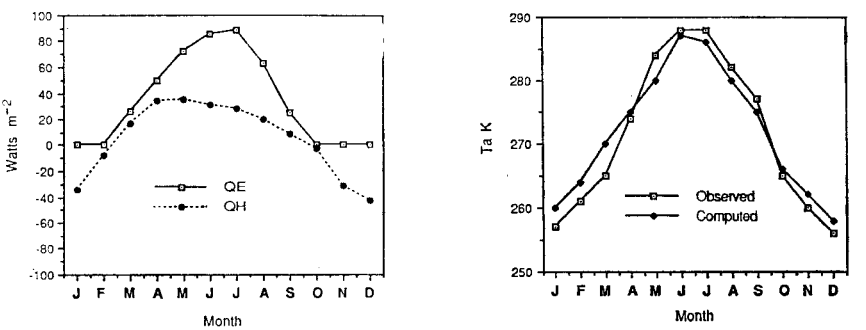

Fig. 4. **Partitioning of energy terms in a full forest stand**

Fig. 5. **Simulated vs observed air temperature. The observed values are the mean for Bevearlodge**

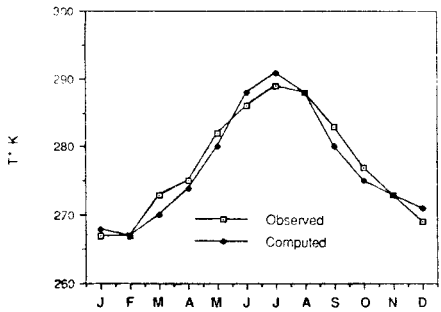

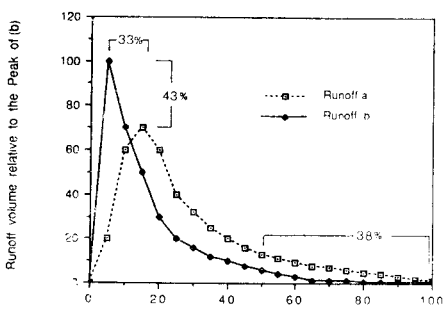

Fig. 6. Simulated vs measured ground surface temperature

Fig. 7. Unit volume hydrograph showing the distribution of runoff if the water surplus generated from the model is accumulated and discharge. The base of the hydrograph is given in per cent to indicate how the water might be distributed if it were released all at once. (a) and (b) represent treatments I and II respectively. The numbers shown indicate percentage change from treatment I to treatment II. For example (+33) indicates that the peak of the hydrograph (b) is 33 % higher than that of (a)

KLESHCHENKO, L. K., RADIUHIN, V. T.: STATISTICAL ANALYSIS OF NORTHERN HEMISPHERE AIR TEMPERATURES WITH A VIEW TO SPACE-TIME LOCALIZATION OF LONG-TERM CHANGES OF SURFACE CLIMATE

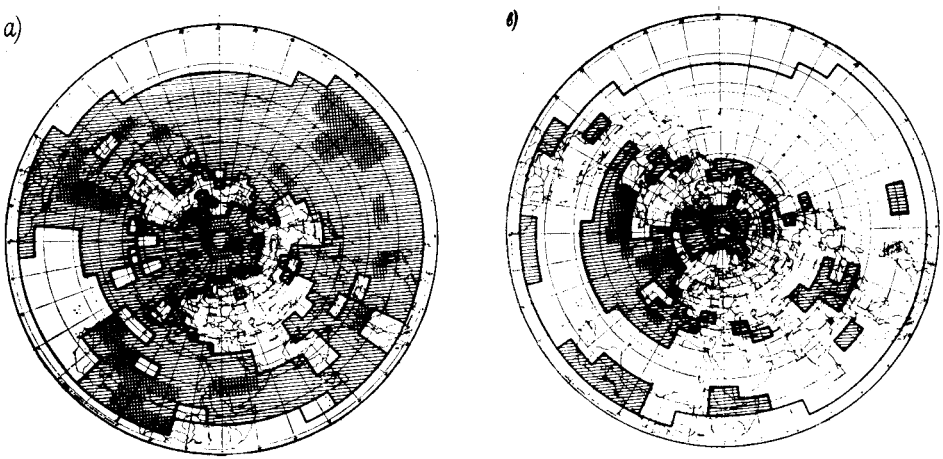

Fig. 1. Northern Hemisphere areas where warming and cooling periods are found with a s/n ratio $\geqq 1.0$ for mean annual data – warming (a), cooling (b)

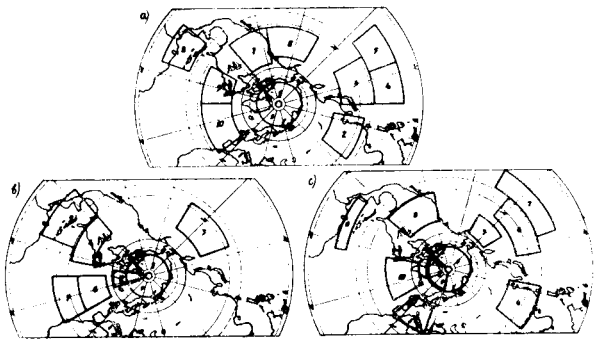

Fig. 2. Northern Hemisphere areas for which mean regional air temperatures were calculated from mean annual (a) and mean seasonal (winter – b, summer – c) data

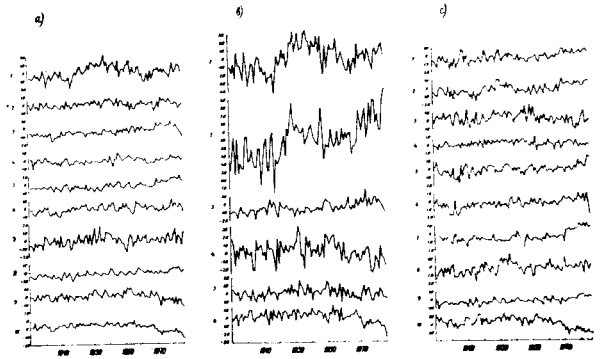

Fig. 3. Long-term regional air temperature changes: mean annual (a) and mean seasonal (winter – b, summer – c) data. The numbers of diagrams correspond to area numbers in *Fig. 2*

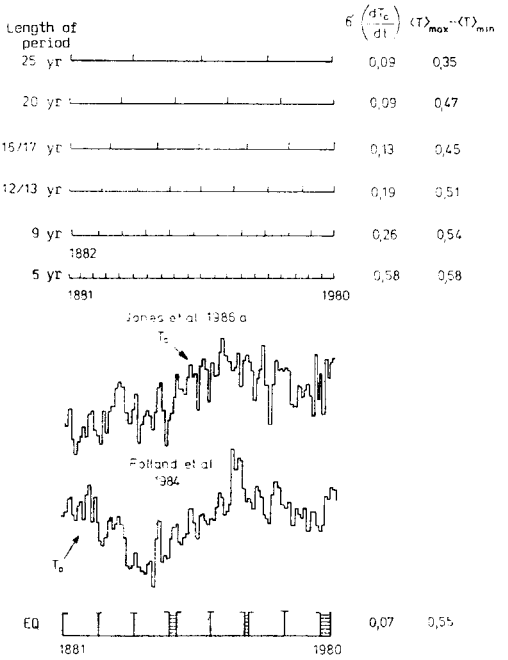

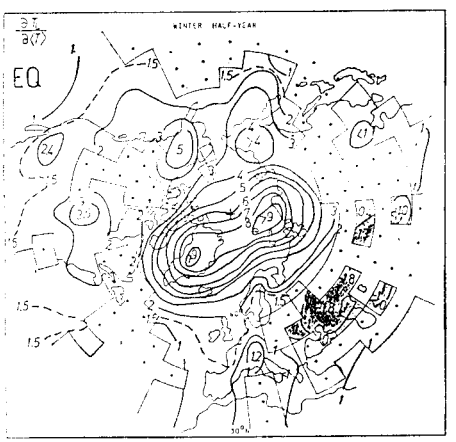

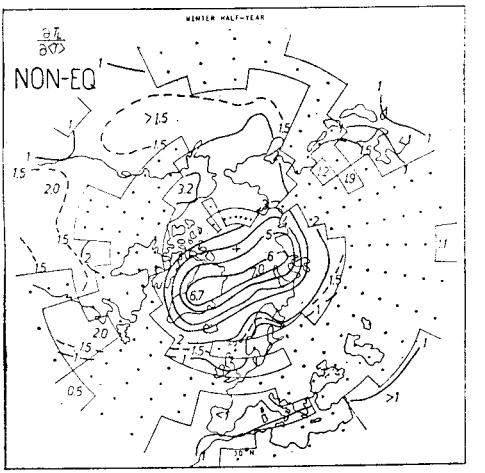

Fig. 1. Time series of average temperatures over the continents (Tc) and oceans (T_o) and the different non-equilibrium and equilibrium (EQ) periods. The first column at the right side represents the standard deviation of linear trends within each period and the second one contains the difference between the highest and lowest hemispherical mean temperatures for given division

Fig. 2. Coefficients of regression for the equilibrium division. No significant coefficients even at the 80 % level are received in the indicated gridpoints

Fig. 3. The same as *Fig.* 2,but for the 5 non-equilibrium divisions in average. In the indicated gridpoints significant coefficients are received in less than 3 divisions

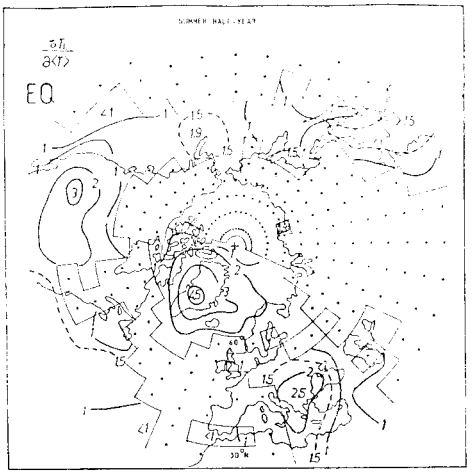

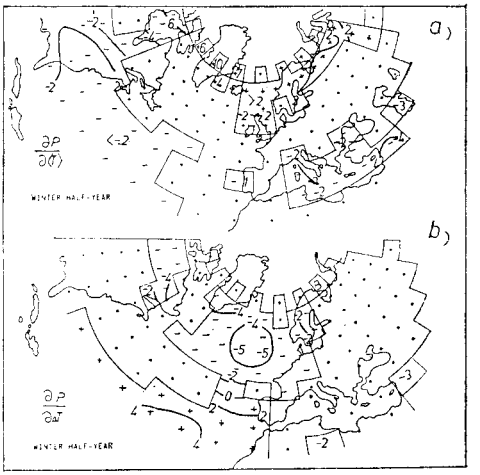

Fig. 4. The same as *Fig. 2*, but for the summer half-year

Fig. 5. The relative sensitivity of sea-level pressure for the with half-year comparing to the hemispherical mean (a) and continent-ocean contrast (b)

BARTHOLY, J.: A DATA SET OF HEMISPHERICAL SNOW COVER FIELDS (1966–1983) AND ITS POSSIBLE EFFECTS ON OTHER METEOROLOGICAL PARAMETERS ON THE GLOBAL AND REGIONAL SCALE

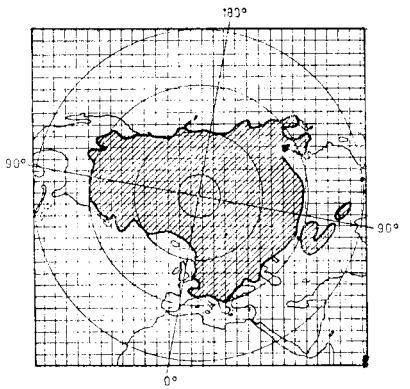

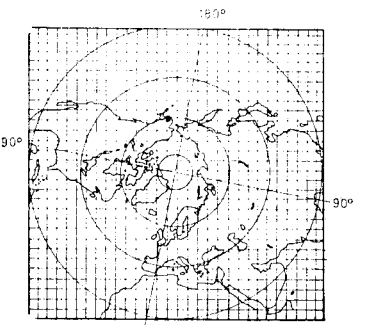

Fig. 1. The monthly hemispherical snow and ice cover map of January of 1967 (the whole area is covered by 89 × 89 grid point)

Fig. 2. The stereographical hemispherical map and the 30 × 30 grid netting which were used for cumulativ codification

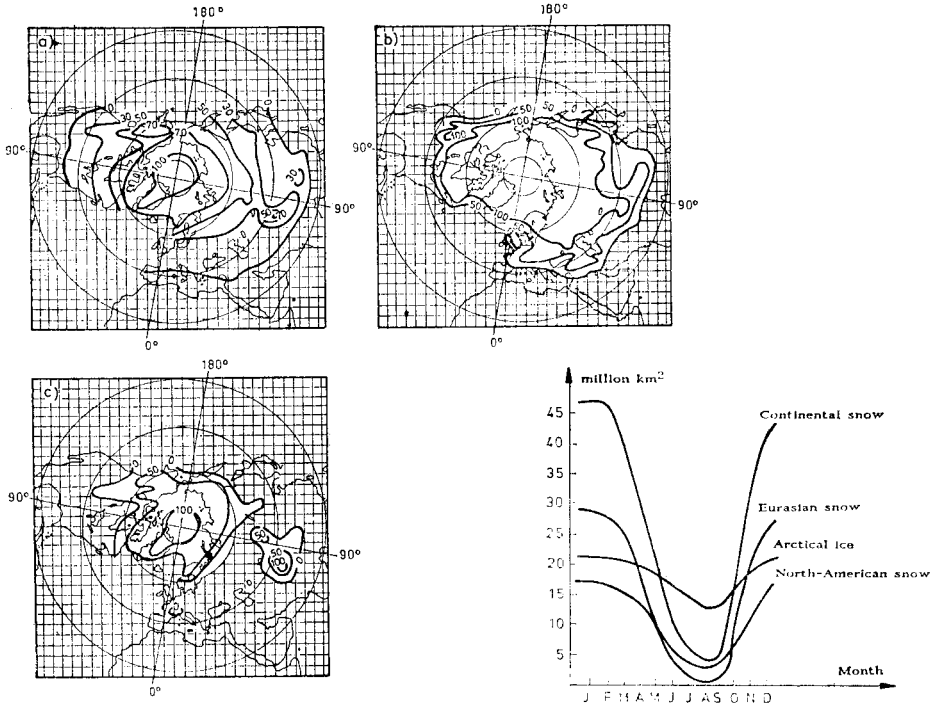

Fig. 3. Mean hemispherical snow and ice cover in percentage: a) yearly, b) in January, c) in July

Fig. 4. The extent of the continental snow and the Arctic ice in million km²

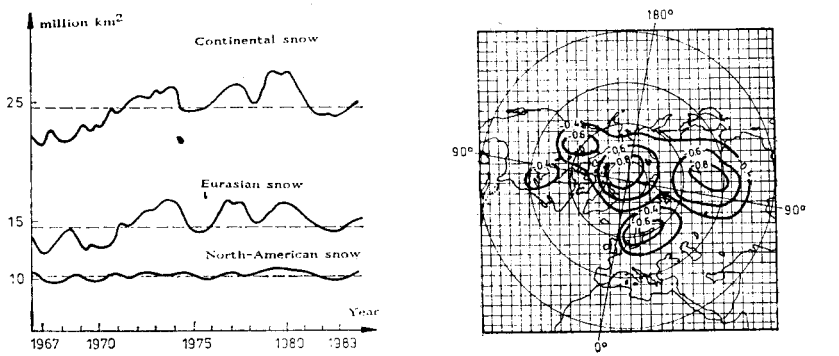

Fig. 5. Yearly changes of the continental snow extent in million km² (computed with the values of the 12-month running means)

Fig. 6. Teleconnection pattern for the winter season between the winter snow cover and the hemispherical temperature anomaly fields

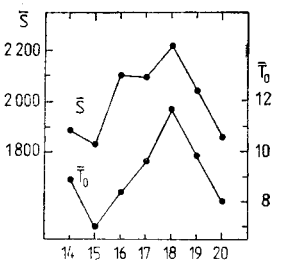

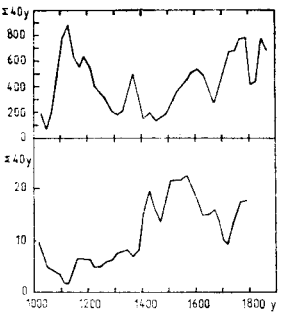

Fig. 1. The top curve $\bar{S}$ represents the annual total number of hours of sunshine record at the Hurbanovo Observatory averaged over the years of the separate 11-year cycles of solar activity. The bottom curve $\bar{T}_0$ give the average lifetime of sunspot groups (in days) in the separate 11-year cycles

Fig. 2. The top curve shows the frequency of aurore borealis at geographic latitudes < 55°. The bottom curve depicts the frequency of floods on the Elbe River and its tributaries

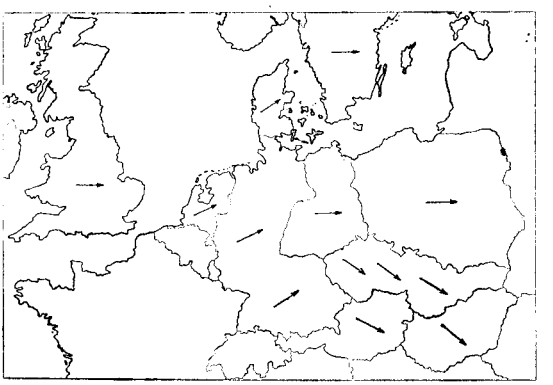

Fig. 3. The basic time trends of atmospheric precipitation changes during the last approximately 100 years are given by the arrows on the map of Europe

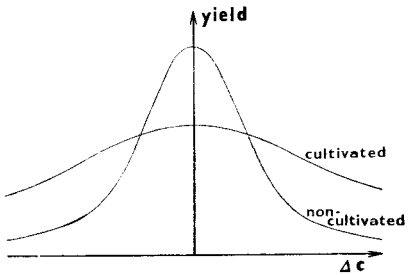

Fig. 1. Idealized relationship between the yield of cultivated (full line) and non-cultivated (dashed line) plants and the departure from climatology

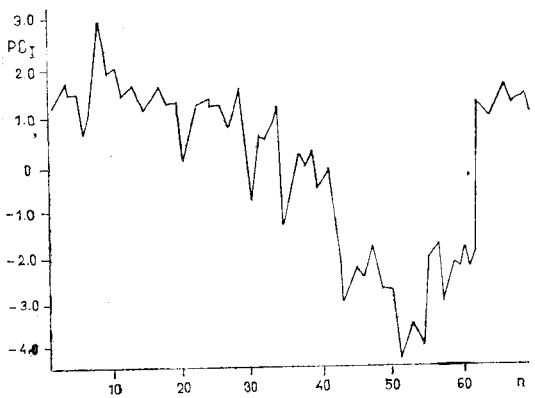

Fig. 1. Change of the first principal component (*PCI*) in space (in point $-n$ of the selection of surface samples)

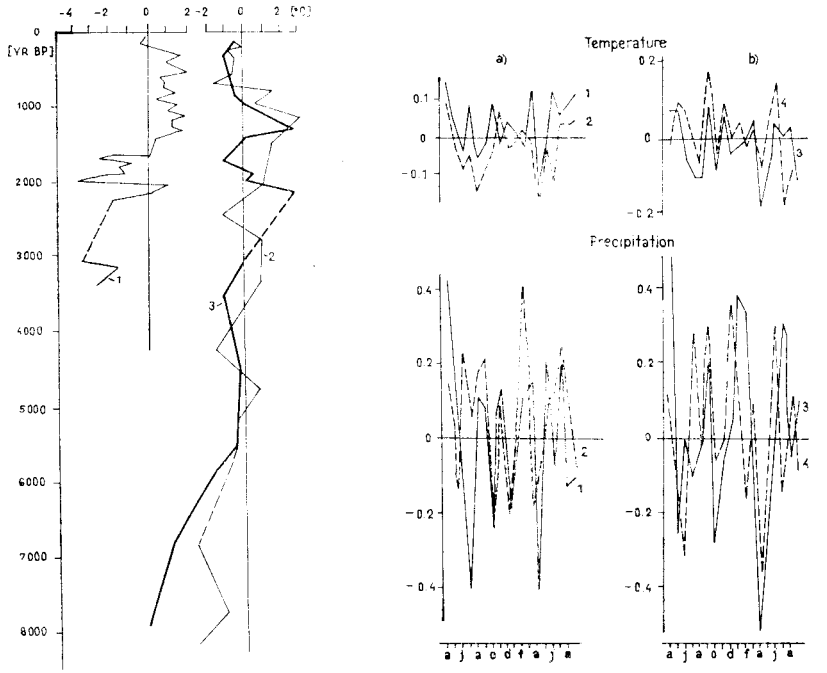

Fig. 2. Reconstructed mean monthly temperature of July: 1 — Carpathian foothills; 2, 3 — Ukrainian Polesye. Vertical lines show contemporary temperature values, dashed lines show parts of the curve with insufficient data

Fig. 3. Response function of the growth of early pine trees in normal conditions (a) and in a high bog (b). Tree groups 1—4

CHERNAVSKAYA, M. M.: MOISTENING CHANGES ON THE RUSSIAN PLAIN DURING THE HISTORICAL PERIOD

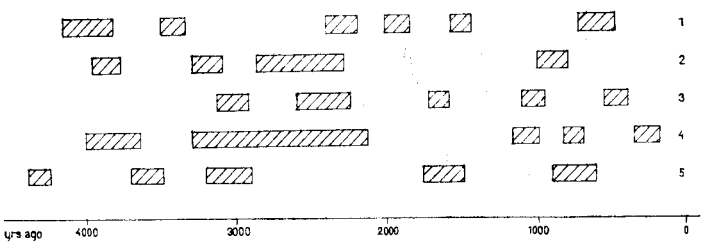

Fig. 1. Dry periods in the forest belt of the Russian Plain and Czech—Moravian Highlands identified from the data of stratigraphic columns of high bogs: 1 — Leningrad region, Shirinskiyr Mkhi bog; 2 — Pskov region, Polistovskoye bog; 3 — Moscow region, Baksheyevskoye bog; 4 — Lithuania, Zhivintas bog; 5 — Czechoslovakia, Velké Dářko bog

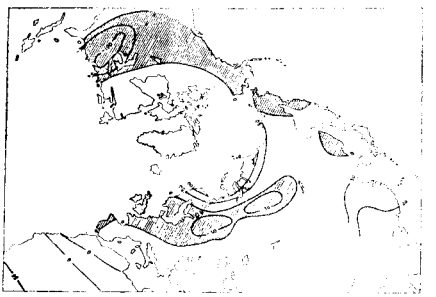

Fig. 2. Deviations of the river runoff of the northern hemisphere in the Holocene climatic optimum from the present-day values (ΔR, mm)

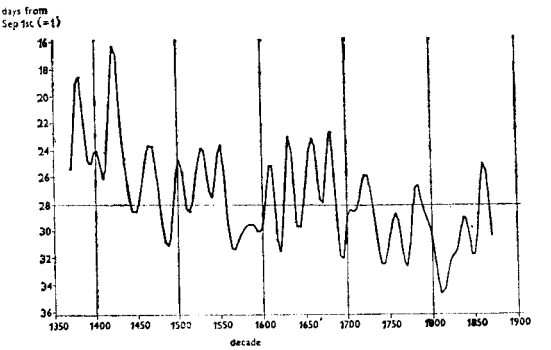

Fig. 1. Mean date of grape harvest in Western Europe (1370—1880) — decennial averages. The years give the beginning of the decade (e.g. 1500 = 1501—1510). Source: 1370 to 1500 — Series Mont d'Or, 1500 to 1880 — area-averaged series W Europe (*Le Roy Ladurie* and *Baulant*, 1980)

MUNZAR, J., PEJML, K.: THE ANALYSIS OF THE INPUT DATA FOR A STUDY OF CLIMATIC FLUCTUATIONS

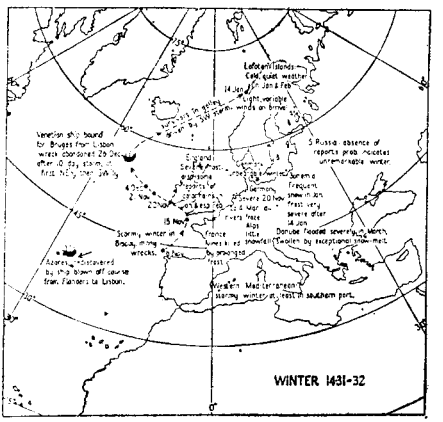

Fig. 1. Reconstruction of weather in Europe in winter 1431/32 after *Lamb* (1980). Extreme weather in the period 1431—1434 contributed to economic calamity in Bohemia towards the end of the Hussite revolutionary era

YOSHINO, M.: RECONSTRUCTION OF RAINY SEASON IN EARLY SUMMER OVER EAST ASIA DURING THE HISTORICAL PERIOD

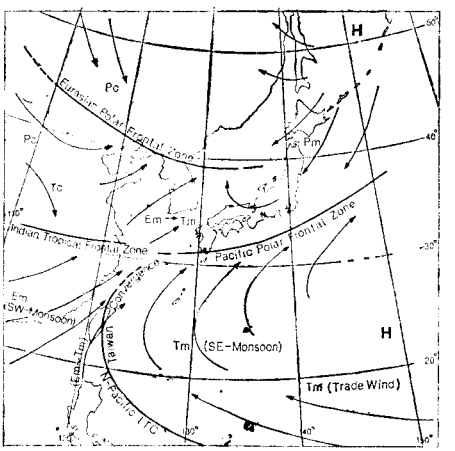

Fig. 1. Schematic illustration of fronts air masses, and air streams in the Bai-u season

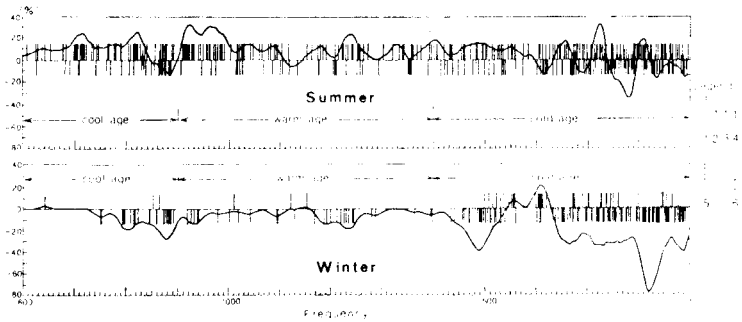

Fig. 2. Weather type of each year and change of its frequency from 601 to 1900 (*Maejima* and *Tagami*, 1986). Legend: Vertical line shows appearance of following type: (1) hot summer, (2) west cool – north hot summer, (3) north cool – west hot summer, (4) cool summer, (5) mild winter, (6) cold winter. Curved line shows change of weather type frequency (weighted running mean for 51 years). They are obtained by following coefficients: type (1) and (2) are +1, type (3) and (4) are −1 in summer while type (5) is +1. type (6) is −1 in winter

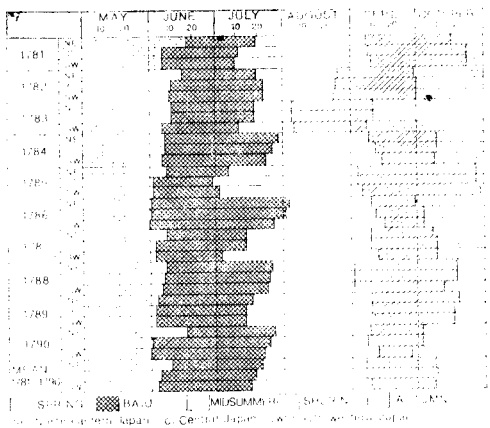

Fig. 3. Classification of natural seasons for the warmer half years for 1781–1790 (*Mikami*, 1988)

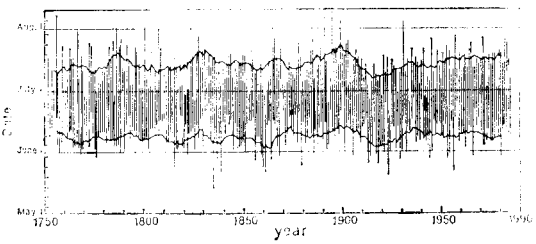

Fig. 4. The secular change of Bai-u season in Kinki District for 1751–1985 (*Mizukoshi*, 1986). Dotted line (lower): date of the onset smoothed by 10 year running mean. Dotted line (upper): date of the end smoothed by 10 year running mean

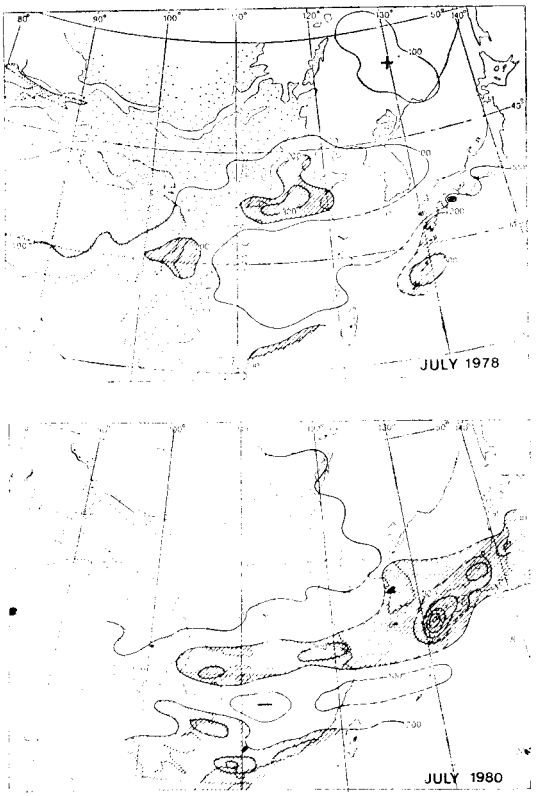

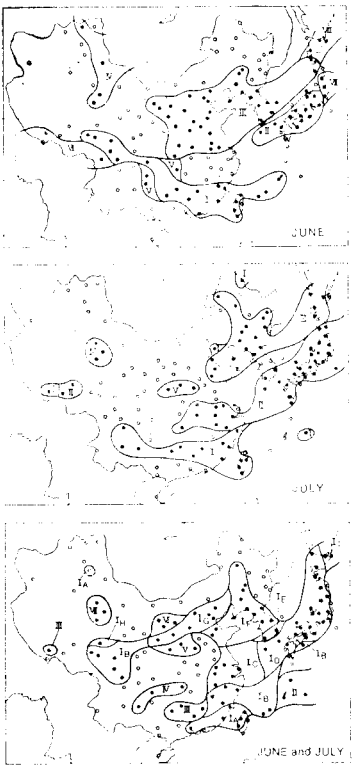

Fig. 5. (a) Distribution of monthly rainfall in July, 1978, an anomalous year and (b) in July, 1980, a normal year (*Mikami*, 1987)

Fig. 6. Regional division of East Asia by interannual variation of rainfall in June, July and June + July, 1956–1980 (*Yoshino* and *Aoki*, 1986)

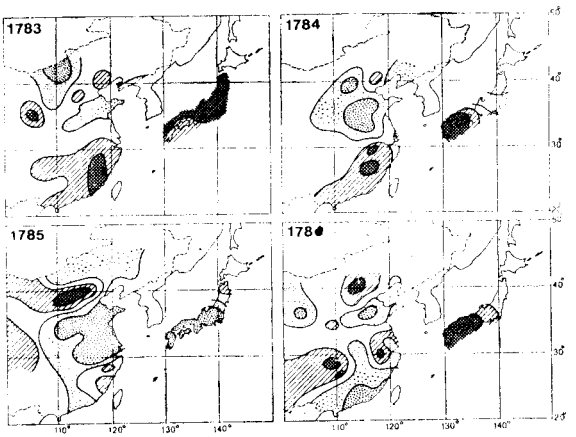

Fig. 7. Composite maps of dryness and wetness over East Asia. Dense hatching, hatching, no marking, stippling, and dense steeppling indicate very wet, wet, normal, dry and very dry areas respectively (*Mikami*, 1987)

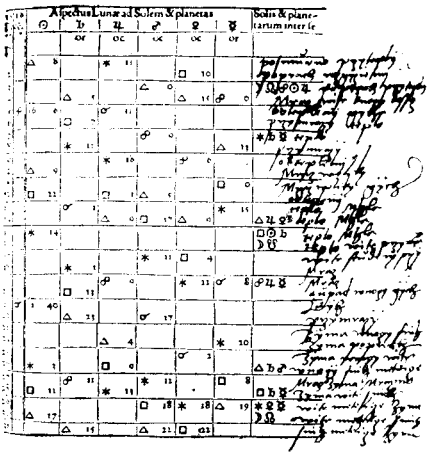

Fig. 1. Czech records in Stoefler's Ephemerides, referring to December, 1538, are the oldest systematic weather observations in Moravia

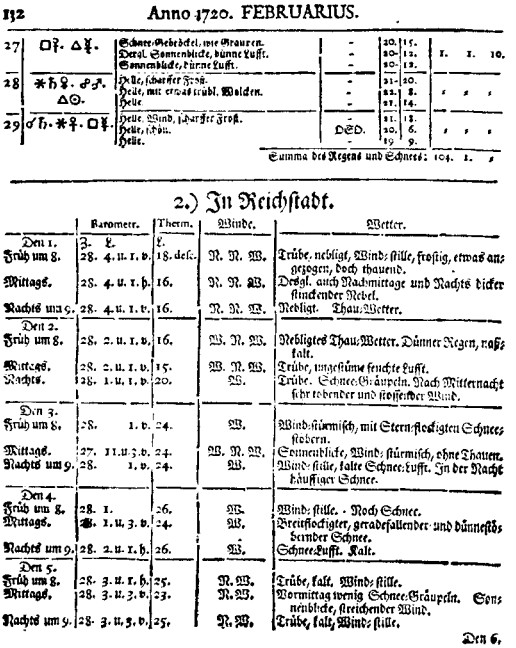

132 Anno 1720. FEBRUARIUS.

27 ☐☽. △☿. Schnee-Gebrödel, wie Grauren. - 20. 15.
Dergl. Sonnenblicke, dünne Lufft. - 20- 12. I. I. 10.
Sonnenblicke, dürne Lufft. - 20- 13.

28 ✱♄☿. ☌☾. Kälte, scharffer Frost. - 21- 20.
△☉. Heüe, mit etwas trübl. Wolcken. - 22. 8. ' ' '
Heüe - 22. 14.

29 ☌♄. ✱☿. ☐☿. Heüe. Wind, scharffer Frost. - 21. 13.
Heüe, schön. DSD. 20. 6. ' ' '
Heüe. - 19 9.

Summa des Regens und Schnees: 104. I. '

2.) In Reichstadt.

	Barometer.	Therm.	Winde.	Wetter.
Den 1.	☽ ☿	☿		
Früh um 8.	28. 4. u. 1. v.	18. def.	N. N. W.	Trübe, neblicht, Winds stille, frostig, etwas angezogen, doch thauend.
Mittags.	28. 4. u. 1. h.	16.	N. N. W.	Desgl. auch Nachmittage und Nachts dicker stinckender Nebel.
Nachts um 9.	28. 4. u. 1. v.	16.	N. N. W.	Neblicht. Thau-Wetter.
Den 2.				
Früh um 8.	28. 2. u. 1. v.	16.	W. N. W.	Nebligtes Thau-Wetter. Dünner Regen, naß kalt.
Mittags.	28. 2. u. 1. v.	15.	W. N. W.	Trübe, ungestüme feuchte Lufft.
Nachts.	28. 1. u. 1. v.	20.	W.	Trübe. Schnee-Gräupeln. Nach Mitternacht sehr tobender und stossender Wind.
Den 3.				
Früh um 8.	28. 1. v.	24.	W.	Winds-stürmisch, mit Stern-flockigten Schnee-flöcken.
Mittags.	27. 11. u. 3. v.	24.	W. N. W.	Sonnenblicke, Winds-stürmisch, ohne Thauen.
Nachts um 9.	28. 1. v.	24.	W.	Winds-stille, kalte Schnee-Lufft. In der Nacht häuffiger Schnee.
Den 4.				
Früh um 8.	28. 1.	26.	W.	Winds-stille. · Noch Schnee.
Mittags.	W. 1. u. 3. v.	24.	W.	Breitflockigter, geradefallender und dünnestöbender Schnee.
Nachts um 9.	28. 2. u. 1. h.	26.	W.	Schnee-Lufft. Kalt.
Den 5.				
Früh um 8.	28. 3. u. 1. h.	25.	N. W.	Trübe, kalt, Winds stille.
Mittags.	28. 3. u. 3. v.	23.	N. W.	Vormittag wenig Schnee-Gräupeln. Sonneblicke, streichender Wind.
Nachts um 9.	28. 3. u. 3. v.	25.	N. W.	Trübe, kalt, Winds stille.

Den 6.

Fig. 2. Meteorological measurements from Zákupy (Reichstadt) are the oldest systematic instrumental observations in Bohemia

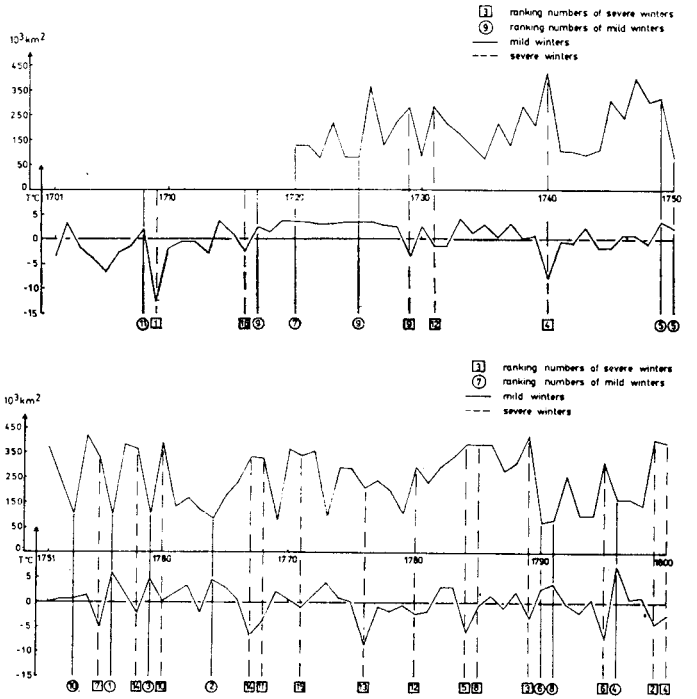

Fig. 1. Changes in area of Baltic Sea ice (after data of *Belin* and *Preobrazhenskij*, 1962) vs. deviations of mean temperature in January from the corresponding 100-year mean temperature in Wrocław during 18th century

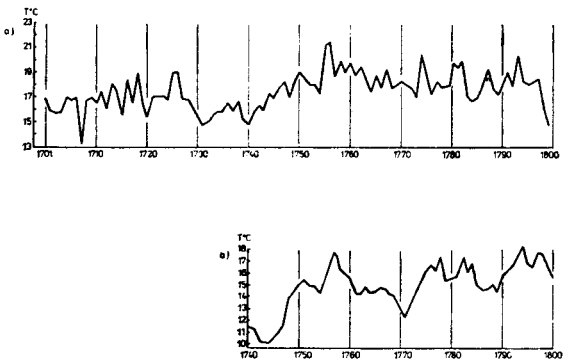

Fig. 2. Mean temperature for June and July $\left(\frac{T_{VI} + T_{VII}}{2}\right)$: a) in Wrocław during 18th century, b) in Zakopane from 1740 to 1800 (after *Bednarz*, 1984)

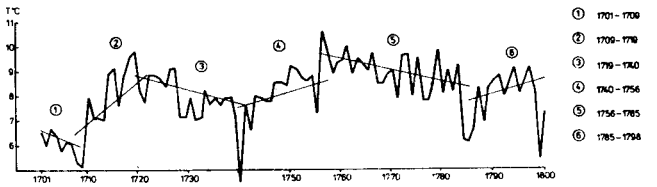

Fig. 3. Trends of annual mean temperature in Wroclaw during chosen several-year-long periods in 18th century

KYNCL, J., DOBRÝ, J., MUNZAR, J., SARAJISHVILI, K. G.: TREE-RING RESPONSE OF CONIFERS IN EUROPE TO WEATHER CONDITIONS IN 1912 (WITH REGARD TO THE VOLCANE KATMAI ERUPTION)

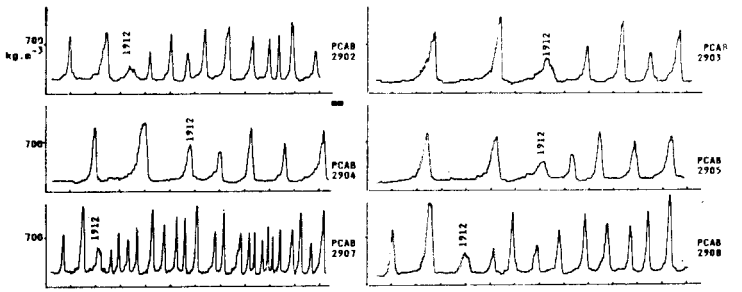

Fig. 1. Densitograms of Norway spruce, site No 29 (Jeseníky Mts.)

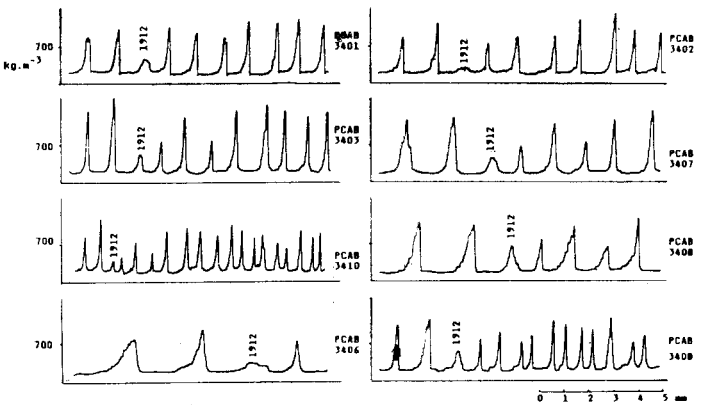

Fig. 2. Densitograms of Norway spruce, site No 34 (High Tatras)

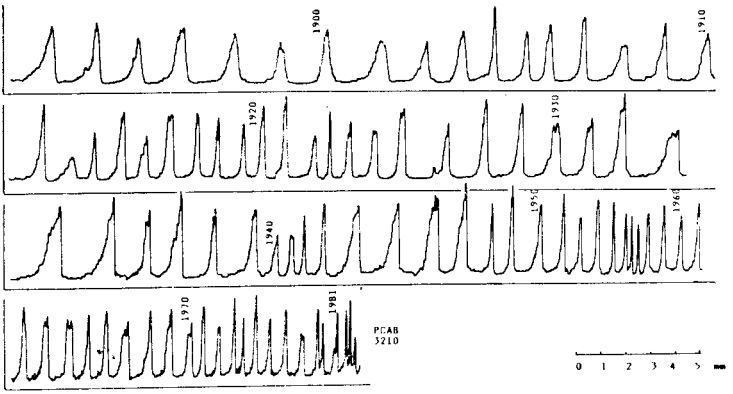

Fig. 3. Densitograms of Norway spruce for the period 1894–1984, site No 32 (Góry-Bystrzyckie Mts.)

SNEYERS, R., VANDIEPENBEECK, M., VANLIERDE, R., DEMAREÉ, G.: CLIMATIC CHANGES IN BELGIUM AS APPEARING FROM THE HOMOGENIZED SERIES OF OBSERVATIONS MADE IN BRUSSELS-UCCLE (1833–1988)

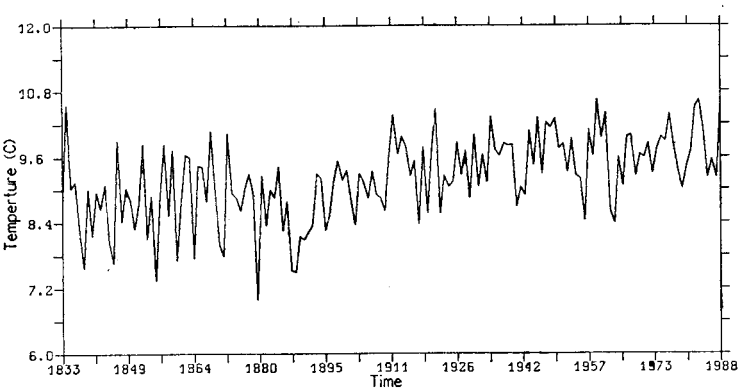

Fig. 1. Year. Average of the air temperature

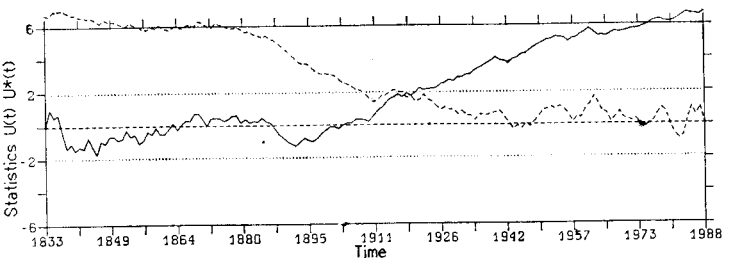

Fig. 2. Year. Average of the air temperature. Progressive trend test

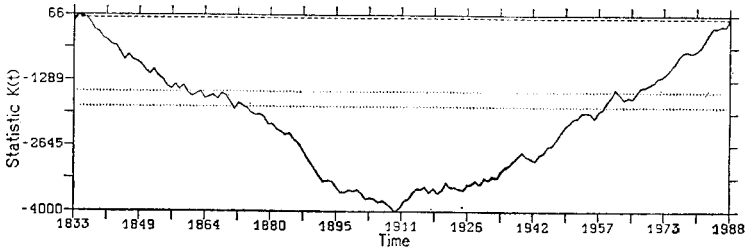

Fig. 3. Year. Average of the air temperature. Petitt's change-point test

OLBERG, M.: METHODS TO RESEARCH TIME DEPENDENT CHANGES IN THE SPECTRAL BEHAVIOUR OF CLIMATOLOGICAL DATA SERIES

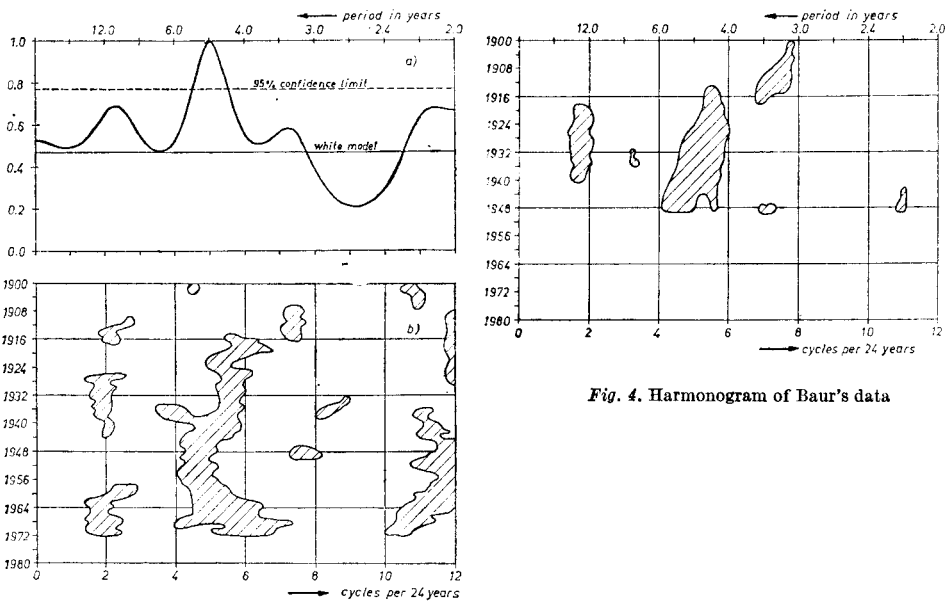

Fig. 4. Harmonogram of Baur's data

Fig. 3. MESA (a) and moving MESA (b) of the annual precipitation totals by *Baur* (1851 – 1985)

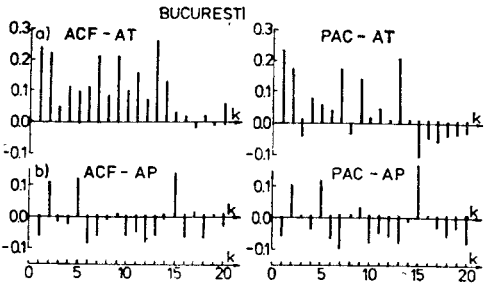

Fig. 1. a) Annual temperatures, b) annual precipitation amounts

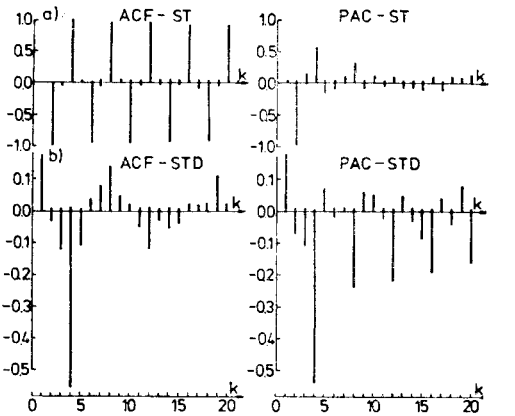

Fig. 2. a) Non-differenciated seasonal temperatures, b) seasonal-differenciated temperatures

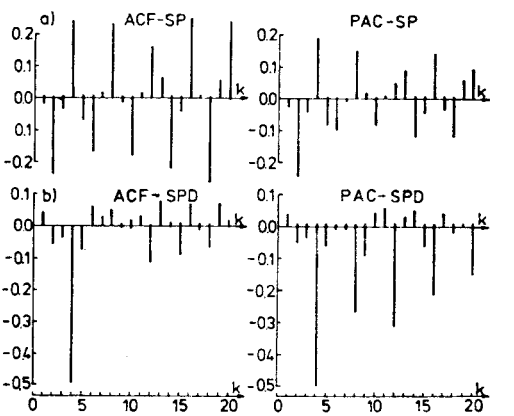

Fig. 3. Non-differenciated precipitation amounts, b) seasonal differenciated precipitation amounts

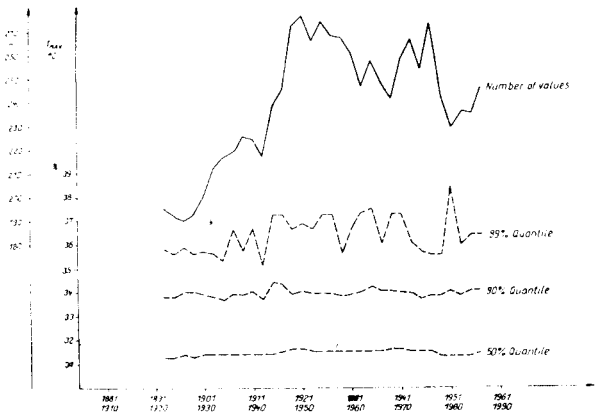

Fig. 1. Quantiles and number of values of the marginal distribution, daily maximum of the air temperature ≧ 30 °C, Potsdam 1893 – 1986 (30-year shifted intervals)

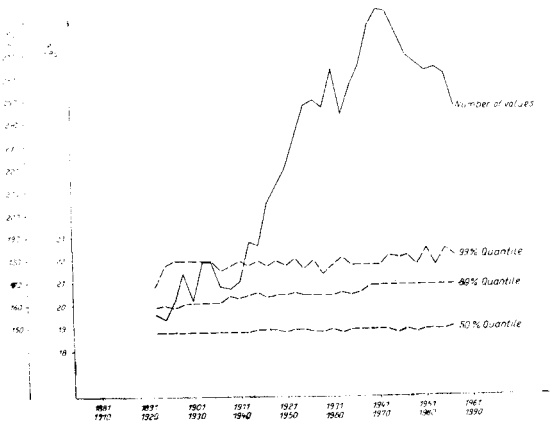

Fig. 2. Quantiles and number of values of the marginal distribution, daily mean value of the vapour pressure ≧ 18 hPa, Potsdam 1893 – 1986 (30-year shifted intervals)

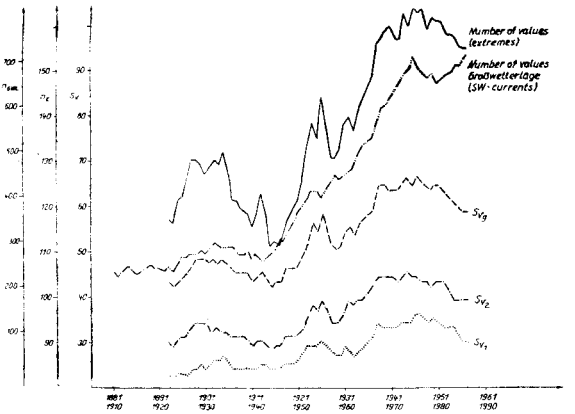

Fig. 3. Vector components and number of values of the extremes of the temperature-humidity complex, daily maximum of the air temperature ≧ 30 °C, daily mean value of the relative humidity ≧ 75 %, Potsdam 1893–1986, and number of values of the Großwetterlagen with south-westerly currents, 1881–1986 (30-year shifted intervals)

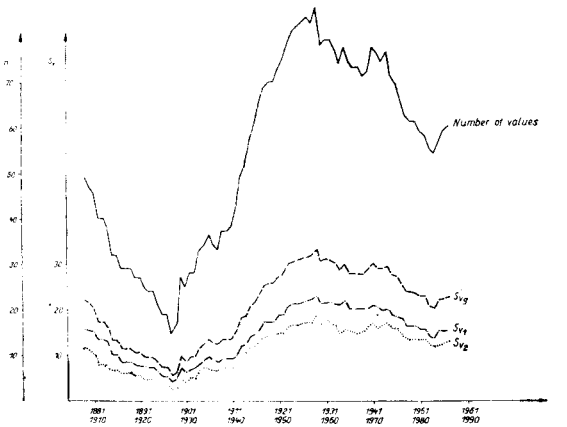

Fig. 4. Vector components and number of values of the extremes of the temperature-humidity complex, daily maximum of the air temperature ≧ 25 °C, daily mean of the vapour pressure ≧ 15 hPa, Hohenpeißenberg 1879–1986 (30-year shifted intervals)

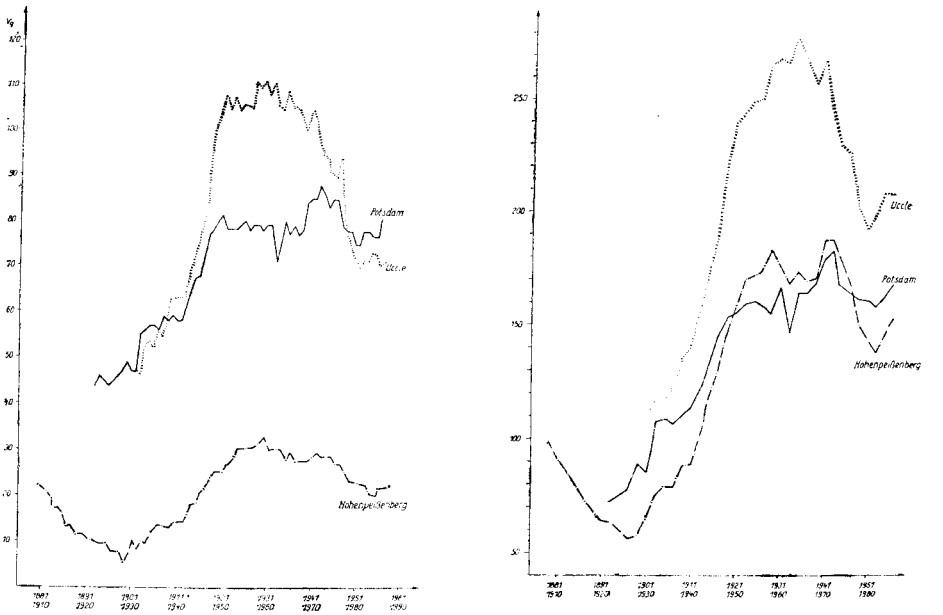

Fig. 5. Sums of the amounts of the vectors of the temperature-humidity complex, daily maximum of the air temperature ≧ 30 °C (Potsdam, Uccle), ≧ 25 °C (Hohenpeißenberg), daily mean value of the vapour pressure ≧ 15 hPa, Potsdam 1893 – 1986, Hohenpeißenberg 1879 – 1986, Uccle 1901 – 1986 (30-year shifted intervals)

Fig. 6. Number of values of the daily mean value of the equivalent temperature ≧ 50 °C (Potsdam, Uccle), ≧ 45 °C (Hohenpeißenberg), Potsdam 1893 – 1986, Hohenpeißenberg 1879 – 1986, Uccle 1901 – 1986 (30-year shifted intervals)

KALVOVÁ, J.: SOME REMARKS ON APPLICATIONS OF ROBUST REGRESSION TO METEOROLOGICAL DATA

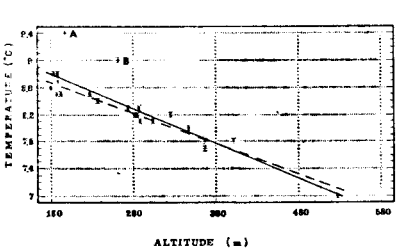

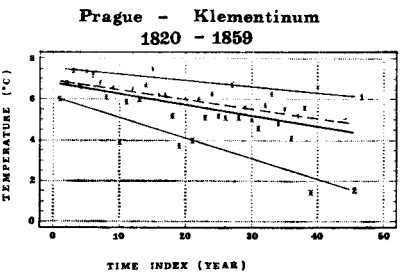

Fig. 1. 50-year averages of annual temperatures for 23 stations as a function of altitude. Solid (dashed) line represents the LSE (TLSE) regression line. A and B denote the outliers

Fig. 2. The trends of annual minimum air temperatures at Prague – Klementinum. Solid (dashed) line represents the LSE (TLSE) regression line. Regression quantiles $\hat{\beta}(\alpha_1)$ and $\hat{\beta}(1 - \alpha_1)$ for $\alpha_1 = 0.07$ are denoted 1 and 2

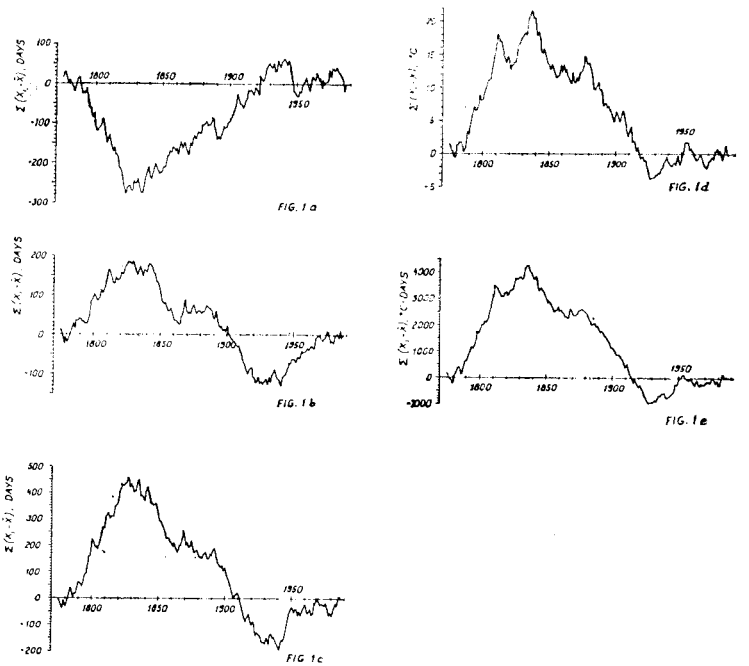

Fig. 1. Season of prevalence of daily average temperatures higher than 15 °C. Cummulated deviations from the 213-years mean of date of the first day of the season (*Fig. 1a*), date of the last day of the season (*Fig. 1b*), duration (number of days) of the season (*Fig. 1c*), mean temperature (°C) of the season (*Fig. 1d*), temperature index (°C . number of days) (*Fig. 1e*)

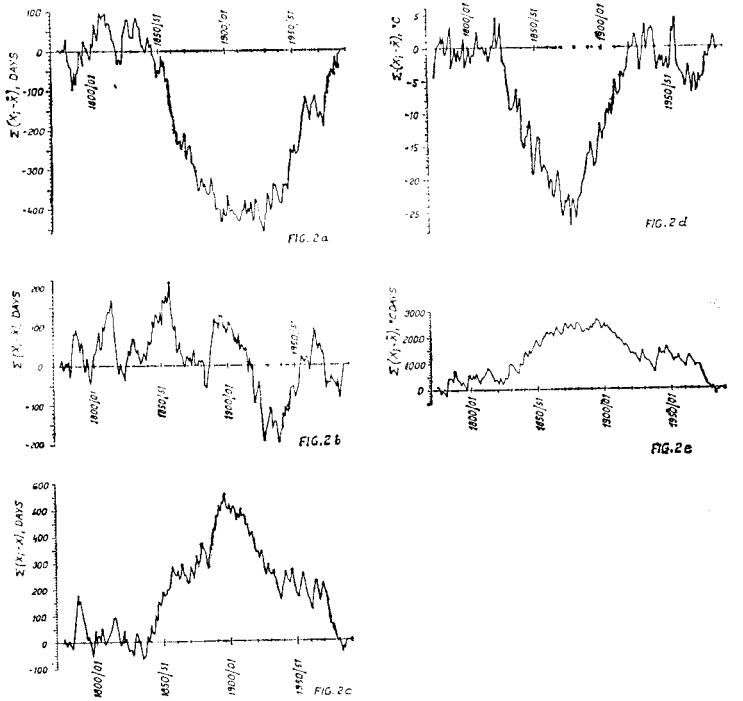

Fig. 2. Season of prevalence of daily average temperatures lower than 0 °C (freezing season). Cummulated deviations from the 212-winters mean of date of the first day of the season (*Fig. 2a*), date of the last day of the season (*Fig. 2b*), duration (number of days) of the season (*Fig. 2c*), mean temperature (°C) of the season (*Fig. 2d*), temperature index (°C . number of days) (*Fig. 2e*)

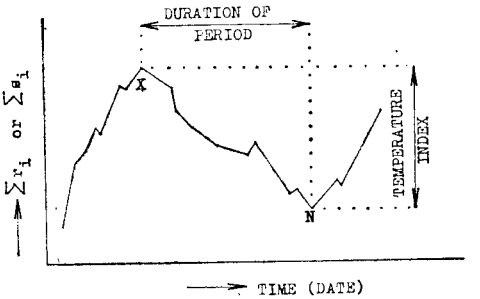

Fig. 3. Scheme of determination of start and end of period of prevalence of temperatures lower or higher than certain value

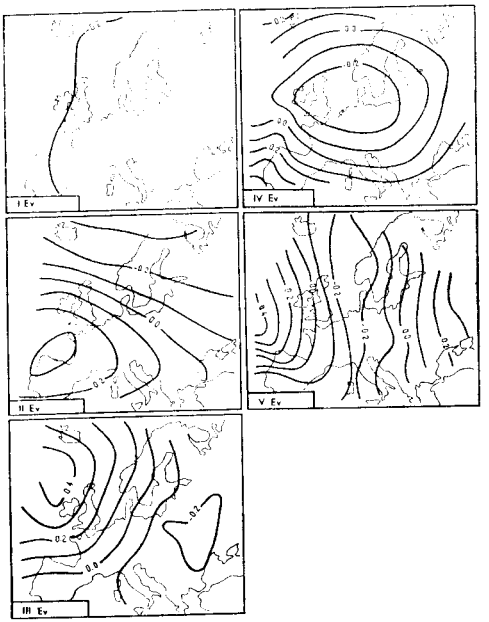

Fig. 1. The spatial distribution of five of first eigenvectors for main isobaric surface 200 hPa

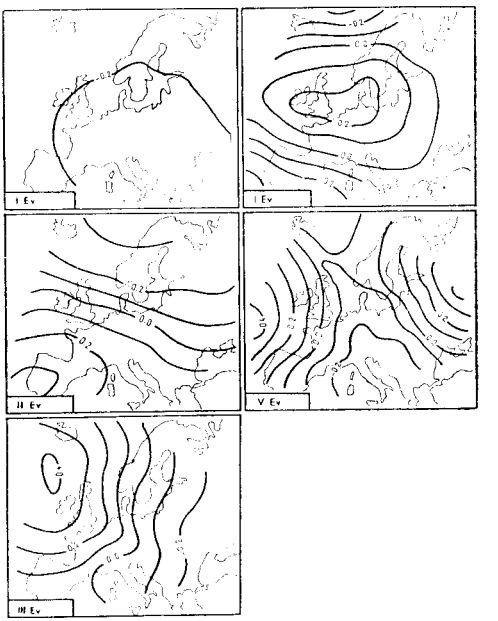

Fig. 2. The spatial distribution of five of first eigenvectors for main isobaric surface 850 hPa

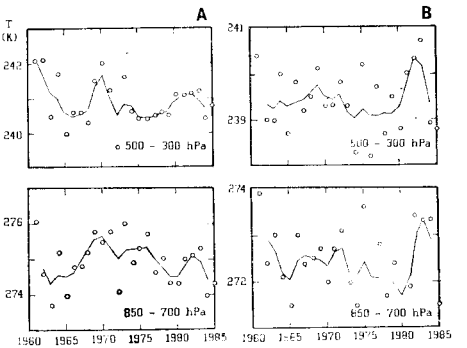

Fig. 3. Yearly means of temperature (dots) and its 3-year overlapping means (continuous line) for Brest (A) and Wroclaw (B)

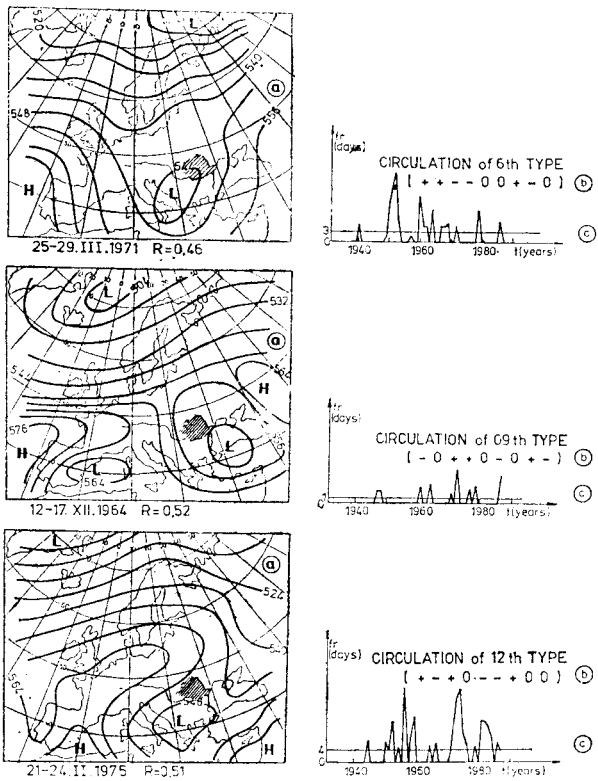

Fig. 1. Anomaly patterns characteristic for the natural synoptic periods: a) representatives, b) the sign $(Xn)_{i=1,9}$ vector, c) frequency of occurrence

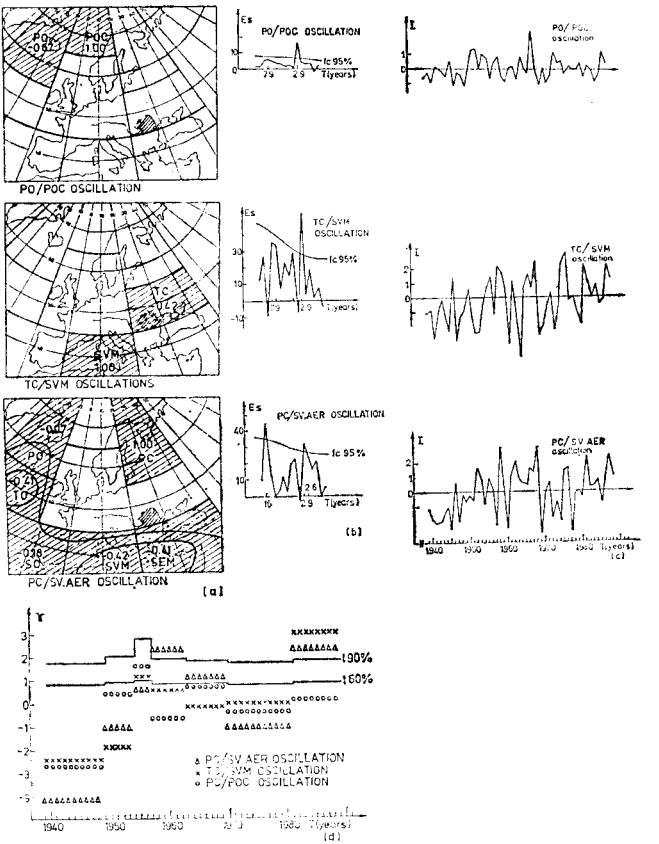

Fig. 3. Oscillations in the Atlantic-European region: a) domain of oscillations and the correlation coefficients between prevailing geopotential anomalies within homogeneous areas; b) spectra of oscillation indices; c) temporal variation of the oscillation index; d) representativeness levels of several homogeneous intervals for the mean climatic state

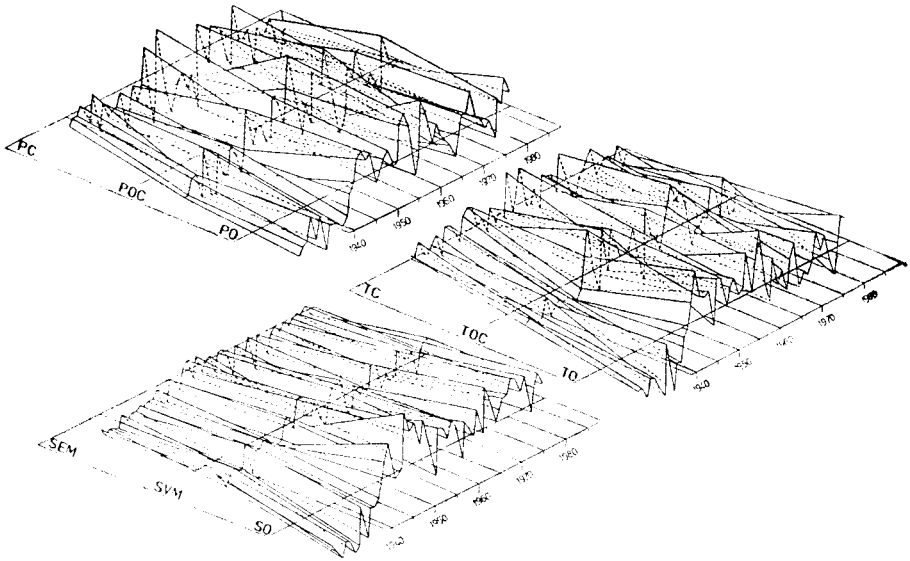

Fig. 2. Temporal evolution of the number of days with predominance of one of the extreme classes of geopotential anomalies

MAKROGIANNIS, T.J., FLOCAS, A.A., KALLIMOPOULOS, P.D.: THE EXTENSIONS OF AZORES ANTICYCLONE TOWARDS SW EUROPE AND THEIR RELATION TO ATMOSPHERIC CIRCULATION ANOMALIES OVER THE MAJOR PART OF EUROPE

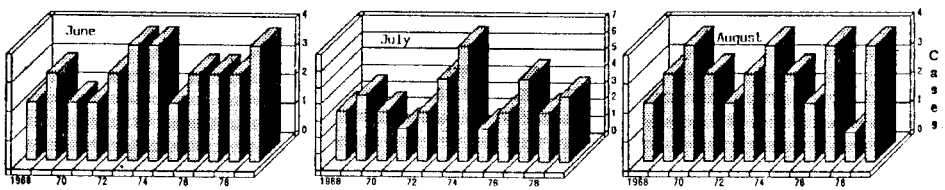

Fig. 1. The interannual distribution of cases of the extensions of Azores anticyclone towards SW Europe, per month

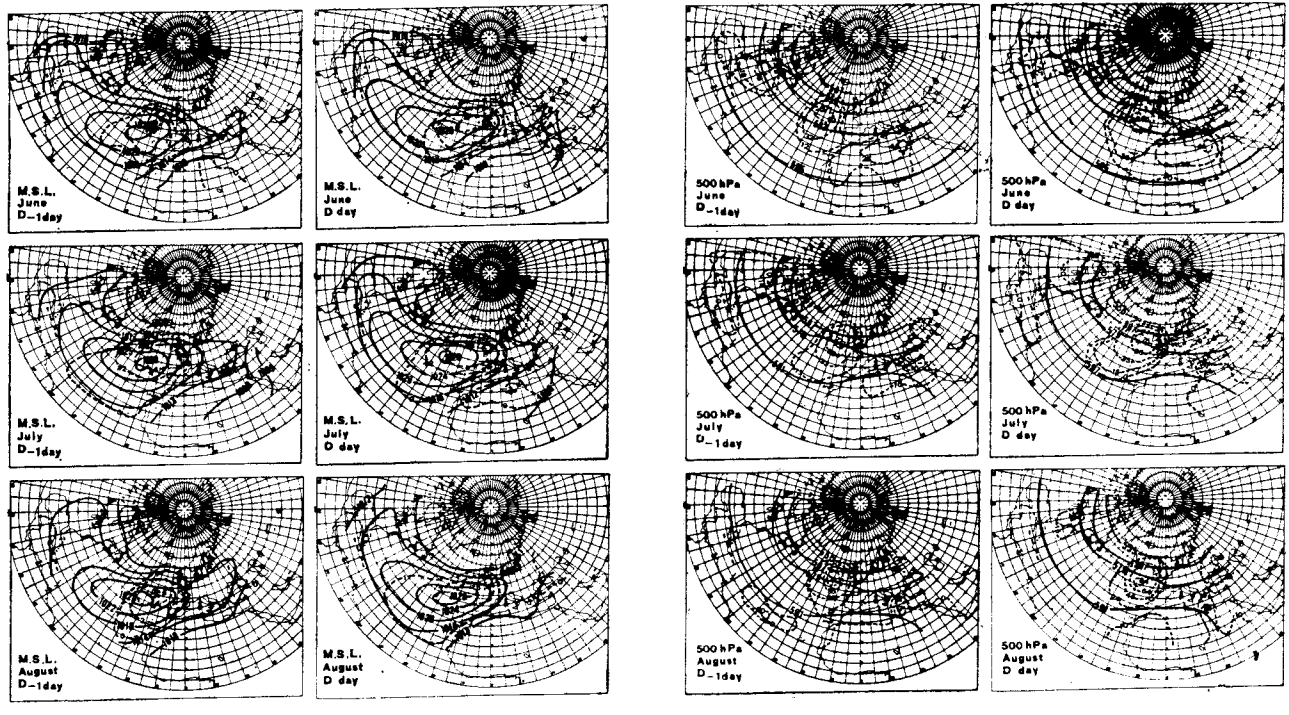

Fig. 2. Mean sea level pressure and patterns of anomalies (hPa). Continuous line -- isobars, dashed line — anomalies

Fig. 3. Mean circulation of 500 hPa surface and patterns of anomalies. Continuous line — isohypses (10 gpm), dashed line — anomalies (gpm)

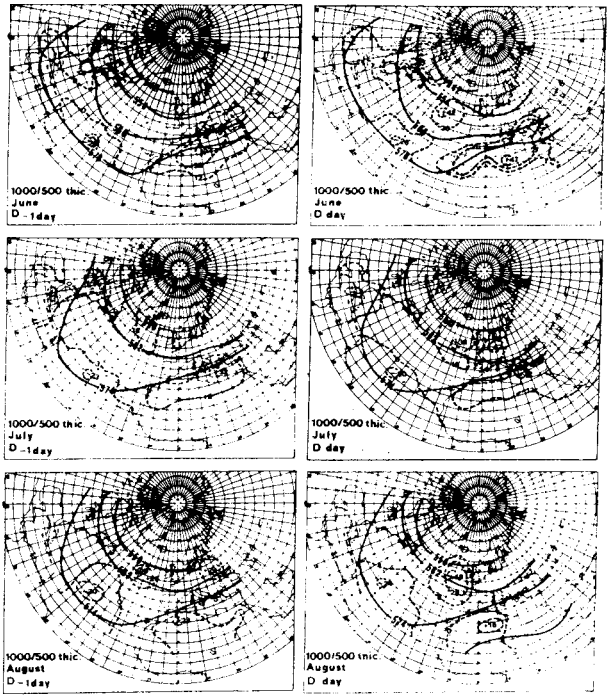

Fig. 4. Mean 1000/500 hPa thickness and patterns of anomalies. Continuous line — thickness (10 gpm), dashed line — anomalies (gpm)

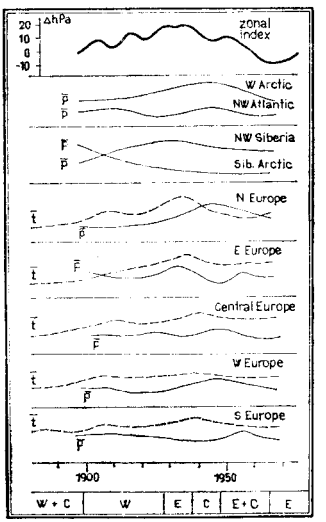

Fig. 1. Pattern of the forming of a tendency of air pressure and air temperature in Europe

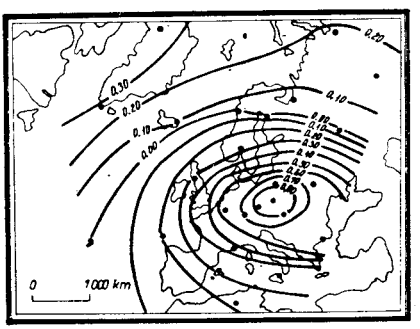

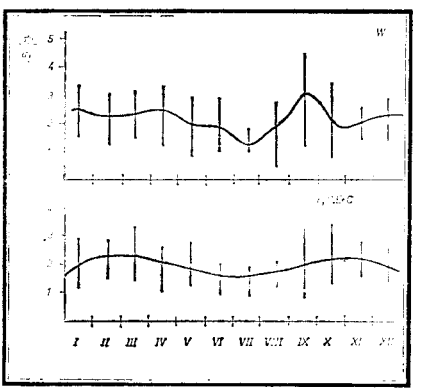

Fig. 2. Determination of mean air pressure in Cracow in relation to air pressure in Europe, March

Fig. 3. Pattern of the forming of the ratio: standard deviations of air pressure to ones of air temperature — during a year in Europe

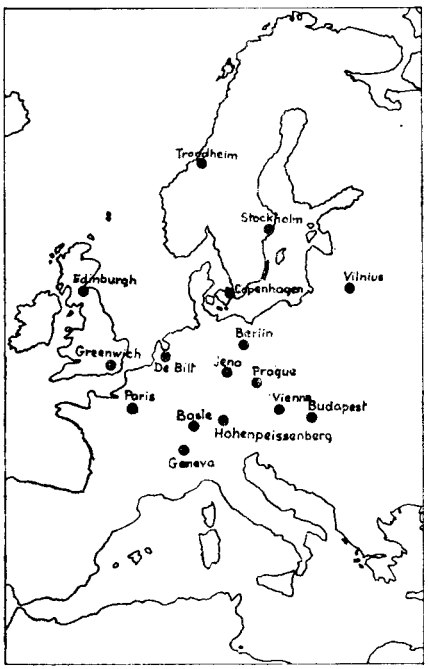

Fig. 1. Positions of climatic stations used in this paper

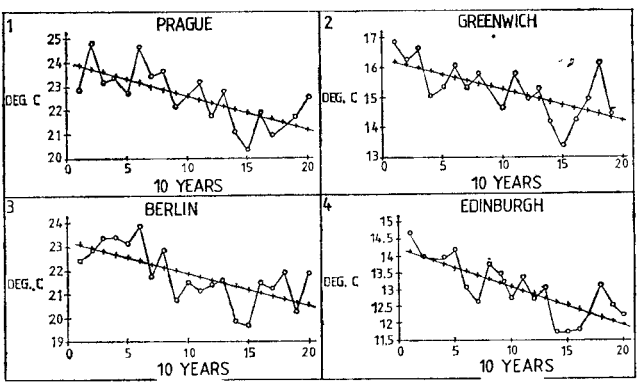

Fig. 2. Variation of decadal average of annual temperature amplitude between 1771 and 1970: Edinburgh, Greenwich, Berlin and Prague

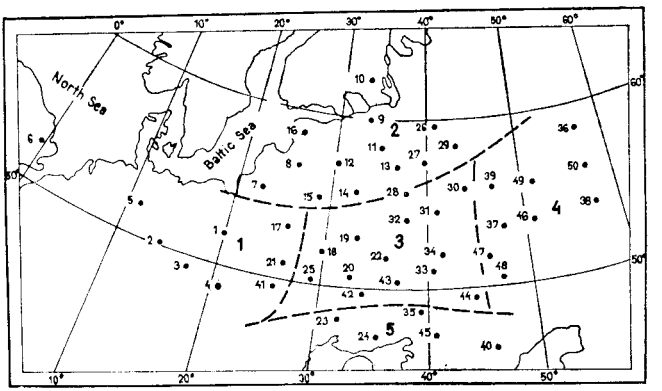

Fig. 1. The regions with homogenous variations of annual precipitation sums. Points and numbers denote centers and numbers of the territories, for which the series of spatial precipitation sums have been used

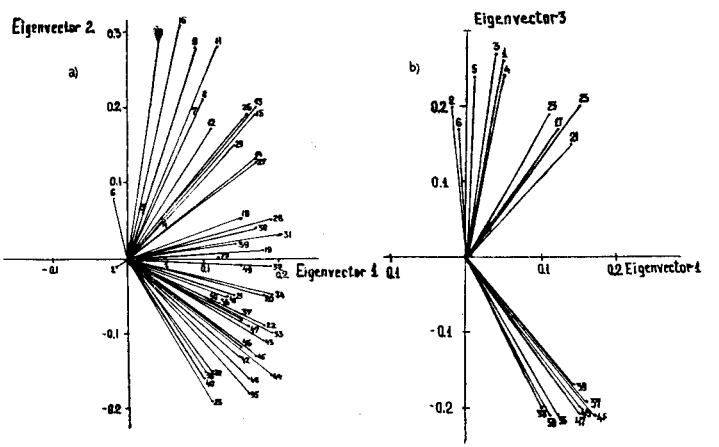

Fig. 2. Projection the points on to the first and second (a) and first and third (b) components

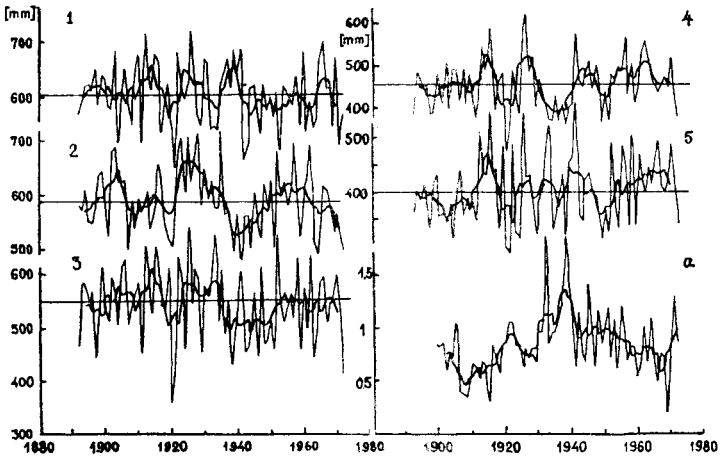

Fig. 3. Patterns of the courses of annual precipitation sums smoothed by five-year running means for different regions in Europe (1 – 5) and the course of Z/M ratio (a)

PERRY, A.H.: WESTERN EUROPE'S CLIMATE DURING THE 1980'S — A COMPARISON WITH EARLIER DECADES

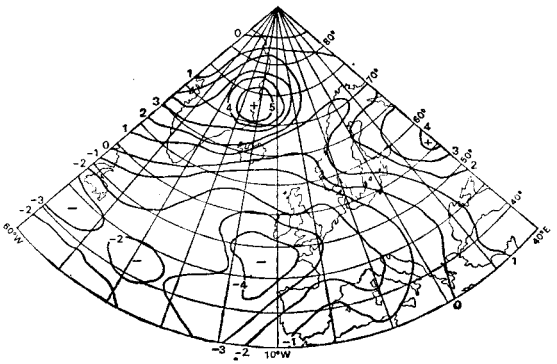

Fig. 1. Surface mean anomaly pattern: January 1970 – 1979

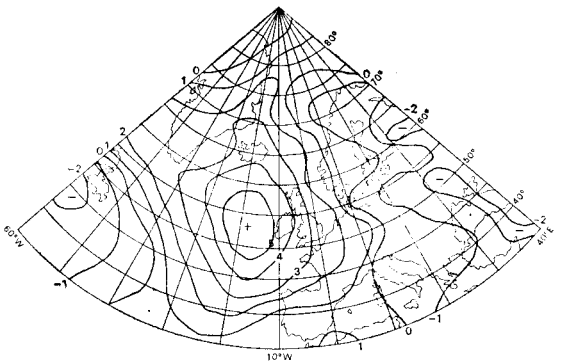

Fig. 2. Surface mean anomaly pattern: April 1970 – 1979

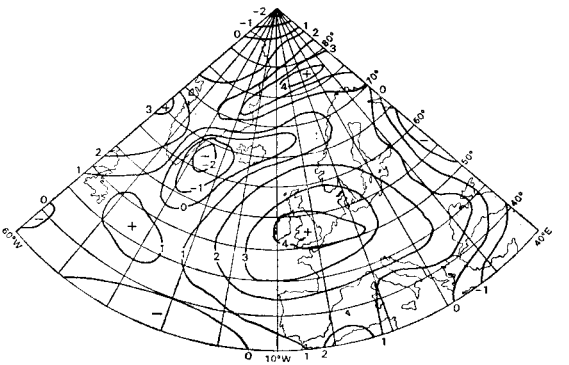

Fig. 3. Surface mean anomaly pattern: October 1970 – 1979

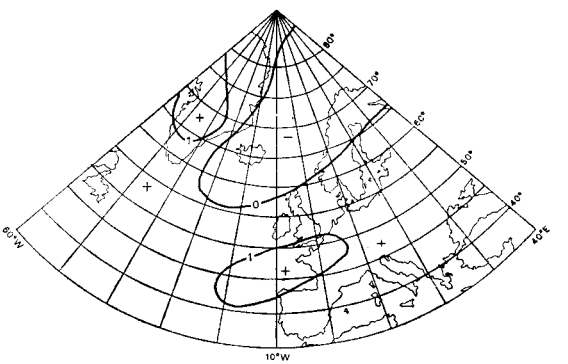

Fig. 4. Surface mean anomaly pattern: Annual 1980 – 1988

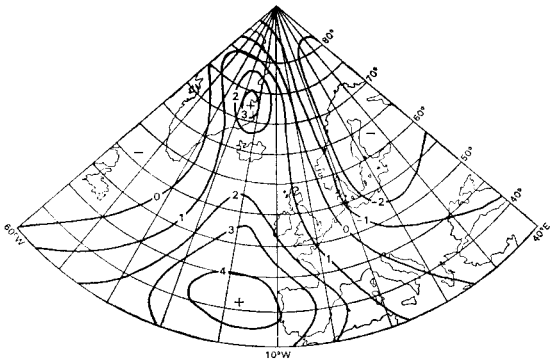

Fig. 5. Surface mean anomaly pattern: January 1980–1988

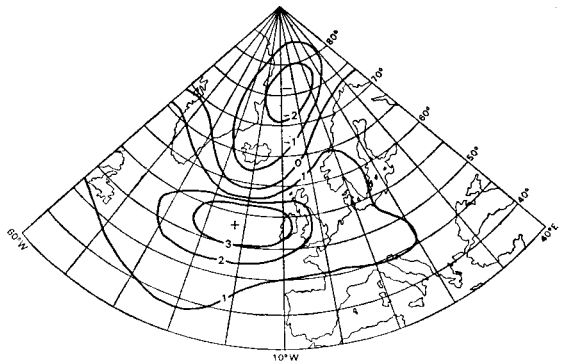

Fig. 6. Surface mean anomaly pattern: April 1980–1988

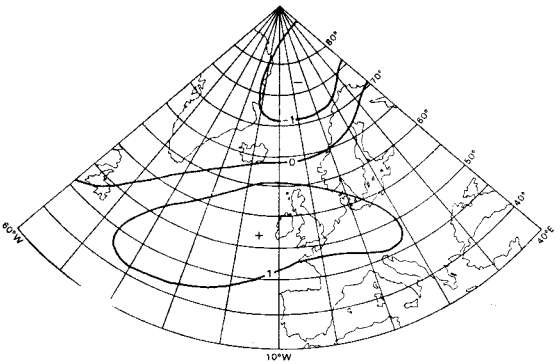

Fig. 7. Surface mean anomaly pattern: July 1980–1988

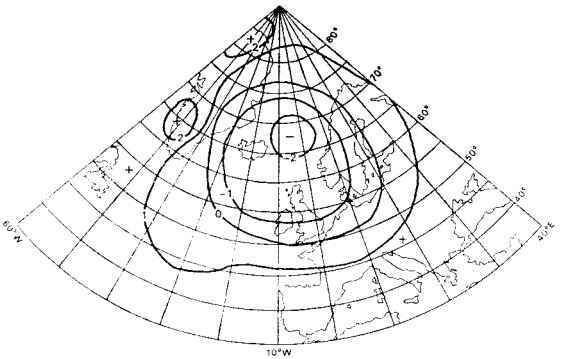

Fig. 8. Surface mean anomaly pattern: October 1980–1988

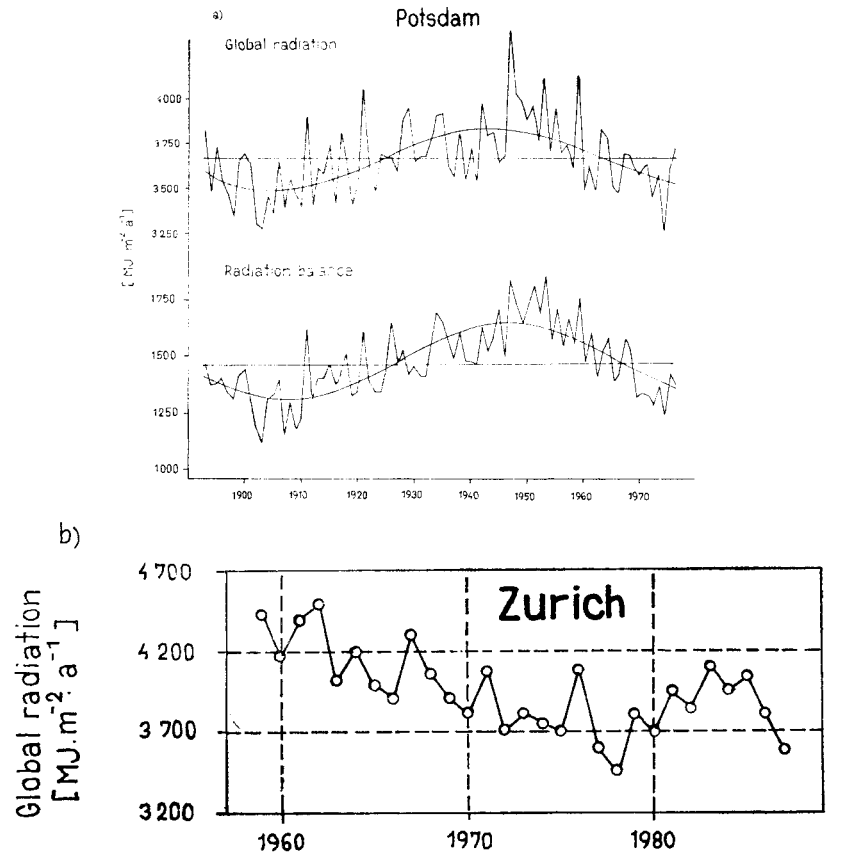

Fig. 1. The course of the annual sums of global radiation and the radiation balance (a) for Potsdam according to *Olberg* (1979) and global radiation (b) for Zurich according to *Ohmura et al.* (1989)

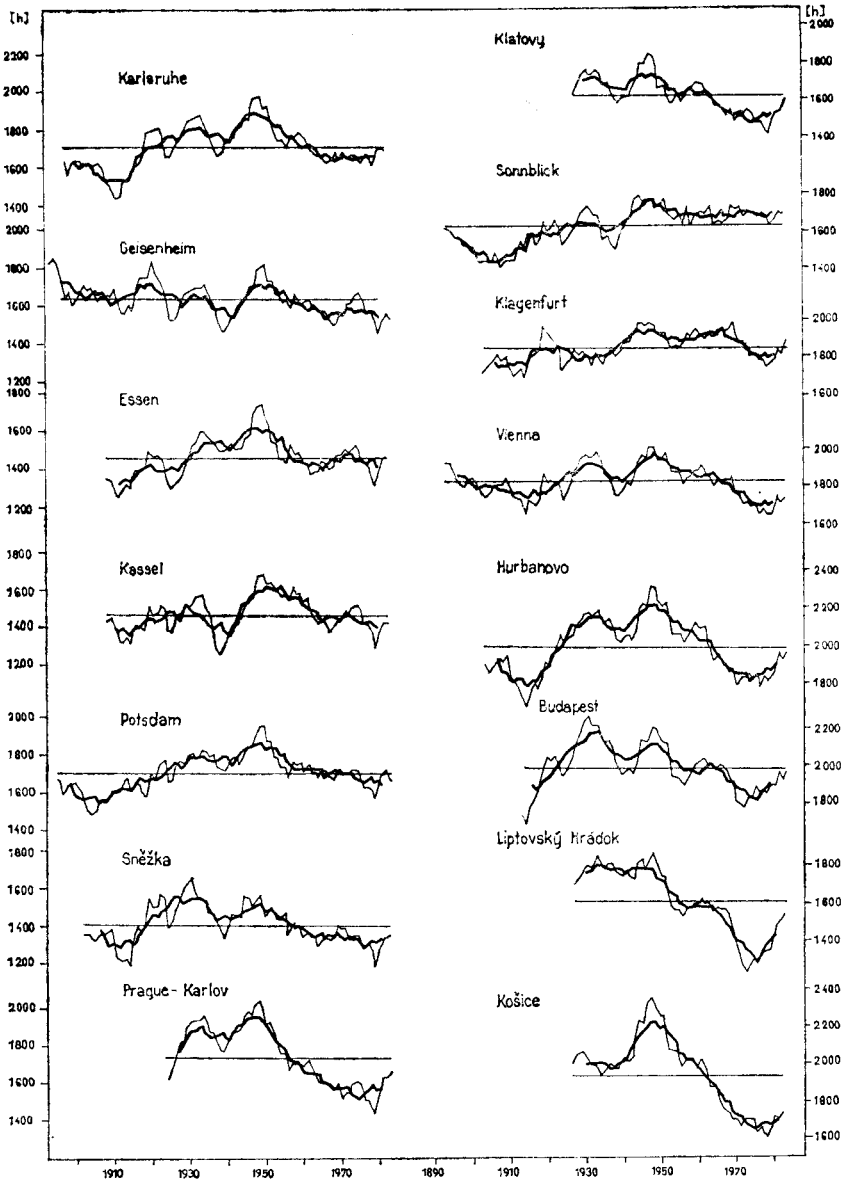

Fig. 2. The course of five-year and ten-year (thick line) running averages of annual sums of sunshine for selected stations in central Europe. The horizontal line expresses the respective long-term average (the same as in *Figs. 3, 4, 5, 6, 7a*)

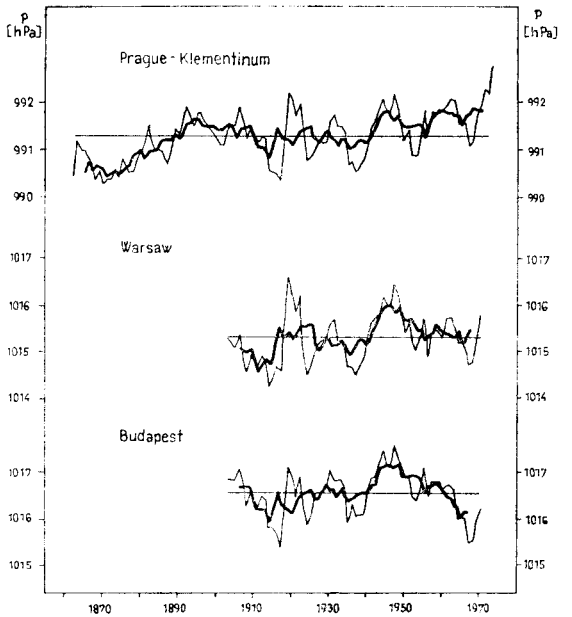

Fig. 3. The course of the five-year and ten-year (thick line) running averages of the annual values of air pressure reduced to sea level (Warsaw, Budapest) and at the level of the station (Prague-Klementinum)

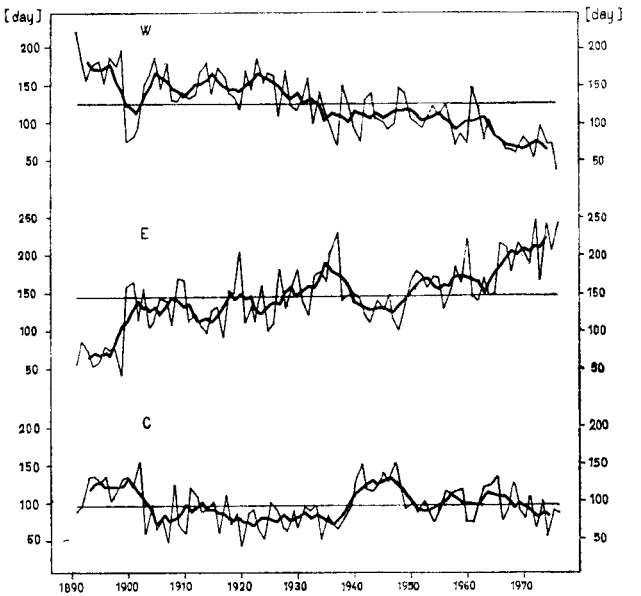

Fig. 5. The course of annual frequencies of occurrences of macrocirculation types *W*, *E*, and *C* according to *Girs* (1971) and *Dydina* (1982) smoothed by five-year running averages (thick line)

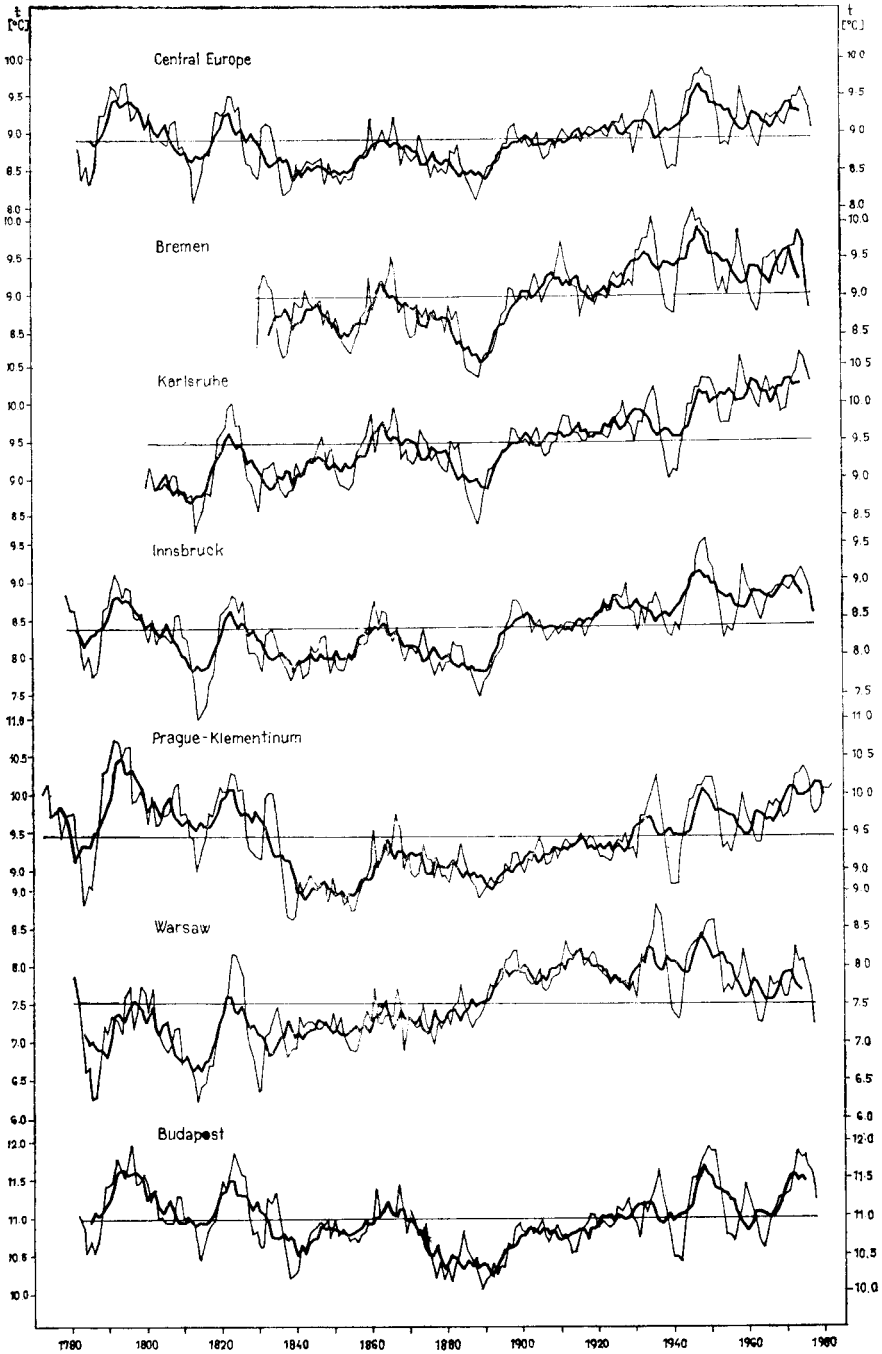

Fig. 4. The course of five-year and ten-year (thick line) running averages of annual air temperature for the model series of central Europe and selected central European stations

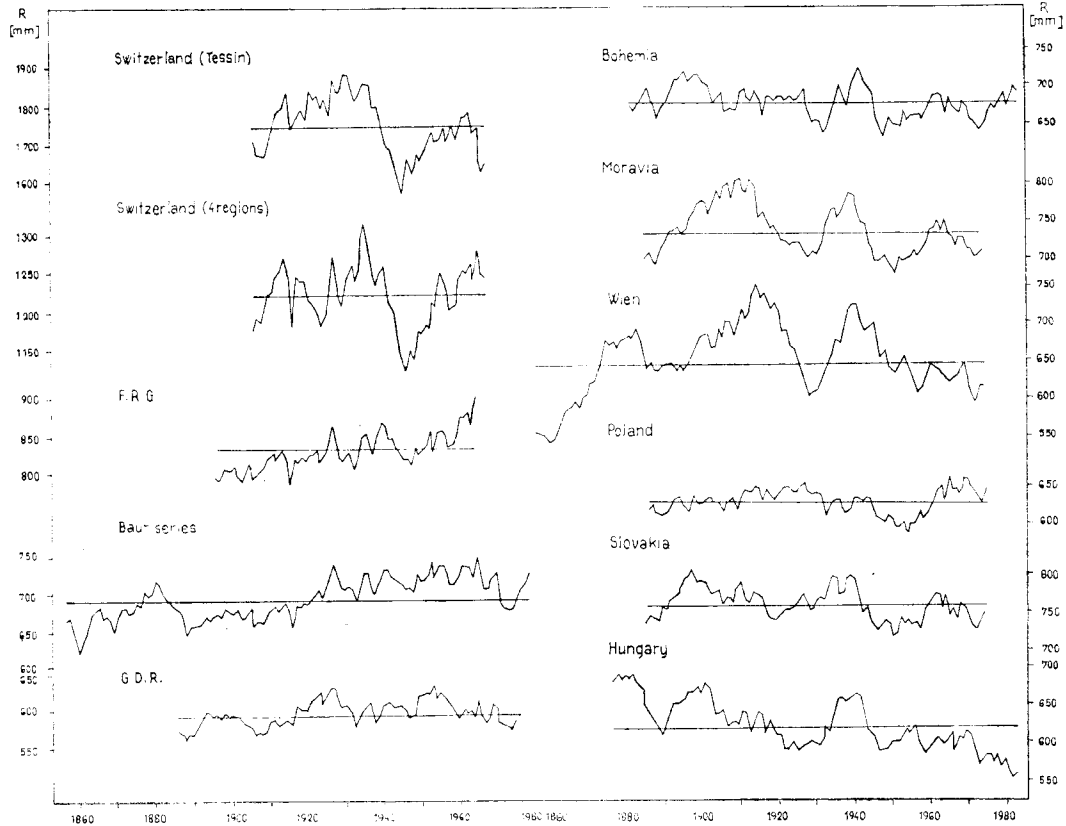

Fig. 6. The course of eleven-year running averages of annual precipitation sums for selected territorial units in the central European region (*Brázdil*, 1986)

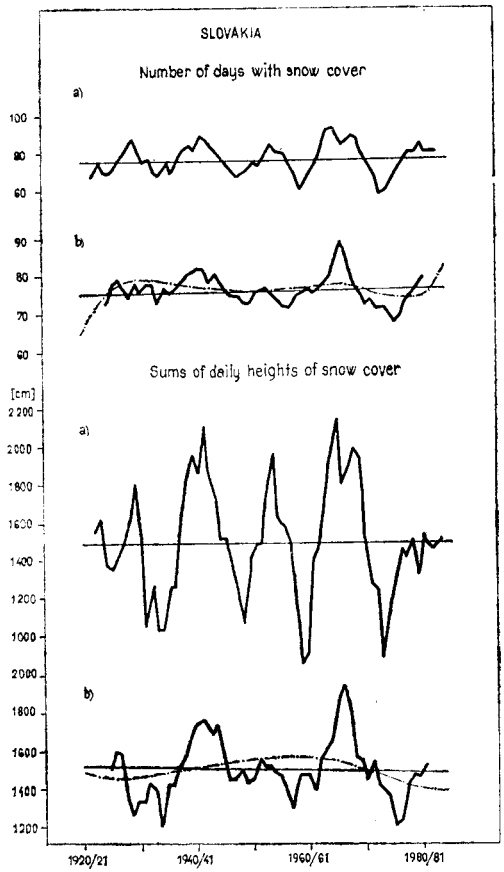

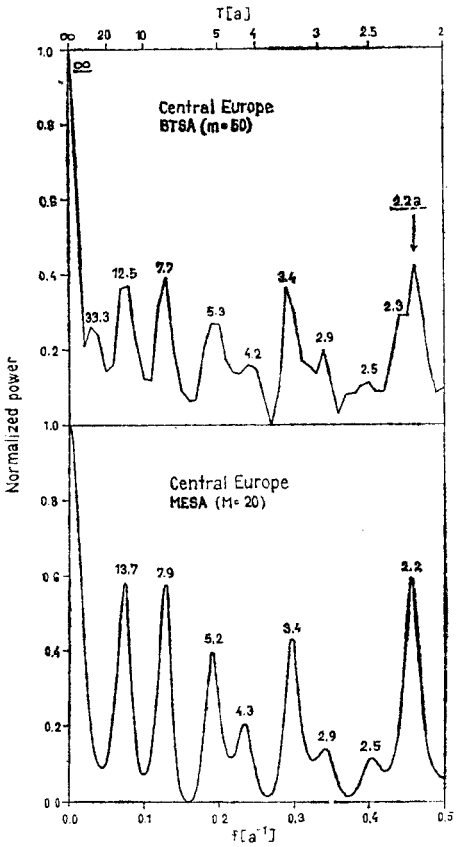

Fig. 7. The course of five-year (a) and ten-year (b) running averages of selected snow pattern characteristics for the territory of Slovakia. In part (b) of the figure the straight line expresses the corresponding straight-line trend, trend of the 4th degree is marked with a dash-and-dot line

Fig. 8. The normalized BT- and ME-spectra of the model series af mean annual air temperatures of central Europe in the period of 1781–1980 with marked periods corresponding to the individual cycles (T — period, f — frequency, a — year). The normalizing was performed in such a way that maximum spectral power was added value 1 and minimum power value 0

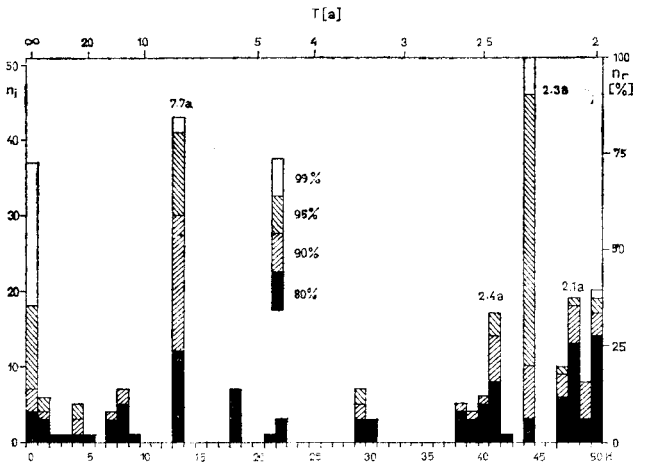

Fig. 9. Absolute (n_i) and relative (n_r) frequencies of statistically significant cycles for 51 central European temperature series in the period of 1881—1980 (completed according to data in *Schönwiese et al.*, 1986): T — period, H — harmonic, calculation for $m = 50$, $T = 2m/H$

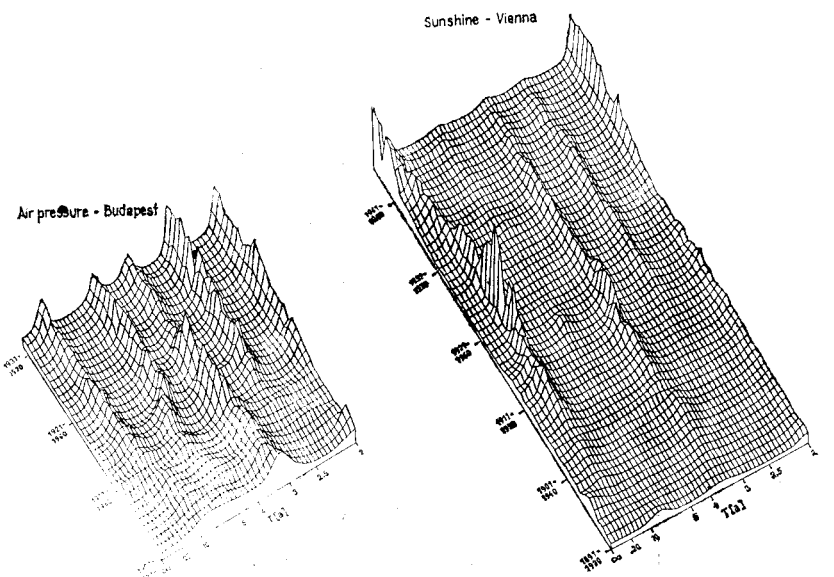

Fig. 10. Three dimensional expression of the dynamical MESA for selected meteorological elements and stations (length of fundamental period 40, $M = 10$, step 1 year)

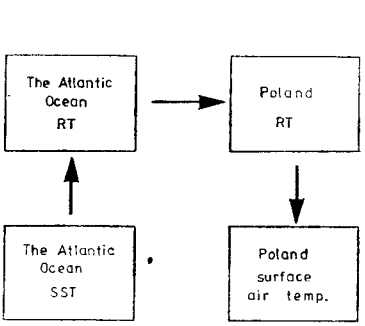

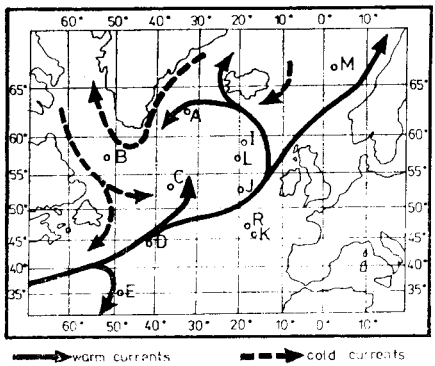

Fig. 1. Pattern of relationship between air temperature and pressure in Poland and SST in the North Atlantic
Fig. 2. Map of weather ships positions in the North Atlantic

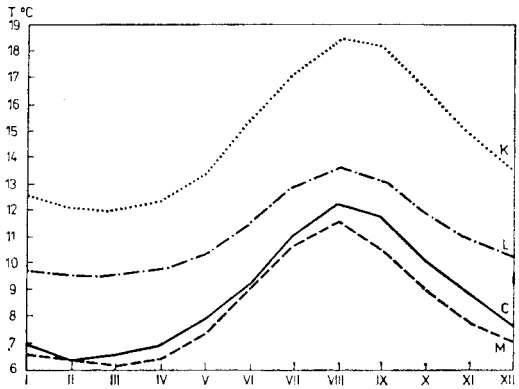

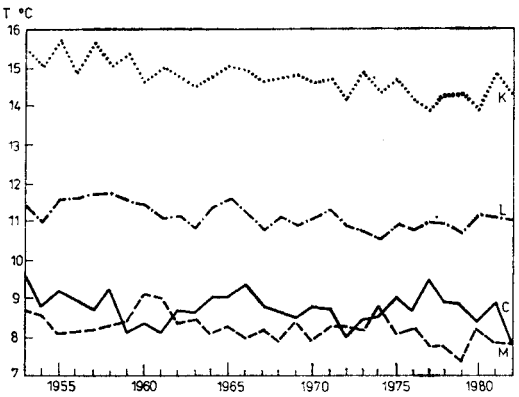

Fig. 3. Annual course of the monthly mean SST values in the North Atlantic for period 1953–1982
Fig. 4. Variability of mean annual values of SST in the North Atlantic (1953–1982)

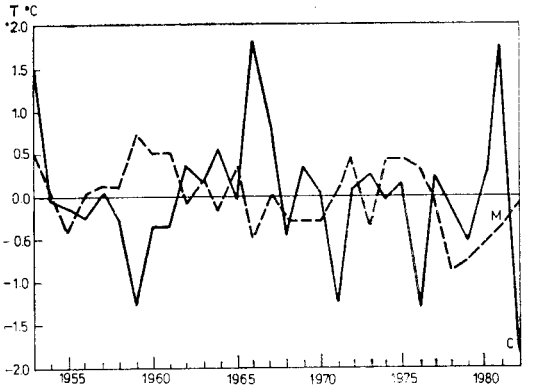

Fig. 5. Annual variations of SST anomalies for region C and **M** (1953 – 1982)

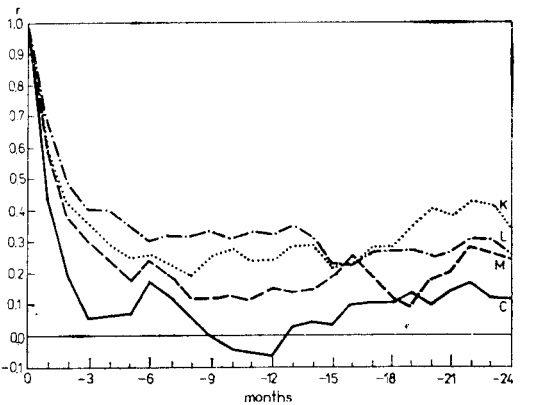

Fig. 6. Autocorrelation function of SST in the **North Atlantic**

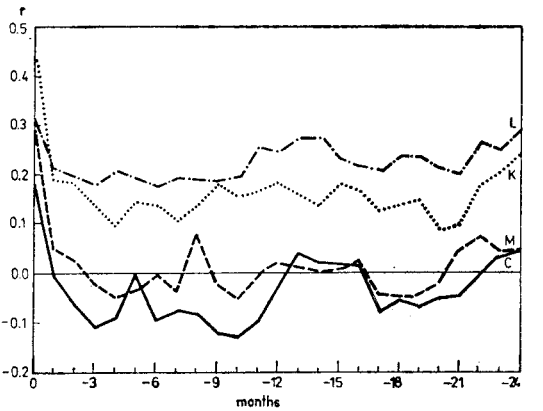

Fig. 7. Correlation function between RT over the North Atlantic and SST

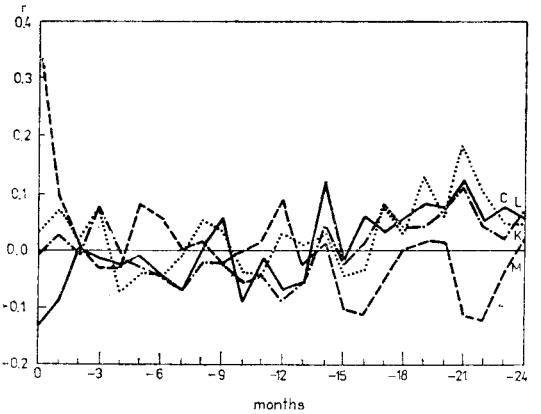

Fig. 8. Correlation function between RT over the North Atlantic and over Poland

BRŮŽEK, V.: LONG—TERM COURSES OF CIRCULATION PARAMETERS AND SOME METEOROLOGICAL ELEMENTS IN BOHEMIA

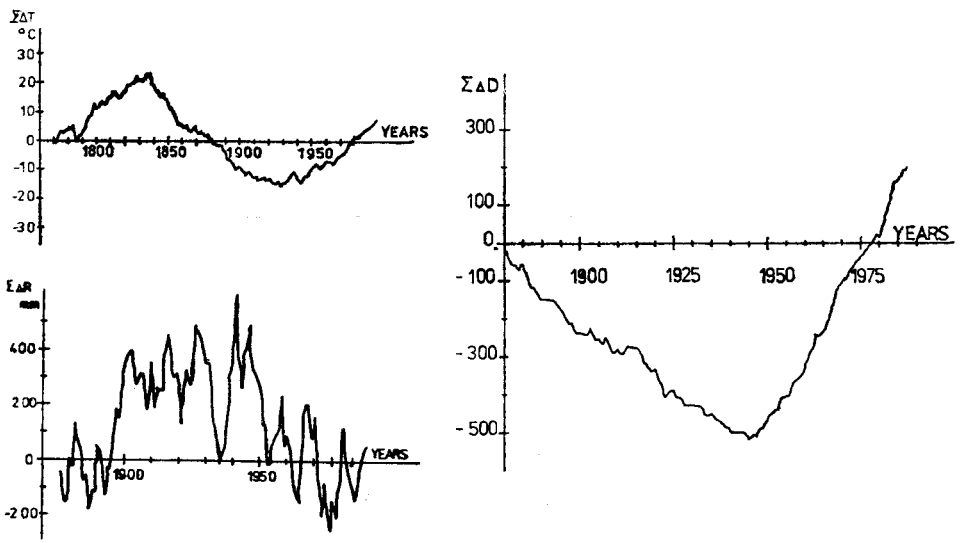

Fig. 1. The integral curve of the mean annual temperature in Prague-Klementinum (1771—1988)

Fig. 2. The integral curve of the annual precipitation sums in Bohemia (1876—1988)

Fig. 3. The integral curve of the south and south-west group of synoptic weather patterns (1881—1988)

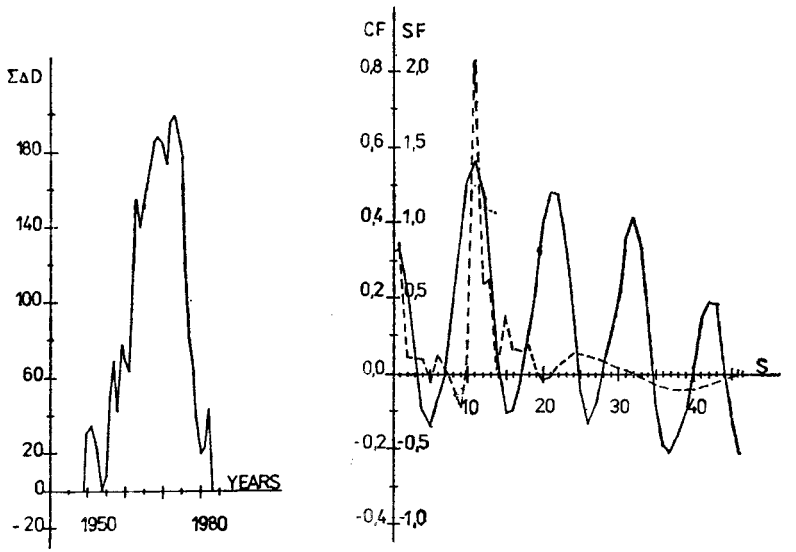

Fig. 4. The integral curve of 500 hPa level at point 55°N, 180°E (1949—1983)

Fig. 5. The correlation CF (full line) and spectral density SF (dashed line) functions between Wolf's numbers and the synoptic weather pattern HFz (1881—1988)

BEDNÁŘ, J.: RECENT CHANGES OF THE SUNSHINE IN PRAGUE REGION

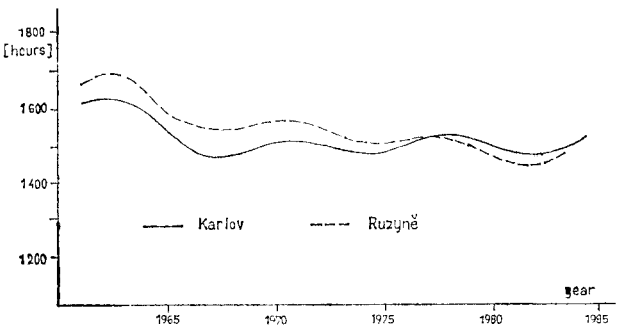

Fig. 1. Values of annual sums of sunshine filtered by Butter-worth method (order 8). Periods shorter than 8 years are supressed

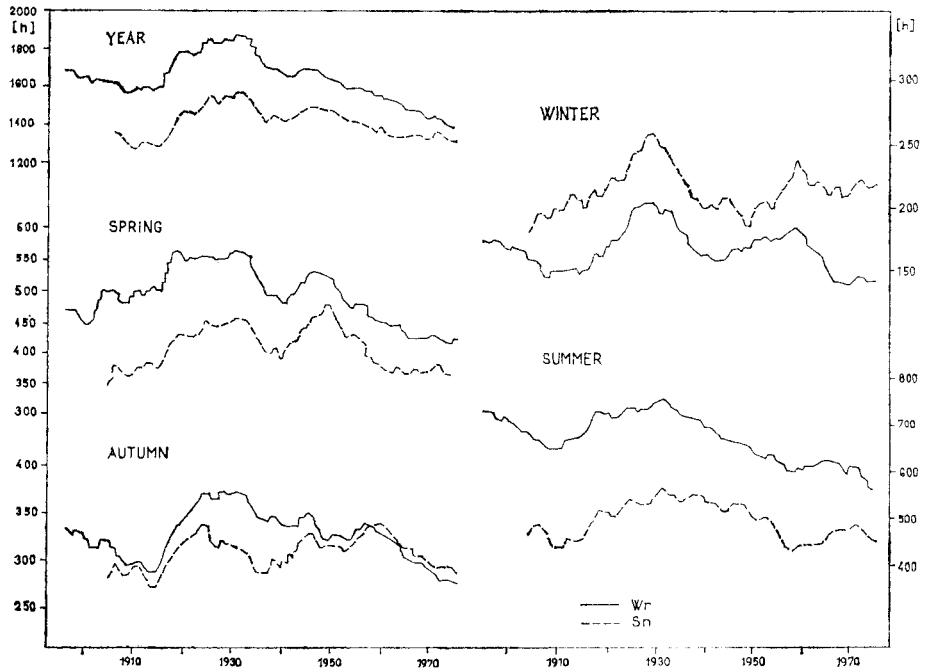

Fig. 1. Sunshine duration in Wrocław (Wr) during 1891—1980 and on Śnieżka Mount (Sn) during 1901—1980 (ten-year overlapping average sums)

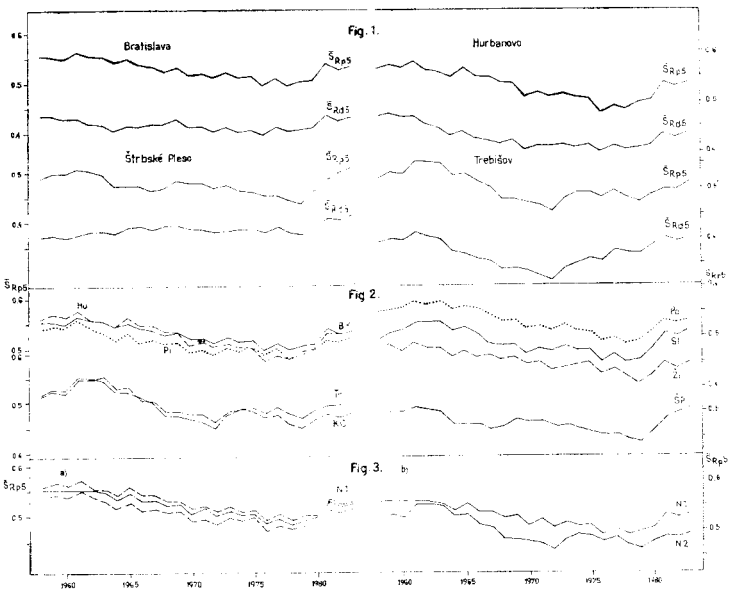

Fig. 1. Comparison between $\overline{S}_{Rd5}$ and $\overline{S}_{Rp5}$ for Bratislava, Štrbské Pleso, Hurbanovo and Trebišov

Fig. 2. The curves $\overline{S}_{Rp5}$ for the stations of the Danube lowland (BK – Bratislava–Koliba, Hu – Hurbanovo, Pi – Piešťany), East Slovakian lowland (Tr – Trebišov, KC – Kamenica nad Cirochou), in hollows (Sl – Sliač, Ži – Žilina, Po – Poprad) and upland locality (ŠP – Štrbské Pleso)

Fig. 3. The mean *N1* curve for the stations of Danube lowland and limits within the framework of which the curves $\overline{S}_{Rp5}$ for the averaged stations are situated (a) and comparison of *N1* (Danube lowland) and *N2* (East Slovakian lowland) curves (b)

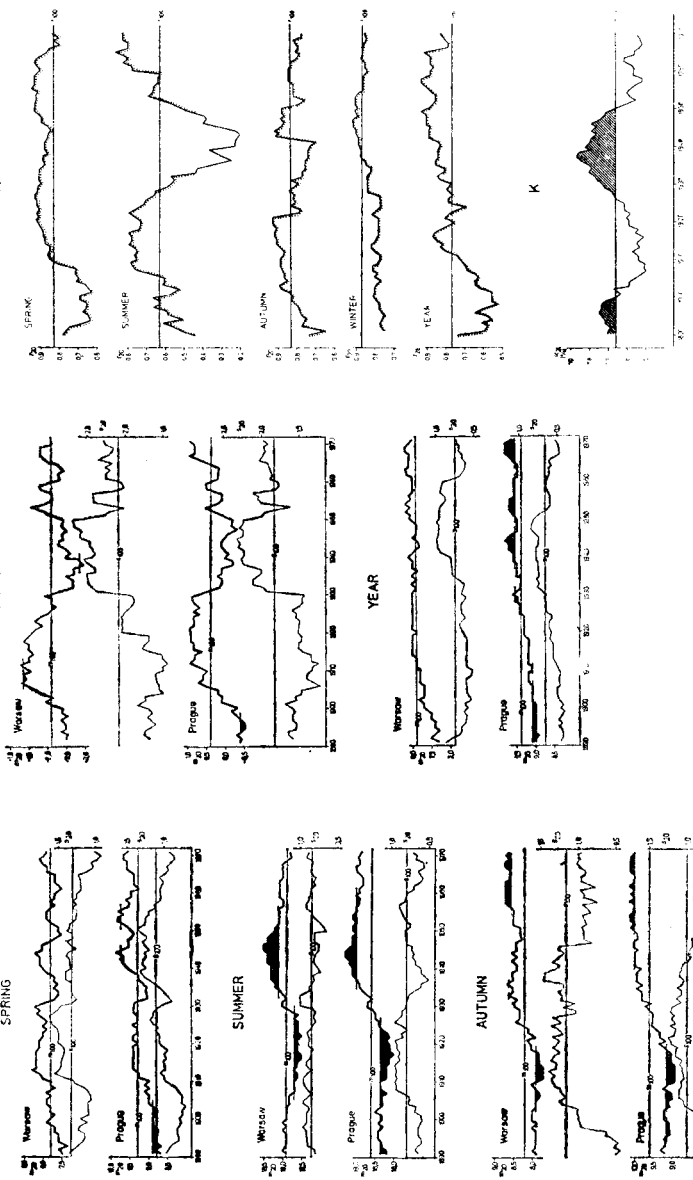

Fig. 1. Seasonal and annual temperatures in Warsaw and Prague in the period of 1881—1980. Explanation: m_{20} — 20-year running means, the significant deviations from 100-year mean marked, s_{20} — standard deviations in 20 year moving periods, m_{100} — mean of the whole 100-year, s_{100} — standard deviation of the whole 100-year period

Fig. 2. The correlation (R) between mean temperatures in Warsaw and Prague in running 20-year periods (1 — significant coeffficients at the 5 % level) and continentality coefficient (K — according to Johansson-Ringleb formula) in Warsaw (20-year running means)

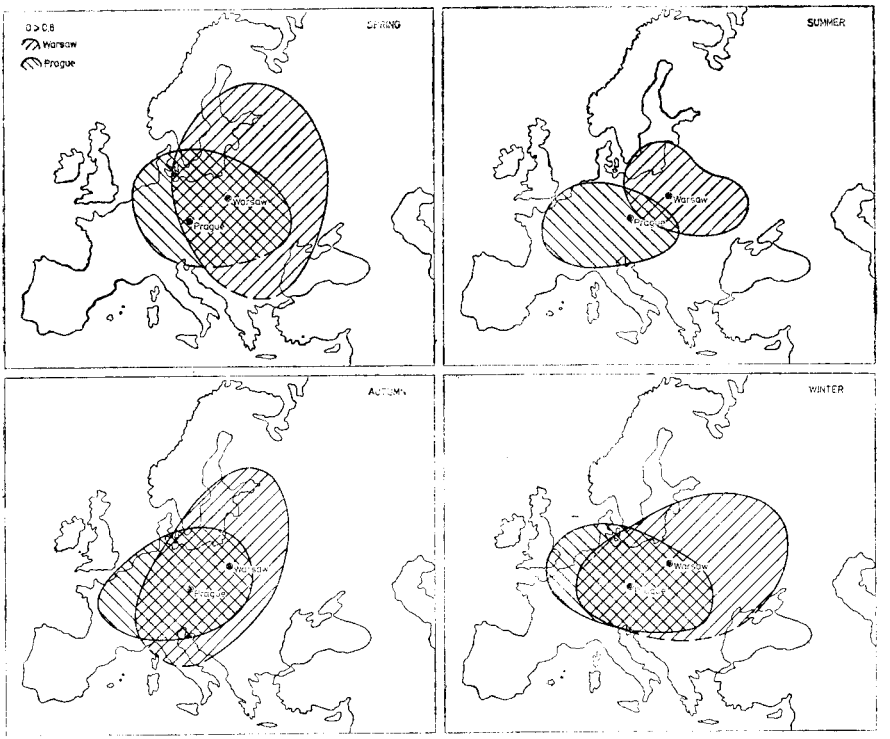

Fig. 3. Convergency of the interannual changes of seasonal and annual temperatures in Europe, with respect to Warsaw and Prague (areas of convergency coefficient $Q \geqq 0.80$ marked)

BLOUTSOS, A.A., SAHSAMANOGLOU, H.S., BRÁZDIL, R.: LONG–TERM AIR TEMPERATURE FLUCTUATIONS IN GREECE AND CZECHOSLOVAKIA

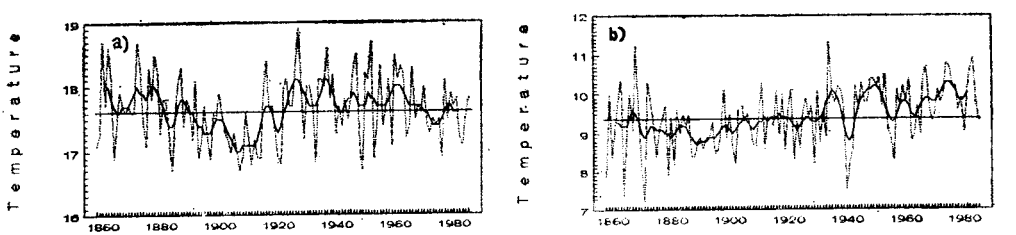

Fig. 1. The course of annual air temperatures for Athens (a) and Prague (b). Dotted line – observed values, thick line – values obtained by nine-weight binomial filter

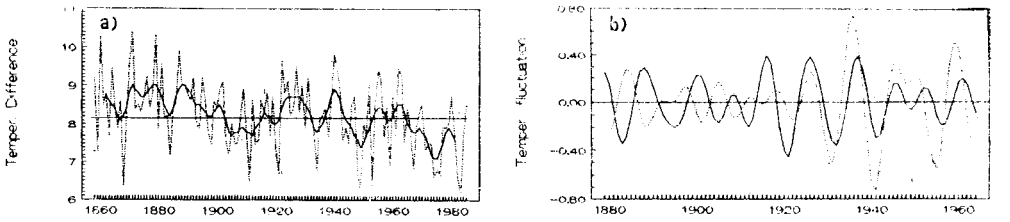

Fig. 2. a) Differences of annual air temperatures between Athens and Prague. Thick line — values obtained by nine-weight binomial filter; b) 11-year air temperature fluctuations obtained by numerical band-pass filtering. Thick line Athens, dotted line — Prague

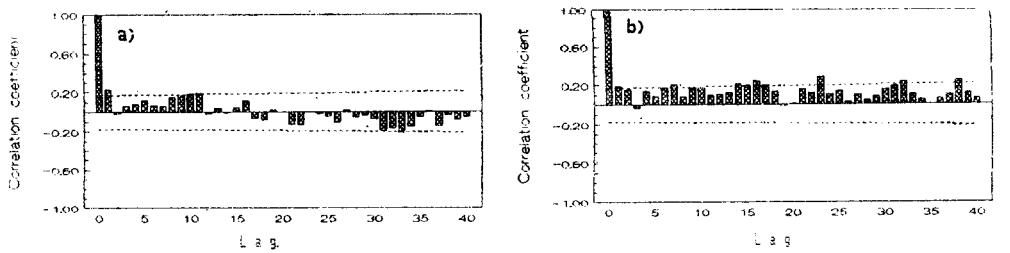

Fig. 3. The course of autocorrelation coefficients of annual air temperatures for Athens (a) and Prague (b). Dotted line — 95 % confidence limit

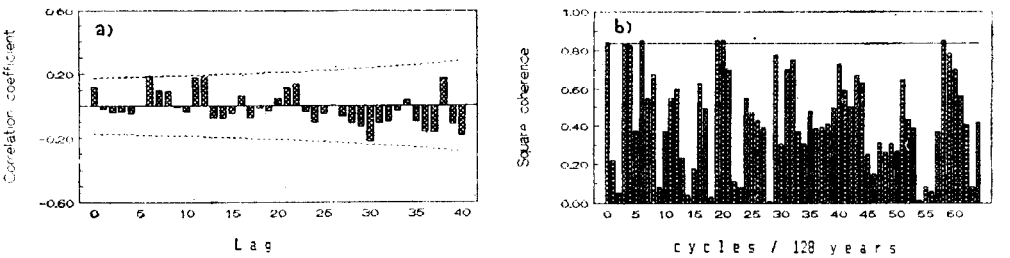

Fig. 4. a) Cross-correlation coefficients between annual air temperatures of Prague and Athens. Dotted line represents 95 % confidence limit; b) Cross spectral analysis between annual air temperatures of Athens and Prague. Continuous line represent the 95 % confidence limit

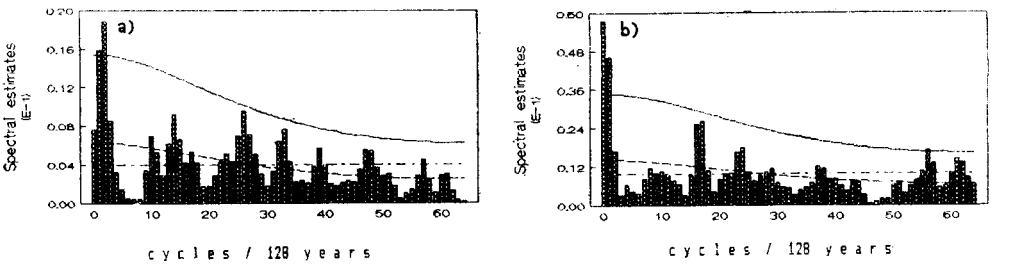

Fig. 5. Power spectral analysis of annual air temperatures for Athens (a) and Prague (b). Continuous line — 95 % confidence limit, dotted line — red noise, broken line — white noise

OSTROŽLÍK, M., MURÍNOVÁ, G.: LONG-TERM ANOMALIES OF AIR TEMPERATURE ON THE TERRITORY OF SLOVAKIA

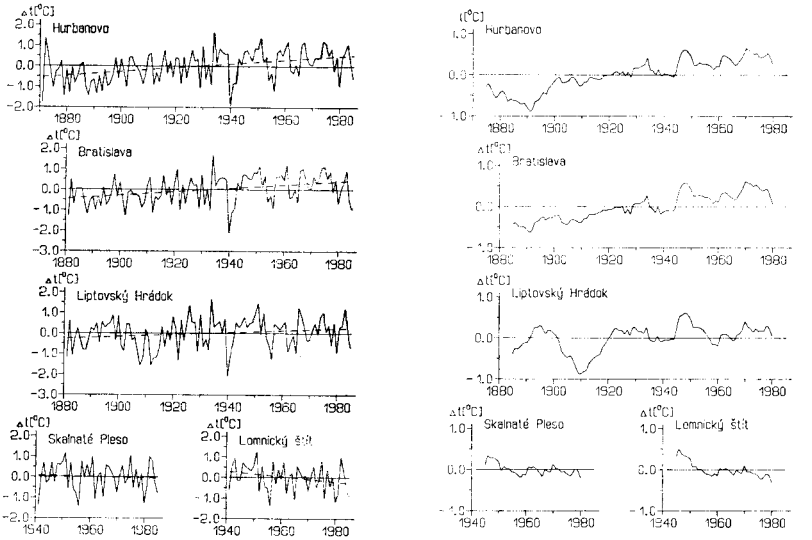

Fig. 1. Course of air temperature deviations from the long-term average and the trend component of these deviations: Hurbanovo (period 1871–1985), Bratislava (period 1881–1985), Liptovský Hrádok (period 1881–1985), Skalnaté Pleso and Lomnický štít (period 1941–1985)

Fig. 2. Course of air temperature deviations from the long-term average smoothed by ten-year running averages: Hurbanovo (period 1871–1985), Bratislava (period 1881–1985), Liptovský Hrádok (period 1881–1985), Skalnaté Pleso and Lomnický štít (period 1941–1985)

ŠOLTÍS, J., TEKUŠOVÁ, M., ZEMAN, V.: LONG-TERM AIR TEMPERATURE AND PRECIPITATION CONDITIONS IN SUMMER AND WINTER PERIODS IN HURBANOVO

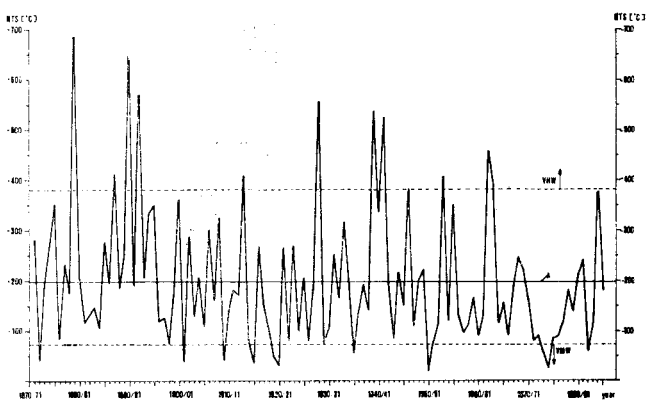

Fig. 1. Course of winter temperature sums of days with average air temperature < 0 °C in individual years of the whole evaluated period in Hurbanovo. Upper dashed line is the boundary of very hard winters (VHW), central full line is the 115-year average (A) and lower dashed line is the boundary of very mild winters (VMW)

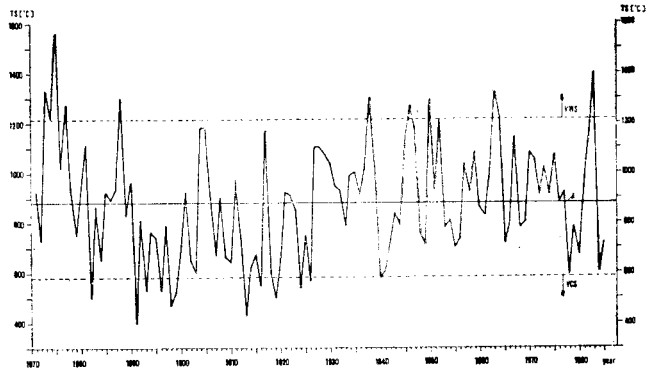

Fig. 2. Course of summer temperature sums of days with average air temperature ≧ 20 °C in individual years of the whole evaluated period in Hurbanovo. Upper dashed line boundary of very warm summer (VWS), central full line is 115-year average (A) and lower dashed line is boundary of very cold summer (VCS)

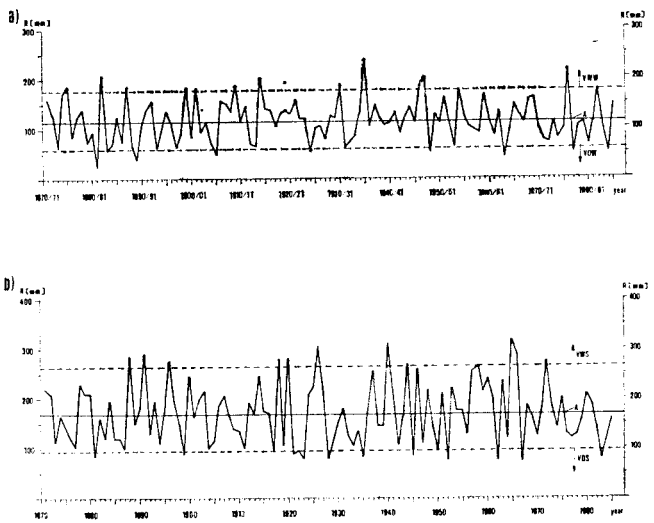

Fig. 3. Course of winter (a) and summer (b) total precipitation in individual years of the whole evaluated period in Hurbanovo. Upper dashed line is the boundary of very wet winters (VWW) (a) and very wet summer (VWS) (b), the central full line is 115-year average (A) and the lower dashed line is the boundary of very dry winters (VDW) (a) and very dry summers (VDS) (b)

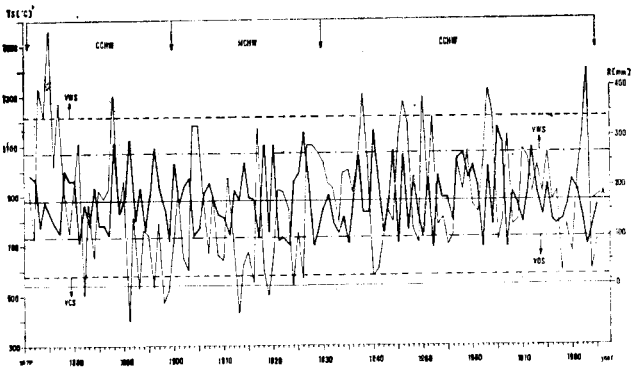

Fig. 4. Results of evaluations of the relationship between temperature and precipitation of the summer seasons in Hurbanovo

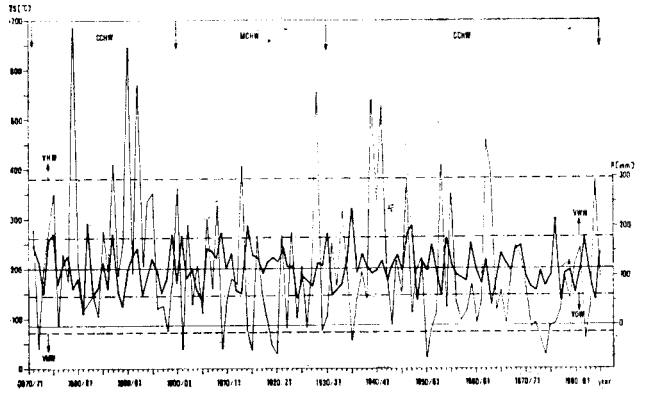

Fig. 5. Results of evaluations of the relationship between temperature and precipitation of the winter seasons in Hurbanovo

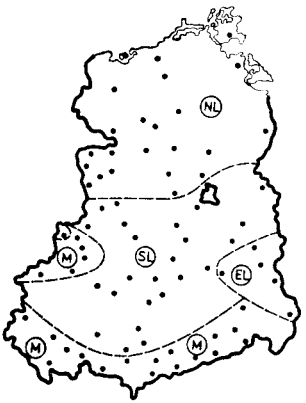

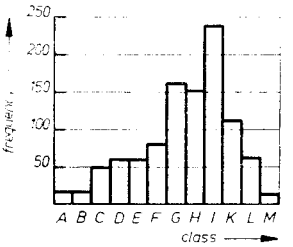

A	$0\ mm \leq P \leq 5\ mm$
B	$5\ mm < P \leq 10\ mm$
C	$10\ mm < P \leq 15\ mm$
D	$15\ mm < P \leq 20\ mm$
E	$20\ mm < P \leq 25\ mm$
F	$25\ mm < P \leq 30\ mm$
G	$30\ mm < P \leq 40\ mm$
H	$40\ mm < P \leq 50\ mm$
I	$50\ mm < P \leq 75\ mm$
K	$75\ mm < P \leq 100\ mm$
L	$100\ mm < P \leq 150\ mm$
M	$P > 150\ mm$

Fig. 1. Geographical distribution of stations used (without numbering): NL – northern lowland, SL – southern lowland, EL – south-eastern part of lowland, M – mountainous areas

Fig. 2. Empirical frequencies of monthly precipitation totals P (station Spremberg, 1901 – 1984)

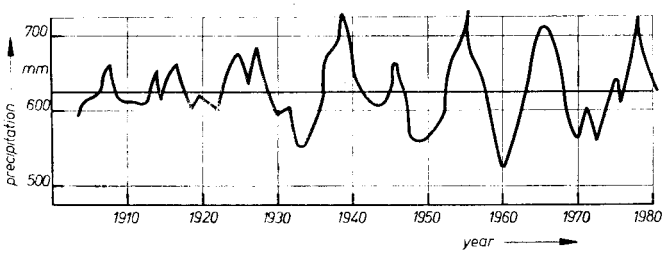

Fig. 3. Course of annual precipitation totals at Spremberg smoothed by 5-year moving means (period 1901 – 1984); horizontal line – mean value for 84 years

MARCINIAK, K.: CERTAIN ASPECTS OF LONG–TERM VARIABILITY OF PLUVIO–THERMAL CONDITIONS IN MIDDLE POLAND IN THE PERIOD 1861–1987 TAKING BYDGOSZCZ AS AN EXAMPLE

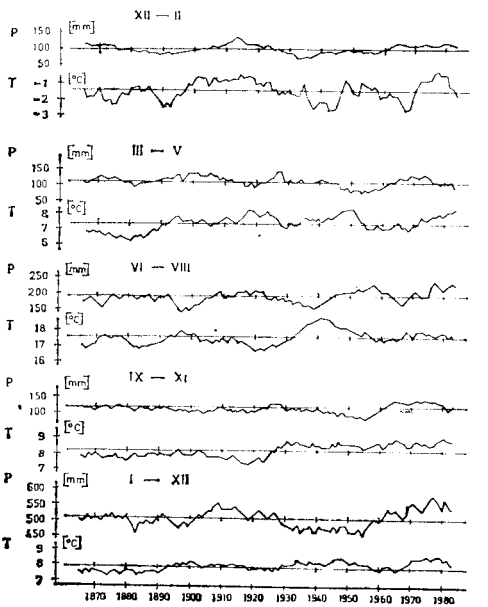

Fig. 1. Running averages of 10-year of atmospheric precipitation totals (*P*) and air temperature means (*T*) in winter (Dec.–Feb.), spring (Mar.–May), summer (June–Aug.), autumn (Sept.–Nov.) and for a whole year (Jan.–Dec.) in Bydgoszcz-IMUZ in the period 1861–1987

PYKA, J.L.: THE METEOROLOGICAL OBSERVATIONS IN WROCŁAW DURING 1881–1980

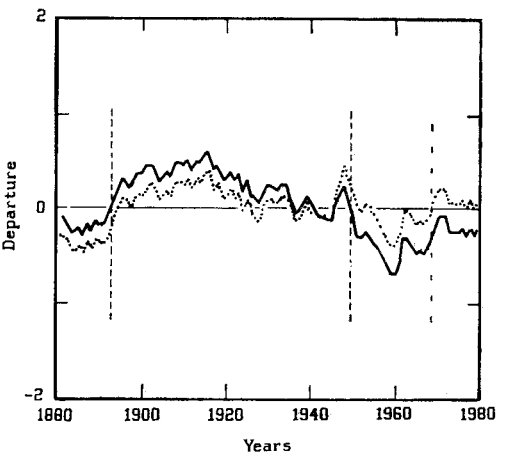

Fig. 1. Eleven-year running averages of temperature departures from 100-year mean (continuous line) and combination of temperature departure from means of periods 1881–1930, 1931–1945 and 1946–1980 (dotted line)

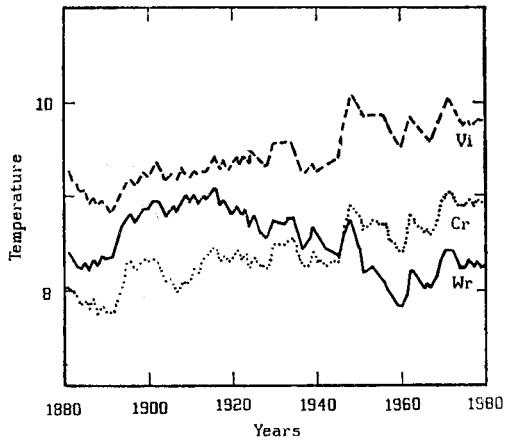

Fig. 2. Eleven-year running averages of temperature of July and year in Wroclaw (Wr), Vienna (Vi) and Cracow (Cr)

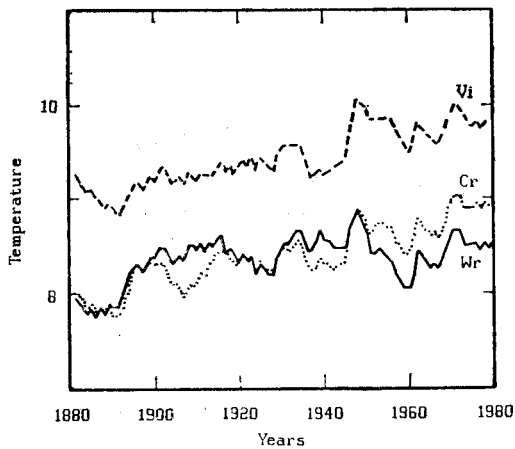

Fig. 3. As same as in *Fig. 2.* For Wroclaw data was corrected using values from *Table 3*

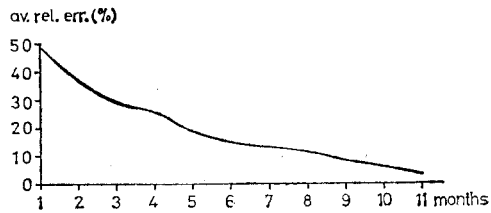

Fig. 1. Mean relative errors of the estimation of the annual sums of precipitation from the mode of monthly relative sums

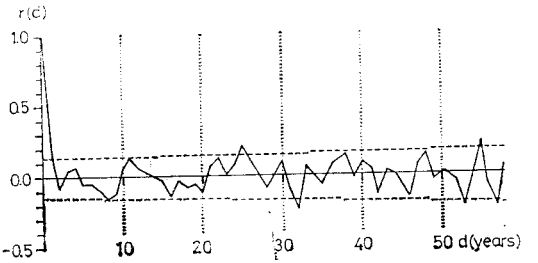

Fig. 2. Autocorrelogram of the annual sums of precipitation

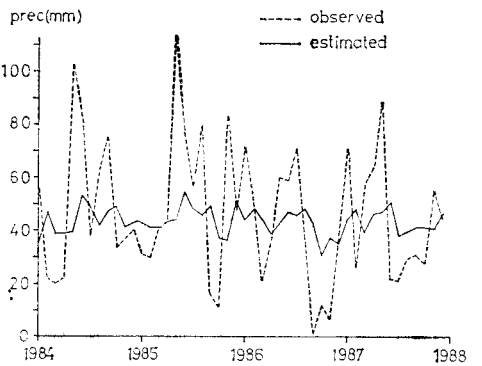

Fig. 3. Monthly precipitations in the years 1984 – 1987 and their estimation with the AR(2) model

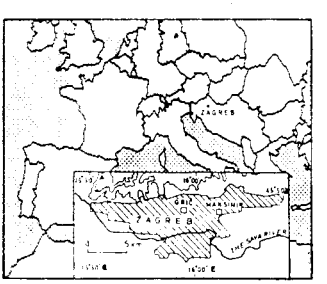

Fig. 1. Location of Zagreb-area in Europe and two stations used in this study

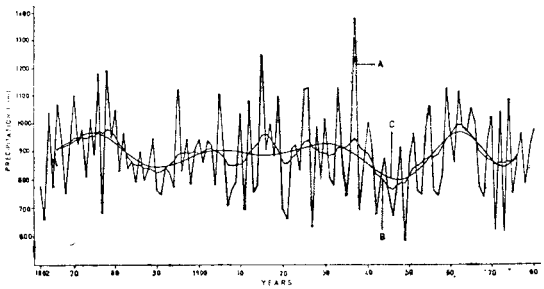

Fig. 2. The time series of annual precipitation amounts at Zagreb-Grič: A — original series, B — the 9-year weighted moving averages and C — the fitted 12-order polynomial

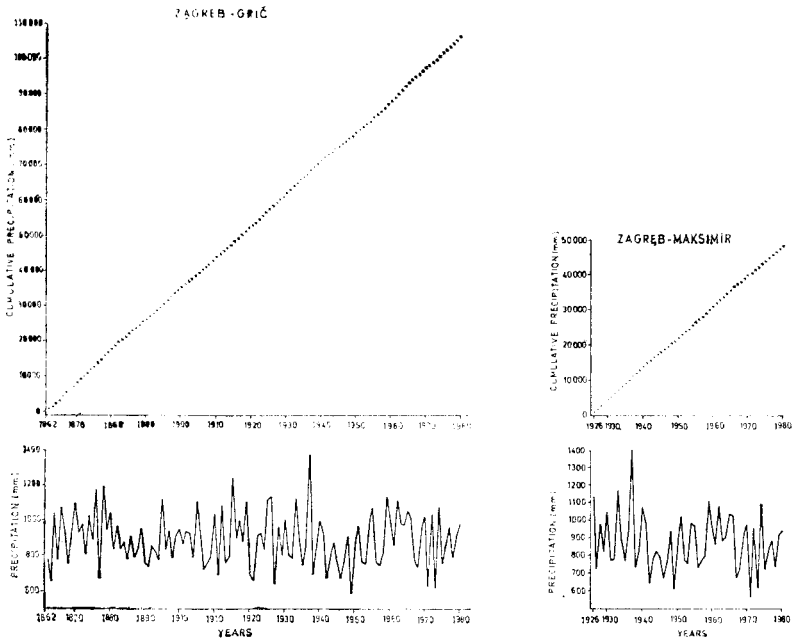

Fig. 3. The mass curves and variations in annual precipitation amounts during the period 1862—1980 (Zagreb-Grič) and 1926—1980 (Zagreb-Maksimir)

BUSUIOC, A., GOLOGUS, L., BOJARIU, R.: POINTING OUT THE VARIATIONS OF THE CLIMATIC CHARACTERISTICS FROM THE TEMPERATURE AND PRECIPITATION STAND-POINT OVER RUMANIA'S TERRITORY

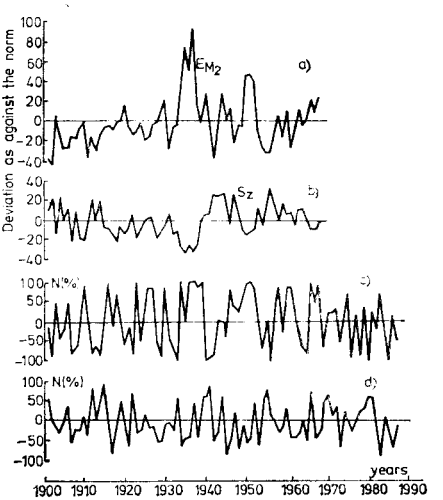

Fig. 1. Anomalies of the annual frequencies of the types of circulation E_{M_2} (a), S_z (b) and the values of the index N (%) for air temperature (c) and precipitation (d)

MIHAILESCU, I.—F., BARBU, A., BUCŞA, I., SABĂU, A.: CHARACTERISTICS OF INTER-ANNUAL VARIABILITY OF THE ATMOSPHERIC PRECIPITATIONS IN RUMANIA

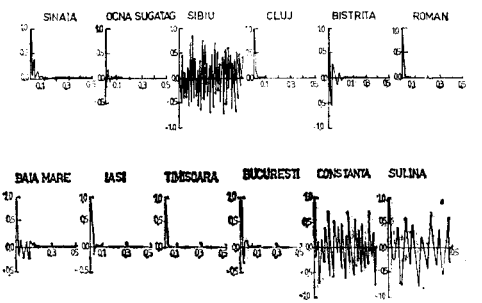

Fig. 2. The function of correlation. The valuation of the maximum entropy

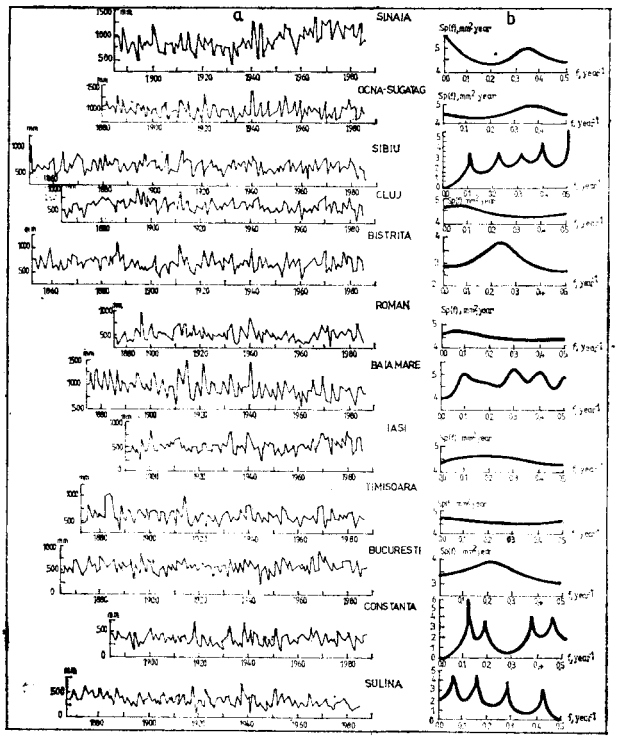

Fig. 1. The variation of the annual totals of precipitations (a) and their spectrum (b)

ADRONACHE, C., MIHA, I.: CLIMATIC VARIABILITY AND QUASI—PERIODICITY OF THE TEMPERATURE REGIME IN RUMANIA

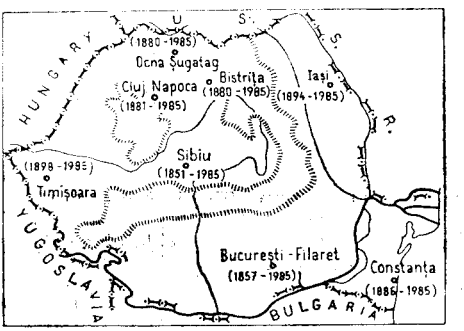

Fig. 1. The selected stations from Rumania and the observation intervals

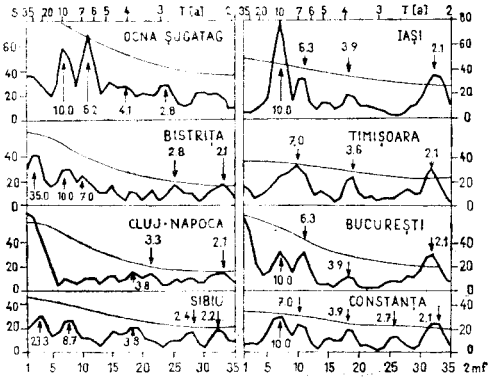

Fig. 2. The power spectra S (10^2K^2) for the series of the annual air temperature means against the frequency $f(2m/an)$ where max lag $m = 35$. The smoothed curve is the 95 % level of confidence. The periods (years) are pointed by arrows

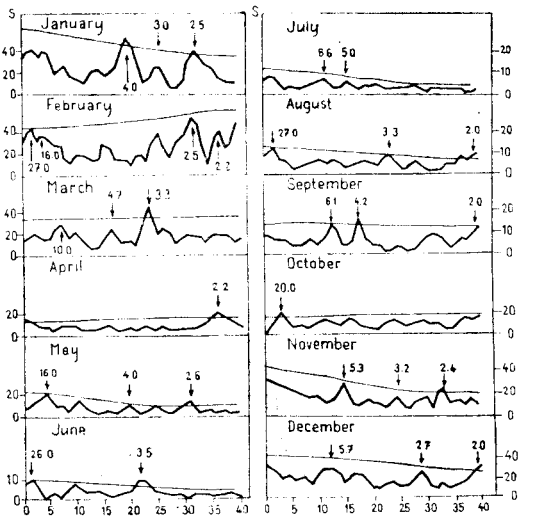

Fig. 3. The power spectra $S(10^2K^2)$ for the series of the monthly temperature means for separate months in Bucharest — Filaret, against the frequency $f(2m/an)$ ($m = 40$)

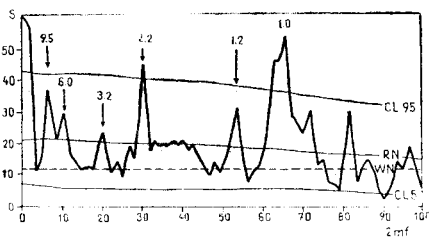

Fig. 4. The power spectrum for the complete series of monthly means (1548 months) in Bucharest — Filaret $S(10^2K^2)$ against the frequency $f(2m/month)$ ($m = 400$)

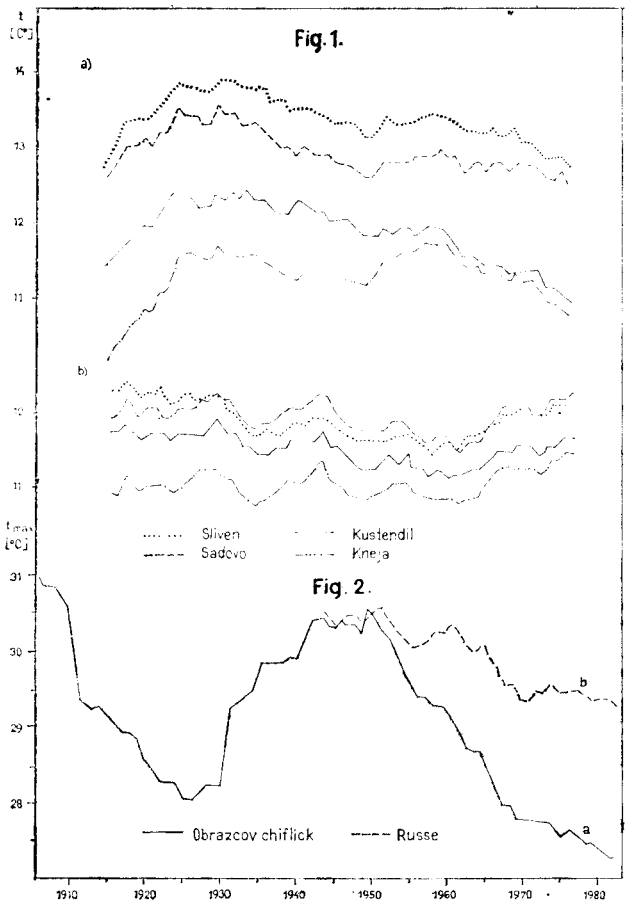

Fig. 1. 20-year running means of mean autumn (a) and spring (b) temperature
Fig. 2. 20-year running means of maximum temperature in country-side (a) and town (b)

Fig. 3. 10-year running means of hot days
Fig. 4. 20-year running means of summer precipitation sums

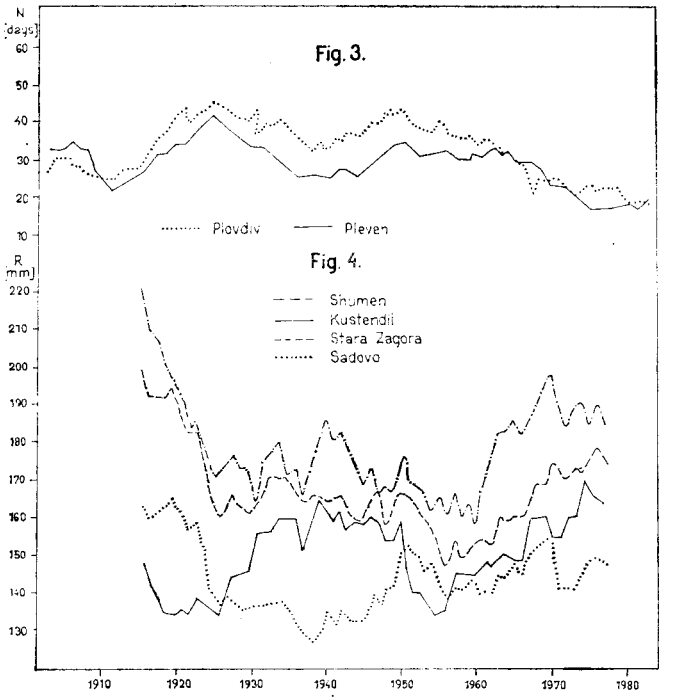

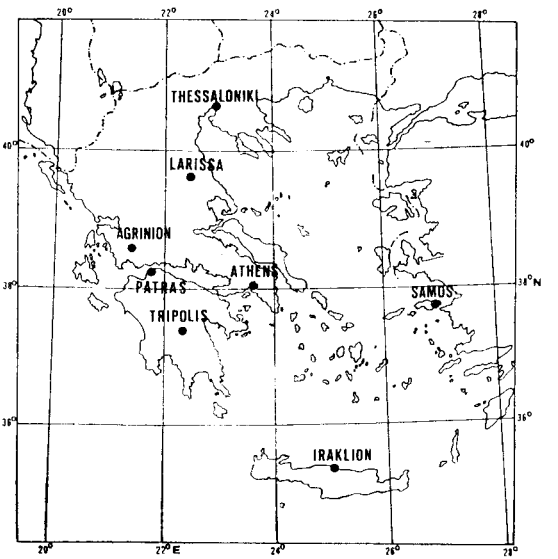

Fig. 1. Location of the 8 stations in Greece

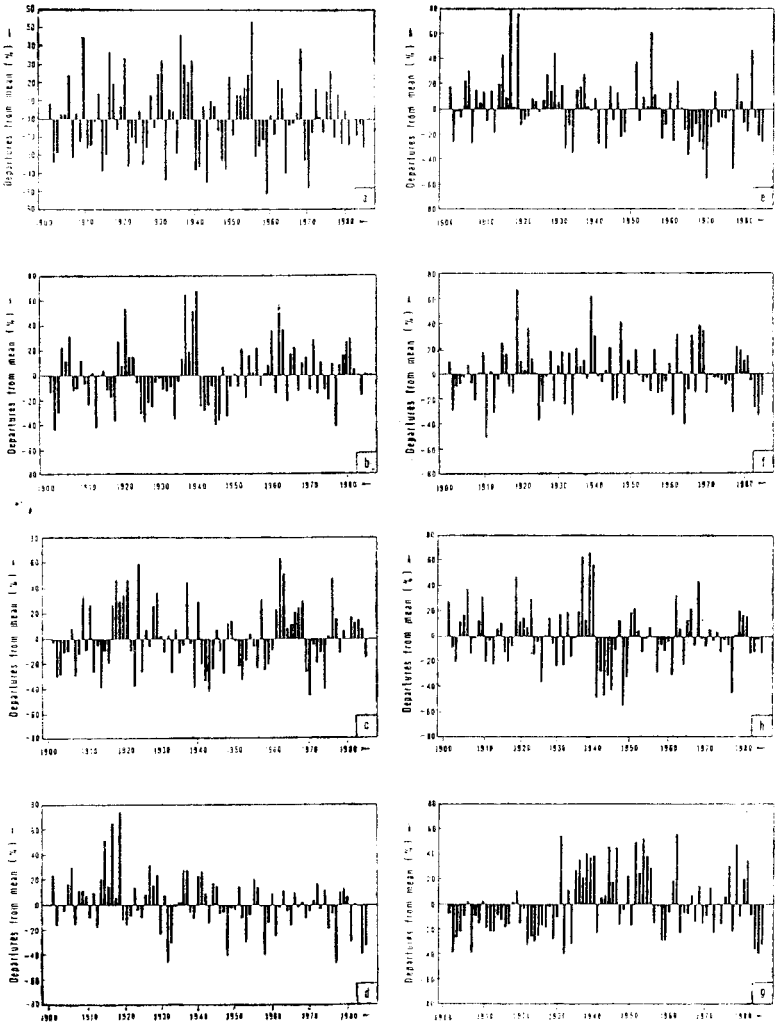

Fig. 2. The annual rainfall in percentage departure from the long-term average at Athens (a), Agrinion (b), Iraklion (c), Thessaloniki (d), Larissa (e), Patras (f), Samos (g) and Tripolis (h)

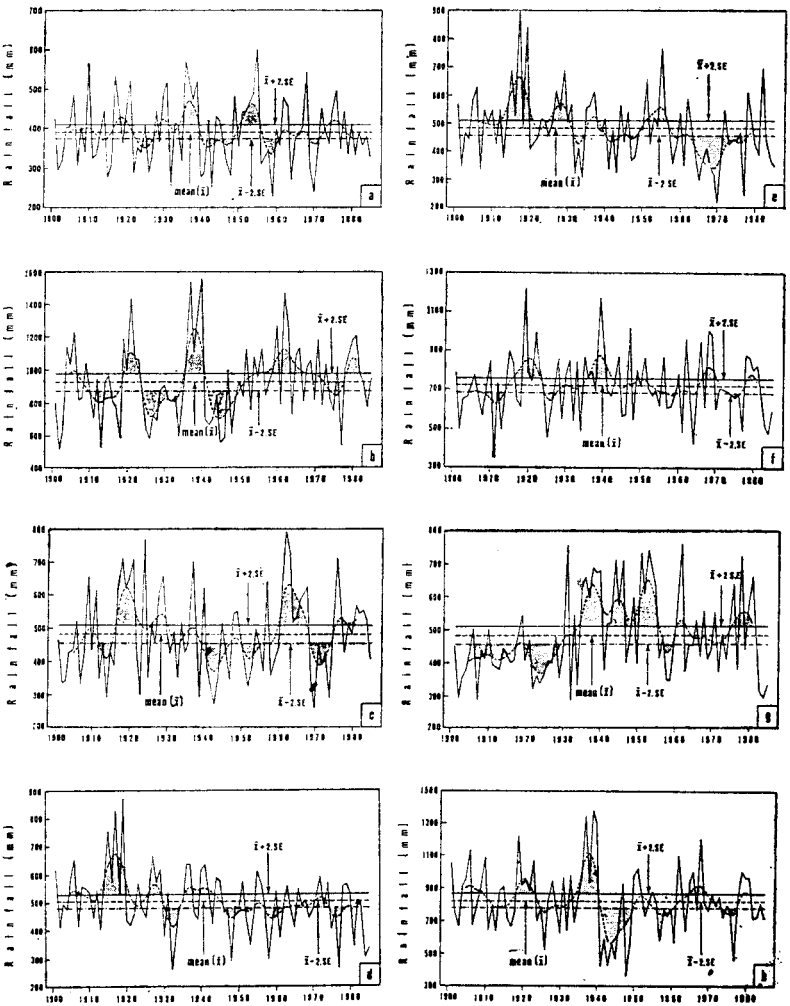

Fig. 3. The original (solid line) and the smoothed (dashed line) rainfall series at Athens (a), Agrinion (b), Iraklion (c), Thessaloniki (d), Larissa (e), Patras (f), Samos (g) and Tripolis (h)

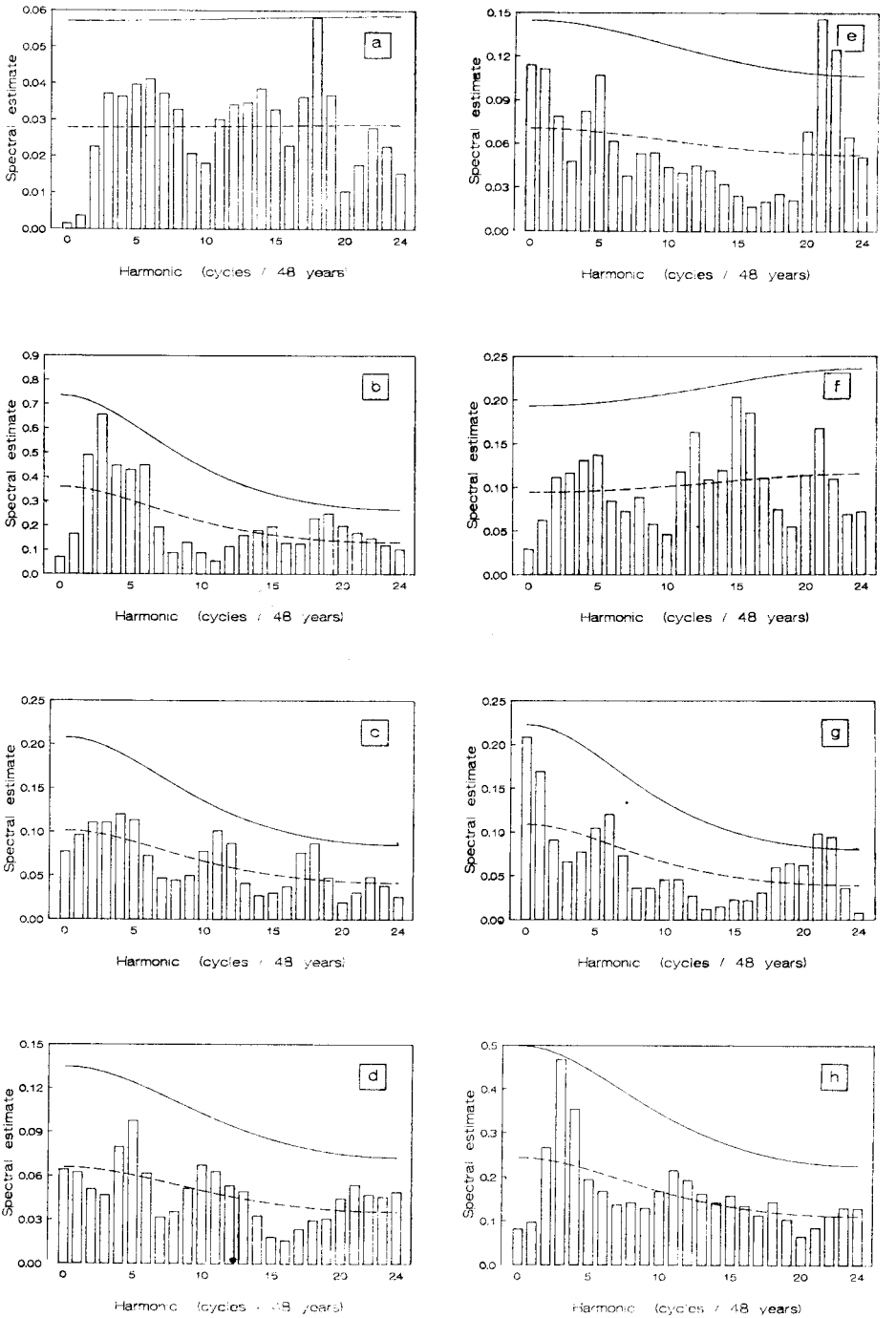

Fig. 4. Power spectrum of annual rainfall amounts at Athens (a), Agrinion (b), Iraklion (c), Thessaloniki (d), Larissa (e), Patras (f), Samos (g) and Tripolis (h)

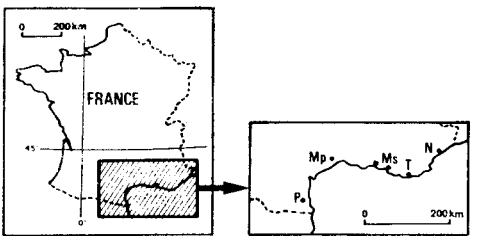

Fig. 1. Situation of the stations. The delimited area is enlarged on the right: N = Nice, T = Toulon, Ms = Marseilles, Mp = Montpellier, P = Perpignan

Fig. 2

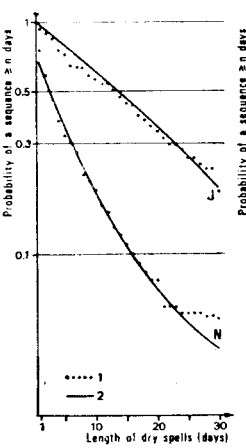

Fig. 3

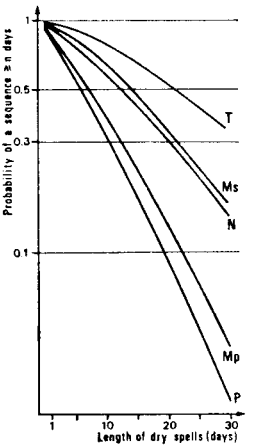

Fig. 2. Dry spells beginning in June $h/d = 0.9$ (J) and November $h/d = 1.5$ (N) in Toulon (1955 – 1984) up to 30 days: 1 – frequency of observed dry spells, 2 – probability of occurrence of a dry sequence $\geqq n$ days according to the SNB model

Fig. 3. Distribution of the probability of a dry sequence (up to 30 days) beginning in July in the 5 stations (1955 – 1984): T, Ms, N, Mp, P – same as *Fig. 1*

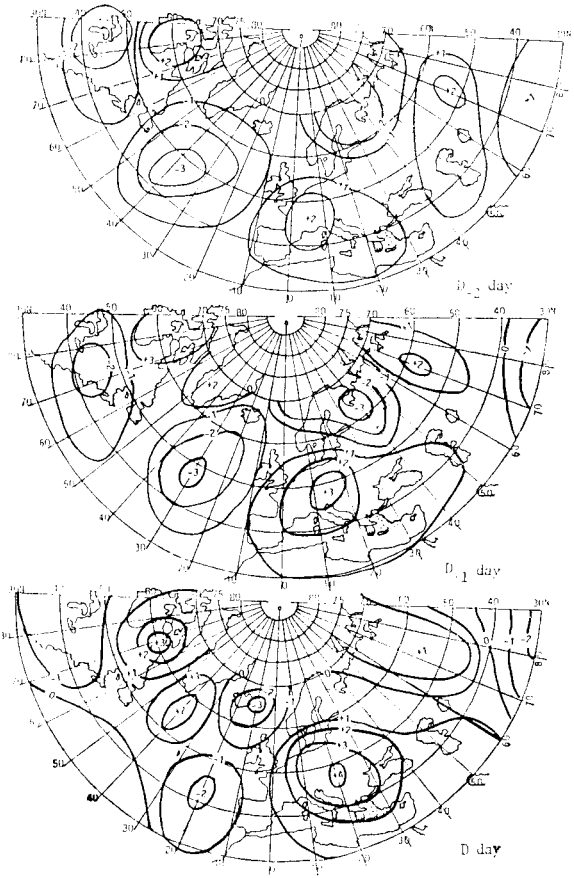

Fig. 1. Centres and their values (hPa) of statistically significant (90 % level) surface pressure anomalies

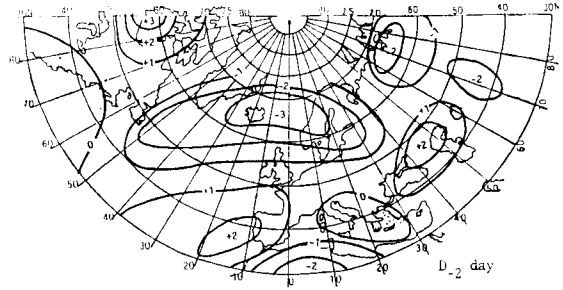

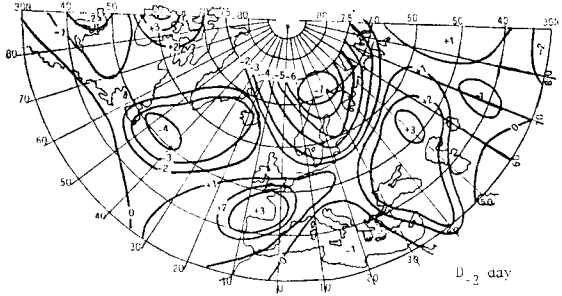

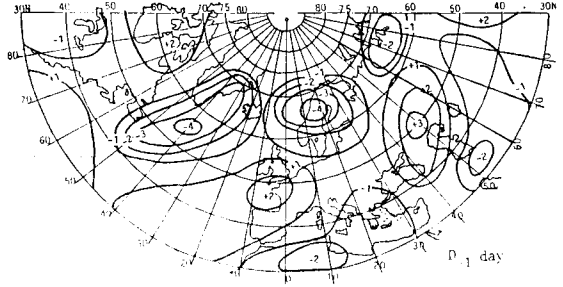

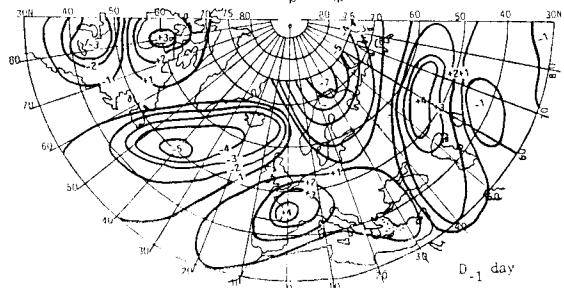

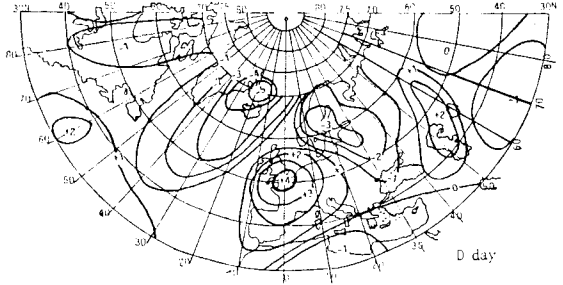

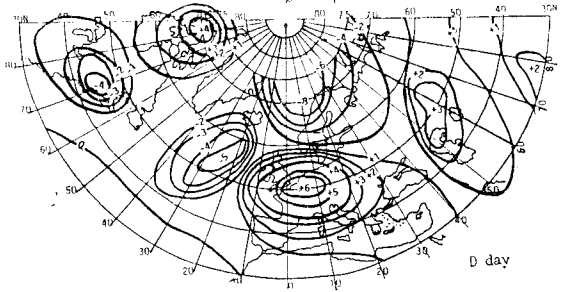

Fig. 2. Centres and their values (dm) of statistically significant (90 % level) 500 hPa surface anomalies

Fig. 3. Centres and their values (dm) of statistically significant (90 % level) 1000/50 hPa thickness anomalies

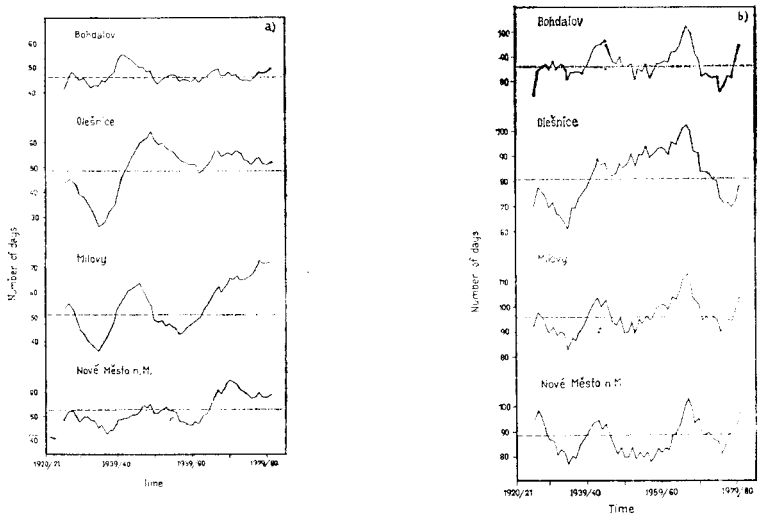

Fig. 1. Course of the annual number of days with the snowfall (a) and with the snow cover (b) smoothed by ten-year running averages in 1920/21 – 1984/85

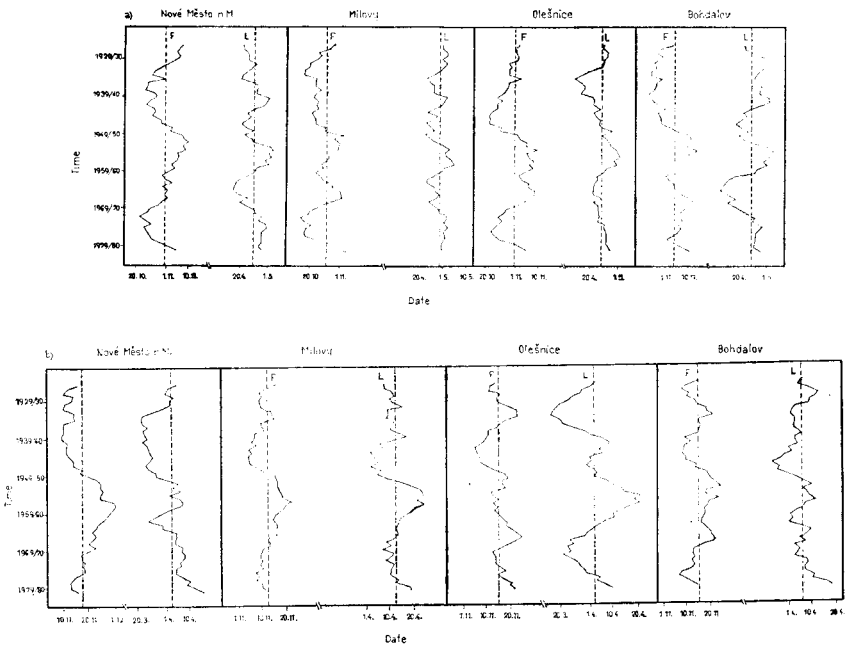

Fig. 2. Courses of the occurrence of the first (F) and the last (L) day with the snowfall (a) and with the snow cover (b) smoothed by the ten-year running averages in 1920/21 – 1984/85

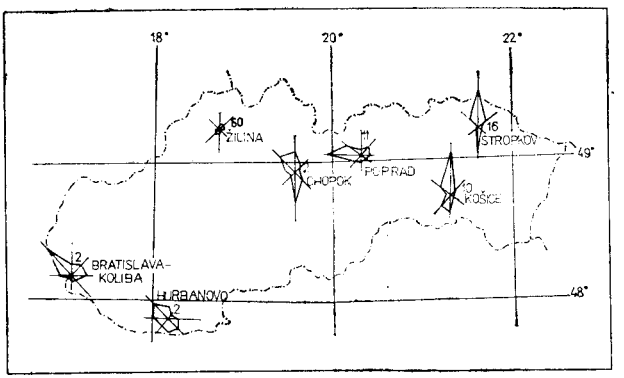

Fig. 1. Relative frequency of the wind direction on seven stations in Slovakia. Number by station indicate frequency of calm by climatological observations (*Šoltis*, 1980)

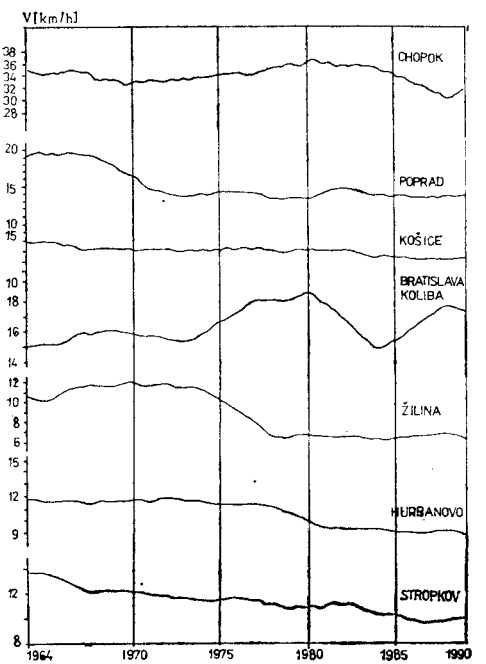

Fig. 2. Annual wind speeds (11-year moving means)

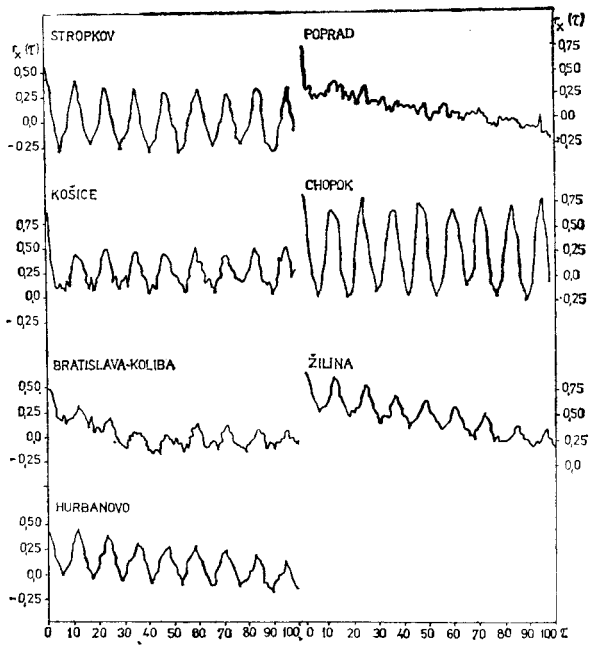

Fig. 3. Autocorrelation coefficients $V_x(\tau)$ of the time series of average monthly wind speeds (τ – time lag)

KAKOS, V.: FLUCTUATIONS IN THE FREQUENCY OF FLOODS ON THE VLTAVA RIVER IN PRAGUE IN RELATION TO METEOROLOGICAL OBSERVATIONS AT PRAGUE–KLEMENTINUM

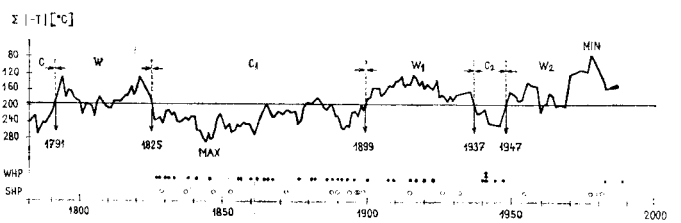

Fig. 1. Occurrence of the floods during the Winter Hydrological Period (WHP) and the Summer one (SHP) in the following years and epochs of the cold (C) and warm (W) winters. Explanation in the text

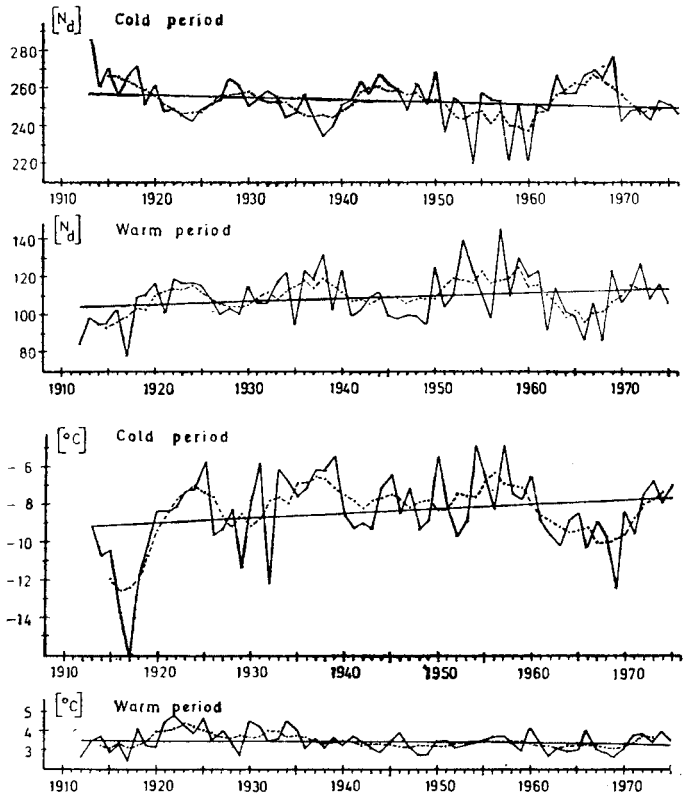

Fig. 1. The length (N_d) and the temperature (°C) of the cold ($t_i < 0.0$ °C) and warm ($t_i \geqq 0.0$ °C) periods in Isfiord Radio in the years 1912 – 1975. Broken line – monthly mean, dashed line – 5-year overlapping monthly mean, straight line – trend lines

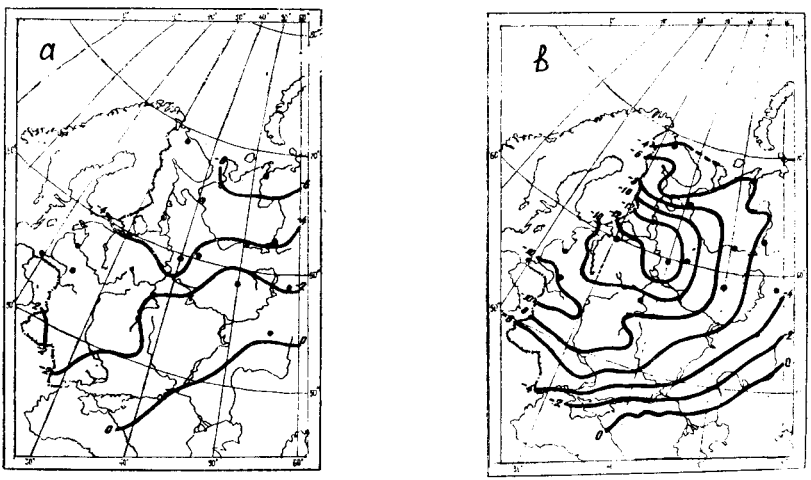

Fig. 1. a) Anomalies of the air temperature seasonal mean for the winter of 1986/87 (°C); b) Anomalies of the January 1987 mean air temperature (°C)

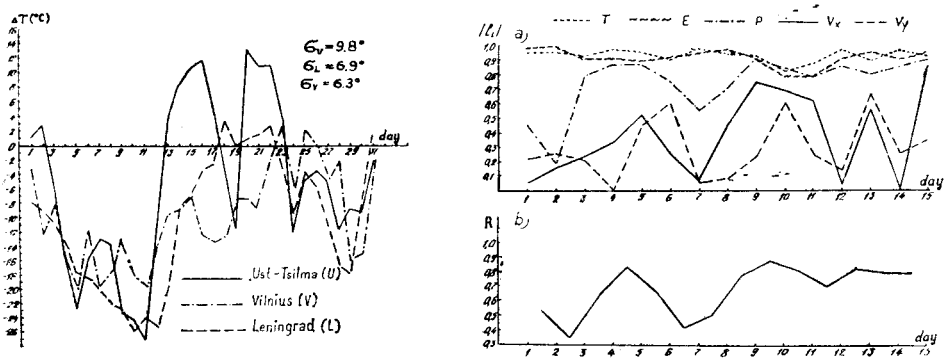

Fig. 2. Anomalies of the mean daily air temperature in January 1987

Fig. 3. a) Factor loadings from meteorological elements on the first factor: air temperature (T), water vapour pressure (E), sea level air pressure (P), wind speed zonal component (V_x), wind speed meridional component (V_y); b) Correlation coefficient between two parts of the first factor vector scores (see the text)

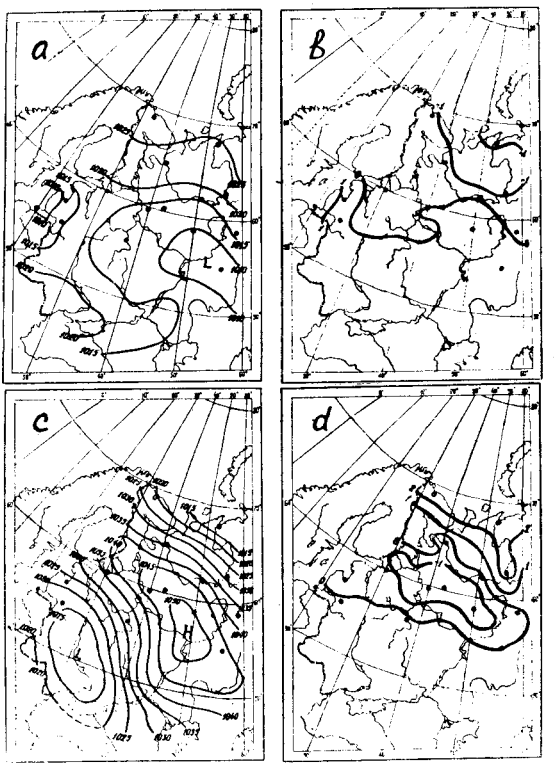

Fig. 4. a) Air pressure on 5 January 1987; b) First factor scores for 5 January 1987; c) Air pressure for 13 January 1987; d) First factor scores for 13 January 1987

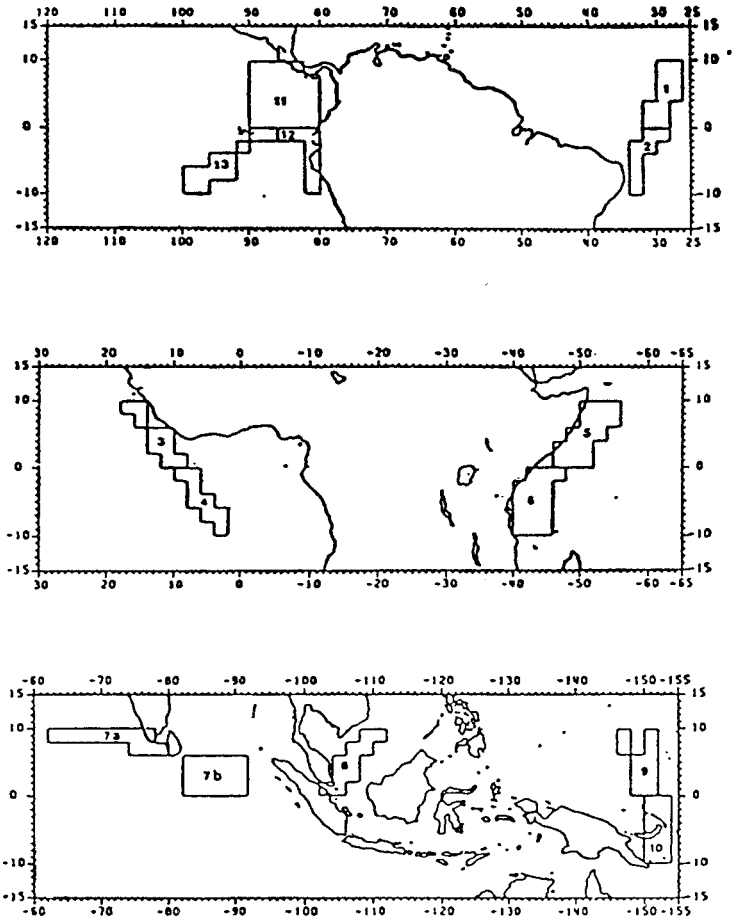

Fig. 1. Map of the selected 14 sections of ship routes in the equatorial belt

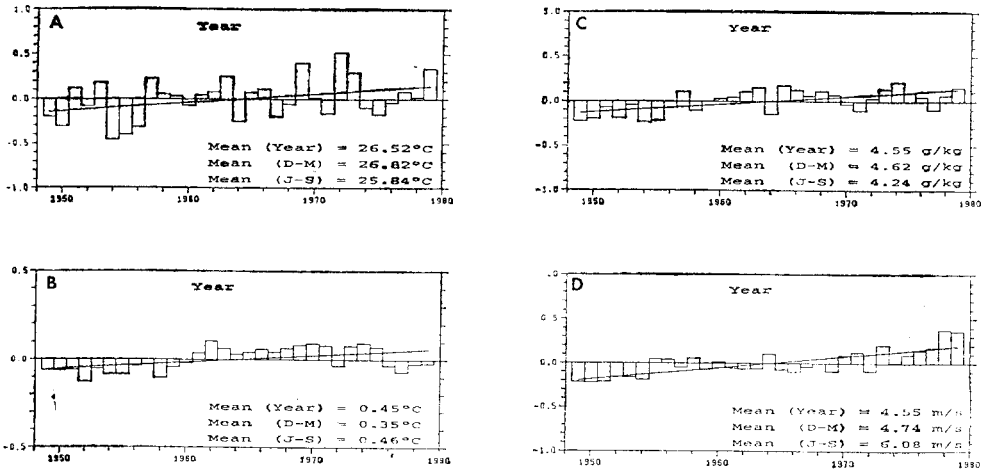

Fig. 2. Time series of selected parameters at the sea-air interface, averaged for 12 sections (only 9–10) annual anomalies with linear trend 1949–1979: A – Sea surface temperature, B – sea-air temperature difference (both in °C), C – saturation deficit (g H_2O/kg air), D – scalar wind speed ($m.s^{-1}$)

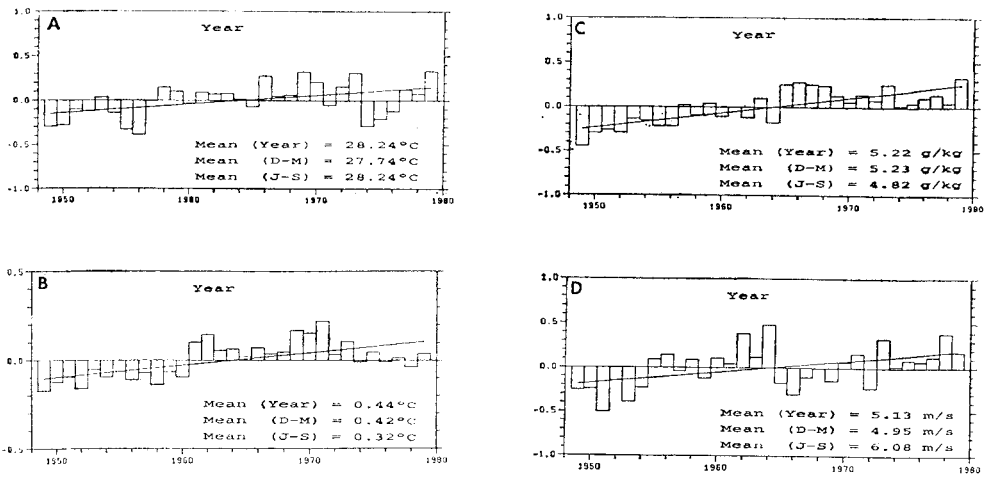

Fig. 3. Time series of selected parameters at the sea-air interface, averaged for sections 7a, 7b, 8 (warmest oceans) annual anomalies with linear trend 1949–1979: A, B, C, D, – see *Fig. 2*

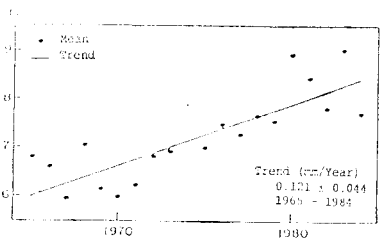

Fig. 4. Time series of annual mean precipitable water between 500 and 700 hPa with annual trend 1965 – 1984, averaged for the stations: Yap, Truk, Majuro and Atuona

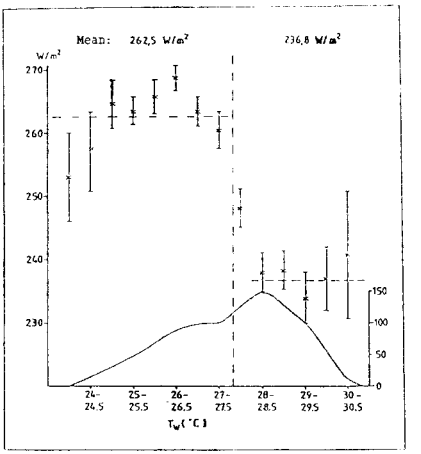

Fig. 5. Outgoing long-wave radiation (Watt.m^{-2}) – representing cloud top temperature and height – as a function of sea surface temperature (T_w) at the surface of the equatorial Pacific Ocean (11). Bottom: frequency of cases

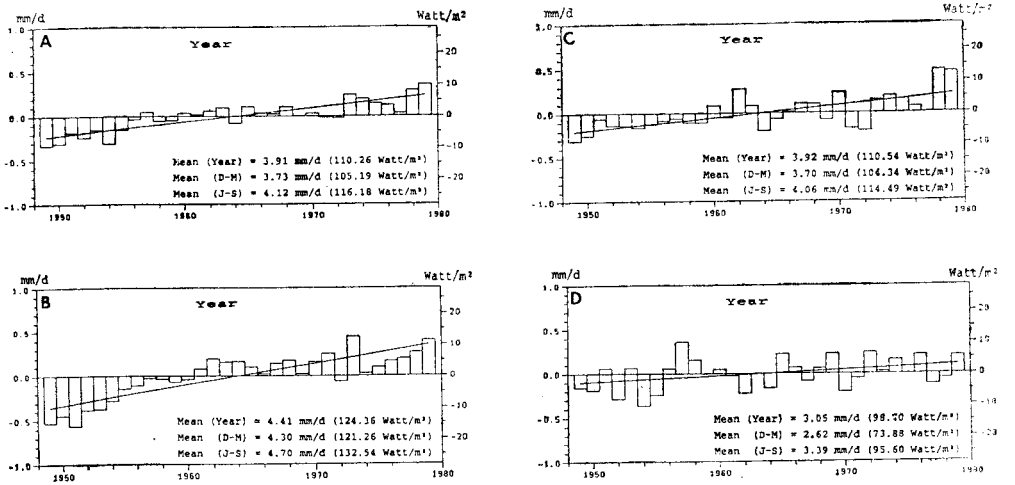

Fig. 6. Time series of the evaporation; annual anomalies and linear trend 1949–1979, averaged for 12 sections (A), sections 7a, 7b, 8 (B), sections 1–4 (C) and sections 11–13 (D)

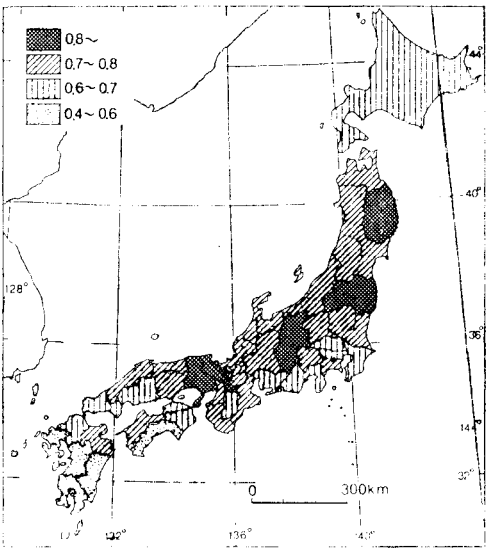

Fig. 1. Distribution of eigenvector for the 1st component

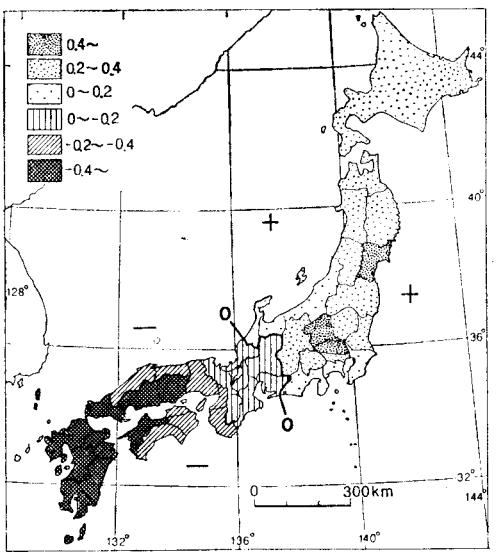

Fig. 2. Same to *Fig. 1*, but for the 2nd component

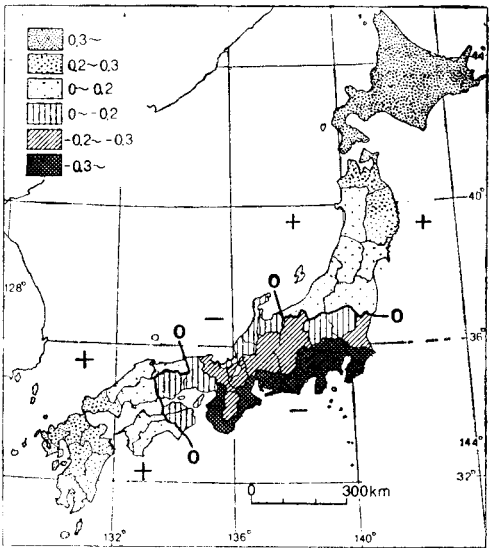

Fig. 3. Same to *Fig. 1.* but for the 3rd component

Fig. 4. Regional division of Japan based on the trends of paddy rice yield during the 104 years, 1883–1986

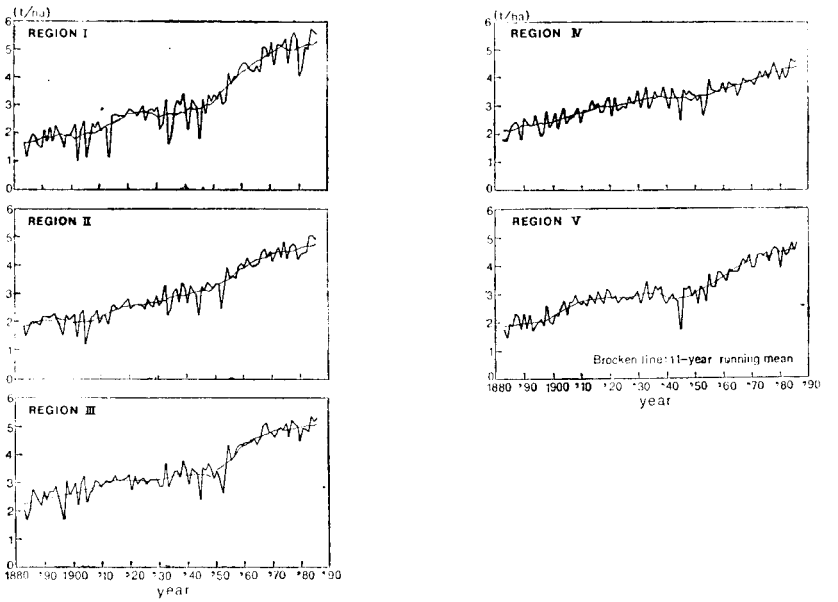

Fig. 5. Secular change of paddy rice yield in Regions I – V from 1883 to 1986. Broken line shows 11-year running mean

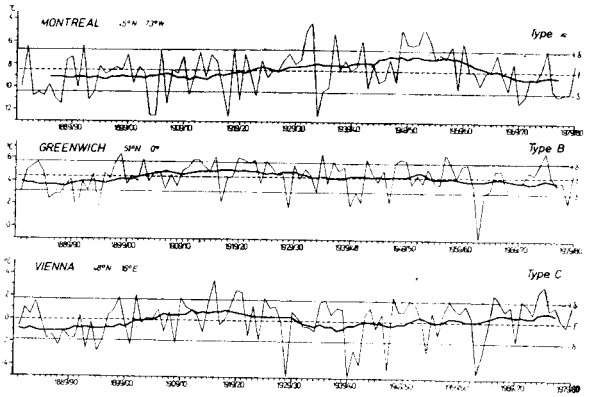

Fig. 1. Course of a mean winter temperature and twenty-year running means at Montreal (type A), Greenwich (type B) and Vienna (type C) in the period 1880/81 – 1979/80 ($\bar{t}$ – mean for 100 winters). For construction of course of running mean data from 1870/71 – 1879/80 and 1880/81 – 1986/87 were used

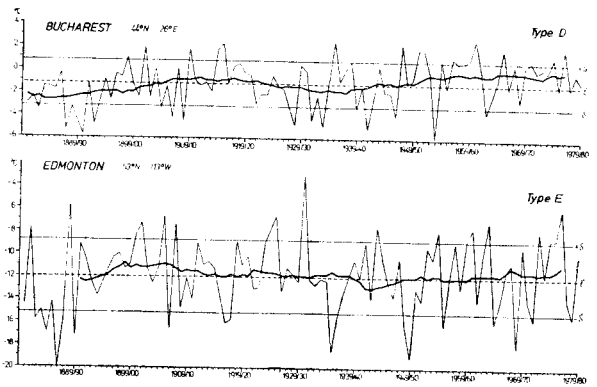

Fig. 2. Course of a mean winter temperature and twenty-year running means at Bucharest (type D) and Edmonton (type E) in the period 1880/81 – 1979/80 ($\bar{t}$ – mean for 100 winters)

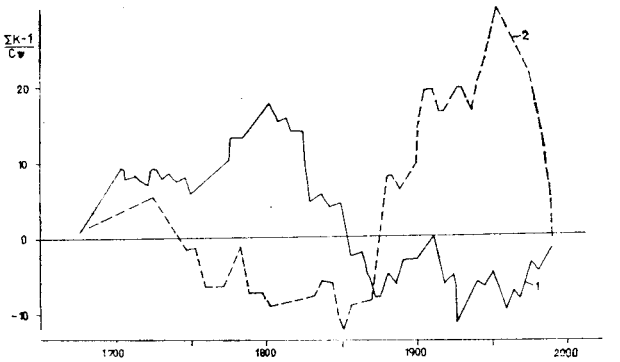

Fig. 1. Accumulative-differential curves of moistening indicators for the centre of the Russian Plain (1) and Eastern Cuba (2)

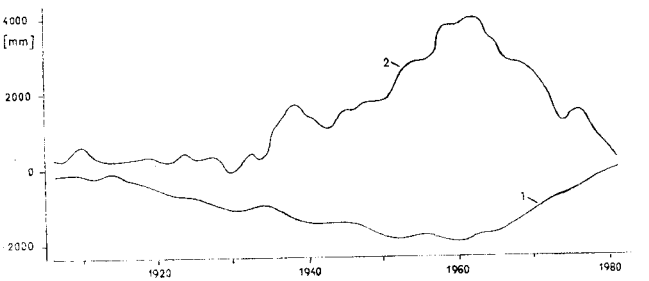

Fig. 2. Accumulative-differential curves of annual precipitation in Moscow (1) and Santiago de Cuba (2)

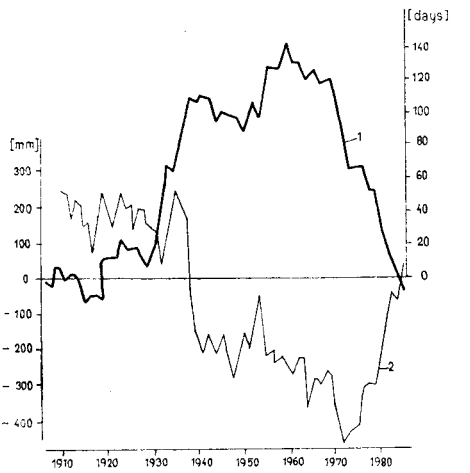

Fig. 3. Accumulative-differential curves of action duration of the latitudinal western ECM group (1) and precipitation totals in Moscow (2) for three summer months